UNIVERSITÉ SETIF1-Ferhat ABBAS

FACULTÉ DE TECHNOLOGIE

THÈSE

Présentée au Département de Génie des Procédés

Pour l'obtention du diplôme de

DOCTORAT

Domaine : Sciences et Technologie

Filière : Génie des Procédés   Option : Génie de l'environnement

Par

BENKOUACHI Oumnia Rayane

THÈME

Adsorption des polluants organiques et minéraux par des matériaux naturels traités en batch

Soutenue le 29/04/ 2025 devant le Jury :

ISSAADI Saifi	**Professeur**	**Univ. Sétif-1-Ferhat ABBAS**	**Président**
BOUGUETTOUCHA Abdallah	**Professeure**	**Univ. Sétif-1-Ferhat ABBAS**	**Directrice de thèse**
BERKAT Djamel	**Professeur**	**Univ. Biskra Mohamed Khider**	**Examinateur**
OMARI Mahmoud	**Professeur**	**Univ. Biskra Mohamed Khider**	**Examinateur**
BAITICHE Milad	**Professeur**	**Univ. Sétif-1-Ferhat ABBAS**	**Examinatrice**
CHEBLI Derradji	**Professeur**	**Univ. Sétif-1-Ferhat ABBAS**	**Invité**

Setif 1 University - Ferhat ABBAS

Setif 1 University-Ferhat ABBAS

FACULTY OF TECHNOLOGY

Thesis submitted to the Process Engineering Department
for a Doctorate Degree

Domain : Science and Technology

Section : Process Engineering   **Option : Environnemental   Engineering**

BY

BENKOUACHI Oumnia Rayane

<u>TITLE OF THE THESIS</u>

Adsorption of organic and mineral pollutants by natural materials treated in batch

Defended on 29/04/ 2025 in front of the Jury:

ISSAADI Saifi	**Professor**	**SETIF1 University-Ferhat ABBAS**	**Chairman**
BOUGUETTOUCHA Abdallah	**Professor**	**SETIF1 University-Ferhat ABBAS**	**Supervisor**
BERKAT Djamel	**Professor**	**Univ. Biskra Mohamed Khider**	**Examinator**
OMARI Mahmoud	**Professor**	**Univ. Biskra Mohamed Khider**	**Examinator**
BAITICHE Milad	**Professor**	**SETIF1 University-Ferhat ABBAS**	**Examinator**
CHEBLI Derradji	**Professor**	**SETIF1 University-Ferhat ABBAS**	**Guest**

Acknowledgments

First and foremost, I am grateful to Allah for leading me and providing me with the health, endurance, bravery, and capacity to carry out this task.

I would like to express my deepest gratitude to my advisor, **Abdallah BOUGUETTOUCHA**, for their unwavering guidance, encouragement, and expertise throughout my doctoral journey. Their support has been instrumental in helping me navigate the challenges of my research and in reaching this milestone.

I extend my sincerest gratitude to my best friend, **Dr. MADI Kamilia**, whose unwavering support and companionship have been with me every step of my academic and personal journey. Her generous assistance will always be cherished and never forgotten

I want to thank my colleague **Dr. LATOUI Mourad** who made this research journey much easier.

I am also deeply thankful to the members of my dissertation committee, Mr. President **ISSAAIDI Saifi**, and the examining members **Pr. OMARI Mahmoud**, **Pr. BERKAT Djamel**, and **Pr.BAITICHE Milad**, for their insightful comments, constructive feedback, and valuable suggestions, which have significantly improved the quality of this work.

I am particularly indebted to my family, whose love, patience, and encouragement have been my source of strength. To my parents, thank you for your sacrifices and for always believing in me.

Finally, I extend my gratitude to all who have contributed to this research, directly or indirectly. This work would not have been possible without your support.

Thank you all

Dedication

To my dear parents,

You who have given me the most precious gift: love, education and a sense of duty. You have always believed in me, even when I myself had doubts. Your patience, sacrifice and dedication have been my compass throughout this journey. This work is the fruit of your encouragement and silent prayers.

To my brothers and sisters: Sife, Houssem, Rafaa, Narimene, and Rihab

For your love, encouragement and solidarity in the moments when I needed it most. Your comforting words and presence have given me immense support.

To my friends, KAmilia, Mimi, Assala, Selma

For your constant encouragement, sharing and understanding. Your friendship has been a breath of fresh air during these years of hard work.

To my dear friend Mouhamed,

For your infinite patience and unfailing support. You have been my refuge in difficult times and my source of motivation when I lacked energy. And for that, I dedicate this thesis to you.

To all those who, from near or far, have contributed to the accomplishment of this work,

I express my infinite gratitude and humbly dedicate this work to you.

International publications

1. **Benkouachi, O. R**.; Bouguettoucha, A.; Tahraoui, H.; Guediri, A.; Chebli, D.; Kebir, M.; Knani, S.; Zhang, J.; Amrane, A. Advanced Green Peel Utilization for Efficient Methylene Blue Removal: Integrated Analysis and Predictive Modeling. J. Mol. Liq. 2024, 125951. https://doi.org/10.1016/j.molliq.2024.125951.

International Communications

1. **Benkouachi, O. R**.; Bouguettoucha, A.; Madi, K.; Tahraoui, H.; Chebli, D.; Kebir, M. Removal of cationic dye –Methylene blue– from aqueous solution by adsorption onto biosorbent, (Chemex Africa 23) Algiers 23 September to 04 October 2023.

2. **Benkouachi, O. R**.; Bouguettoucha, A.; Madi, K.; Chebli, D.Studing the dye removal process kinetically and equilibrium using a modified biosorbent, (ICMRE2023), November 18, 2023 – November 19, 2023 Setif.

National Communications

1. **Benkouachi, O. R**.; Bouguettoucha, A.; Madi, K. Adsorption of Biebrich Scarlet Dye into Peels of vegetables and fruits as Adsorbents, (SNEGD'23), 09 & 10 December 2023 RELIZANE, ALGERIA.

2. **Benkouachi, O. R**.; Bouguettoucha, A.; Madi, K.; Tahraoui, H.; Chebli, An Empirical and Theoretical Investigation into the Adsorption of Methylene Blue on a Novel Untreated Biosorbent - A Statistical Physics Analysis, FEBRUARY 13-14, 2024; BISKRA, ALGERIA.

Table of contents

Acknowledgment

List of figures

List of tables

List of abbreviations

Table of contents

Table of contents

Table of contents

Abstract

List of figures

Chapter I :

Chapter II:

Chapter III:

List of figures

List of figures

Chapter V

List of table

List of table

Nomenclature

C	the intercept of Intraparticle diffusion function
C_o	initial concentration of MB ($mg \cdot L^{-1}$)
Ce	final concentration of MB in the solution
C_t:	concentration of MB at time t ($mg \cdot L^{-1}$)
CR:	Cupule raw (biosorbent)
$C_{1/2}$	the concentration at half–saturation ($mg \cdot L^{-1}$)
C_1	concentrations at half saturation for the first active site ($mg \cdot L^{-1}$)
C_2	concentrations at half saturation for the second active site ($mg \cdot L^{-1}$)
E_{int}	System internal energy ($J \cdot mol^{-1}$)
G	Gibbs free enthalpy ($J \cdot mol^{-1}$)
GP	Green pea
h	Planck constant ($J \cdot s$-1)
K_B	Boltzmann constant ($J \cdot K$)
k_1	equilibrium rate constant of PFO equation ($L \cdot min^{-1}$)
k_2	equilibrium rate constant of PSO equation ($L \cdot min^{-1}$)
K_F	Freundlich constant ($g \cdot L \cdot mg$)
K_{id}	the rate constant of intraparticle diffusion($mg \cdot g$-1$ \cdot min^{-0.5}$)
K_L	Langmuir constant ($L \cdot mg^{-1}$)
k_n	equilibrium rate constant of PNO equation ($L \cdot min^{-1}$)
K_s	Sips constant ($L \cdot mg^{-1}$)
M	mass of the mixture (g)
MWA	Mix waste activated (biosorbent)
m_s	the exponent of the Sips model
MB	methylene blue
n	number of ions per site
n_1	number of ions per site for the first site receptor
n_2	number of ions per site for the second site receptor
nf	Freundlich (R-P) constant
n_o	biosorption reaction order N number of experimental points performed

Nm	sites receptor density (mg•g^{-1})
PFO	pseudo-first-order,
PSO	pseudo-second-order
PNO	pseudo-nth-order
Qe	amount of dye adsorbed at equilibrium (mg•g^{-1})
Qt	quantity adsorbed at time t (mg•g^{-1})
R	the correlation coefficient
RMSE	Root Mean Squared Error
Sa	Entropy (J•mol•K^{-1}) t time (min)
T	temperature (°C or °K)
V	volume of the mixture (L)
Z$_v$	Translation partition function per unit volume
Z$_{gtr}$	translation partition function
β	the constant of desorption (g/mg).
α	the constant of initial sorption rate (mg/(g·min))
ϑ	the fractional power kinetic model constant.
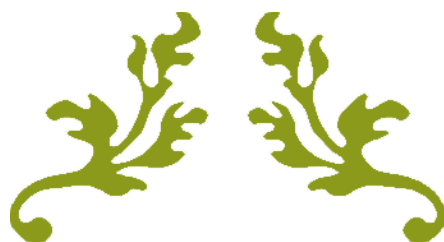
GENERAL INTRODUCTION

{ **General Introduction** }

Ensuring water protection is fundamental to the continuity of life and preserving ecological balance on the planet [1]. The quest for human development and increased comfort over time has contributed to the deterioration of the natural environment. This has caused a decline in air quality, overuse of soils resulting in their depletion due to unsustainable practices, and severe pollution of natural water systems an urgent challenge that must be addressed [2].

The accumulation of numerous organic xenobiotic compounds due to global human-induced pollution has detrimental effects on human health and ecosystems' functionality.

Annually, pollutants from industrial and metallurgical effluents, including metal ions, organic dyes, chemicals, and residual antibiotics, cause water pollution [3], [4]. When these effluents are saturated with dyes, they harm the environment and pose significant risks to human well-being [5]. Therefore, the removal of these dyes from wastewater is critical for the protection of human health and the conservation of environmental resources [6]. A range of techniques for the remediation of dye pollutants (physical, chemical, and biological strategies), including flotation, reverse osmosis, coagulation/flocculation [7], electrochemical processes, ultrasonic treatments, biological treatment [8], photodegradation [9], and adsorption [10], has been developed to confront contemporary degradation challenges.

Even while every technique has advantages of its own, adsorption is an advantageous technique because it is straightforward, efficient within pipeline systems, economically viable, environmentally sustainable, does not produce sludge, is non-destructive, biocompatible, and easy to apply [11], [12].

The versatility of the precursor selection, which can be utilized as an adsorbent or as a foundation for the creation of an adsorbent, is another advantage of the adsorption process.

Accordingly, a wide variety of adsorbents, such as activated carbon, zeolites, biosorbents, and clays, have been used in published studies (reference). In this regard, the primary goal of this thesis is to value regional by-products by creating novel, inexpensive adsorbent materials from food and agricultural wastes, where the final adsorbents must meet certain requirements, such as:

- Readily available and easily sourced raw materials (precursors).

- Non-toxic adsorbents that pose no health risks to operators.

- Adsorbents with well-defined and controllable preparation processes.

- Economically viable production.

- High adsorption efficiency for effective water decolorization.

- Ease of regeneration following the adsorption process.

This thesis valorizes three regional by-products: green pea peels, restaurant agricultural waste, and cupules of oak residues.

The efficacy of the developed adsorbents will be tested in powdered form, and the findings from this PhD thesis will be articulated as articles across the next five chapters.

The first chapter will focus on a comprehensive literature review that aims to contextualize the research problem of this thesis. This section will initially present general information about various types of dyes, their classification according to different criteria, and the associated risks of their usage. Subsequently, an overview of the various water discoloration techniques will be provided, with a detailed examination of the adsorption method. Furthermore, sources of low-cost adsorbents, including natural, industrial, and agricultural residues, will be identified and discussed, alongside comparative tables showcasing different powdered precursors utilized in the literature and their adsorption efficacy with various pollutants. In addition, composite materials proposed as alternative adsorbents to address the

limitations of traditional powdered materials will be introduced. Finally, various parameters that may influence adsorption efficiency—such as adsorbent mass, initial dye concentration, contact time, pH, temperature, particle size, ionic strength, and others—will be identified and discussed at the end of this chapter.

In the second chapter, a comprehensive description of the characterization methods applied in this thesis, as well as the procedures for preparing the adsorbent materials, will be provided. Additionally, the chapter will detail all the experimental protocols used for adsorption tests, covering a range of parameters. Quantum chemical calculations, including Density Functional Theory (DFT) and Molecular Dynamics Simulations (MDS), utilized in this study, will also be explained. The chapter will conclude with an in-depth discussion of statistical physics modeling based on the grand canonical ensemble.

The focus of **the third**, **fourth, and fifth chapters** will be on preparing adsorbents in powder form from the selected precursors.

The third chapter emphasizes the use of unprocessed green pea peels to develop an environmentally friendly product suitable for water purification. In contrast, the fourth chapter focuses on transforming agricultural waste from restaurants through chemical treatment with KOH to produce a material effective for water treatment. We apply physical statistical models, and molecular modeling based on Density Functional Theory (DFT).
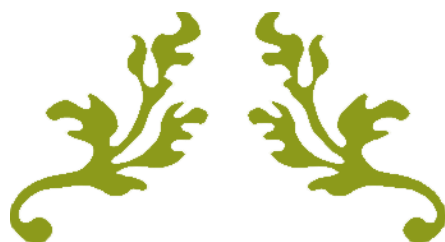
Furthermore, the fifth will be concentrated on the use of unprocessed cupules of oak to develop an environmentally friendly product suitable for water purification. Moreover, this chapter will differ from the fourth by employing the response surface design of experiments.

The characteristics of the prepared materials will be assessed using multiple analytical techniques, such as Fourier Transform Infrared Spectroscopy (FTIR), Scanning Electron

Microscopy (SEM), X-ray Fluorescence (XRF), and Thermogravimetric Analysis (TGA). Their adsorption performance will be evaluated using Methylene Blue (MB) as a model compound, considering various factors that may affect adsorption, including initial dye concentration, contact time, pH, temperature, and ionic strength. The justification for selecting Methylene Blue (MB) as the model molecule will be provided in the following chapters.

In conclusion, this thesis will summarize the investigations carried out and the results obtained, while also proposing future research directions within this field of study.

CHAPTER I

<div align="center">

Part one:

Water pollution

</div>

I.1.   Introduction

The most pressing environmental issue facing the entire planet right now is aquatic pollution, which needs to be addressed immediately. Providing clean water to the public has grown to be a challenging undertaking. Water resources are generally declining, and the main cause of this issue is the discharge of untreated or inadequately treated wastewater from industrial facilities, which mostly contains pollutants like dyes, pesticides, heavy metals, drug byproducts, and wasted chemicals from respective industries (**Figure I.1**) [1], [2].
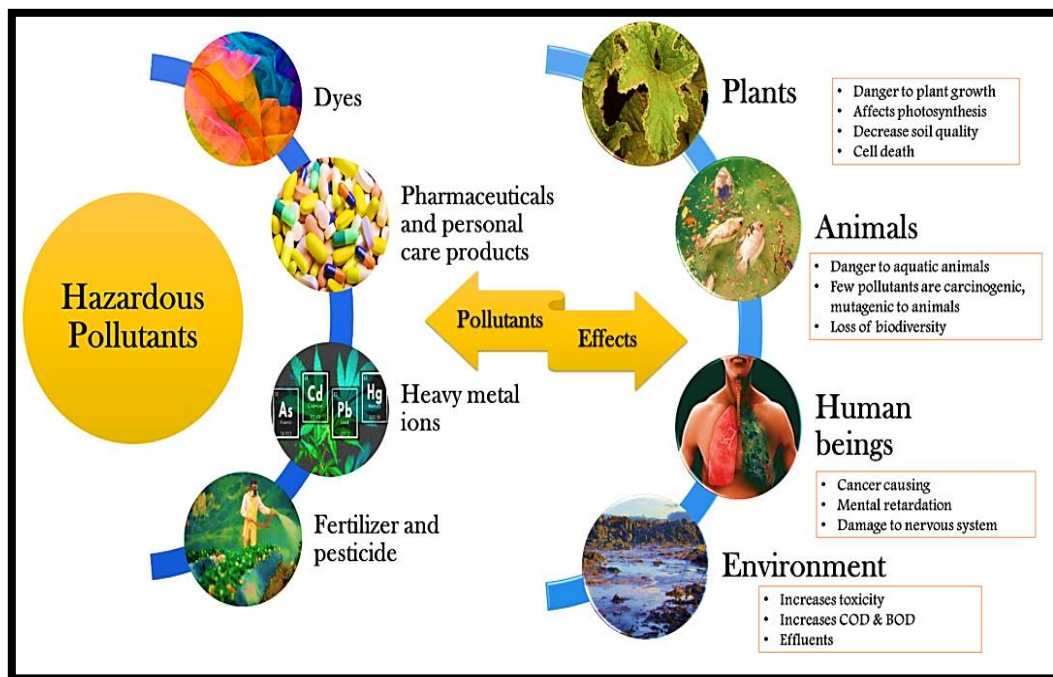
Figure I. 1: The source of hazardous pollutants and their effects are discussed here.

I.2.   Water Quality Indicators

Water quality characteristics are classified into three categories: physical, chemical, and biological. **Table I.1** explains them [3].

Table I. 1: water quality parameters.

Physical parameters	Chemical parameters	Biological parameters
Turbidity	pH	Bacteria
Temperature	Acidity	Algae
Color	Alkalinity	Virus
Odor and Taste	Chloride	Protozoa
Solids	Chlorine residual	
conductivity	Sulfate	
	Nitrogen	
	Fluoride	
	Iron and Manganese	
	Copper and Zinc	
	Hardness	
	Biochemical Oxygen Demand (BOD)	
	Chemical Oxygen Demand (COD)	

Part two:

Overview of Dyes

I.3.   Introduction: resources and consequences of ecotoxicology

Dyes are chromophoric compounds engineered to impart coloration to various materials, including papers, fabrics, or other suitable materials through molecular interactions. Humans have employed dyes for millennia across a wide range of applications [4]. The origin and routes of environmental dyes are depicted in **Figure I.2**, stemming from industries, wastewater treatment facilities, and households, contributing to environmental degradation [5].
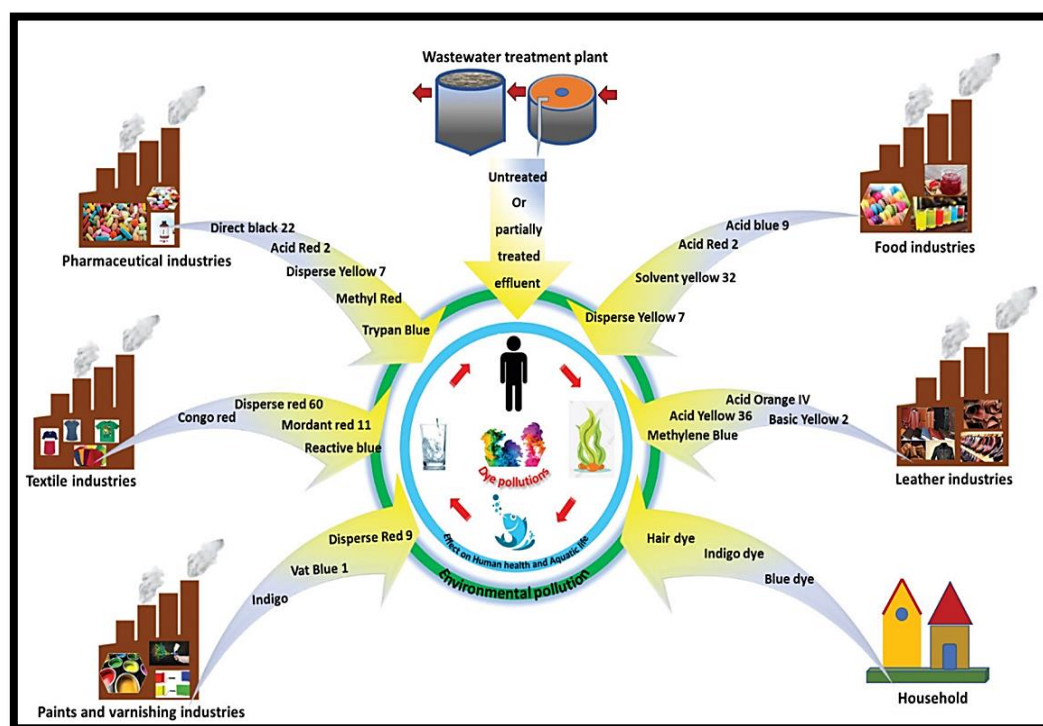
Figure I. 2: Source and routes of dyes.

Structurally, dyes possess aromatic molecular frameworks derived from hydrocarbons such as benzene, toluene, naphthalene, anthracene, and xylene. These compounds are sourced from both natural origins (e.g., plants, insects, animals, and minerals) and anthropogenic processes (synthetic dyes). Artificial dyes, produced from organic molecules, are widely used across

various industries. However, their extensive use and release often alongside other toxic organic and inorganic chemicals through industrial effluents pose significant environmental risks.

The classification of dyes considers their chemical structure, physicochemical properties, origins, and applications, alongside the hazardous nature of industrial effluents [6]. These effluents often contain toxic and carcinogenic compounds harmful to both human health and ecosystems, **Figure I.3**, shows the effect of this pollution.
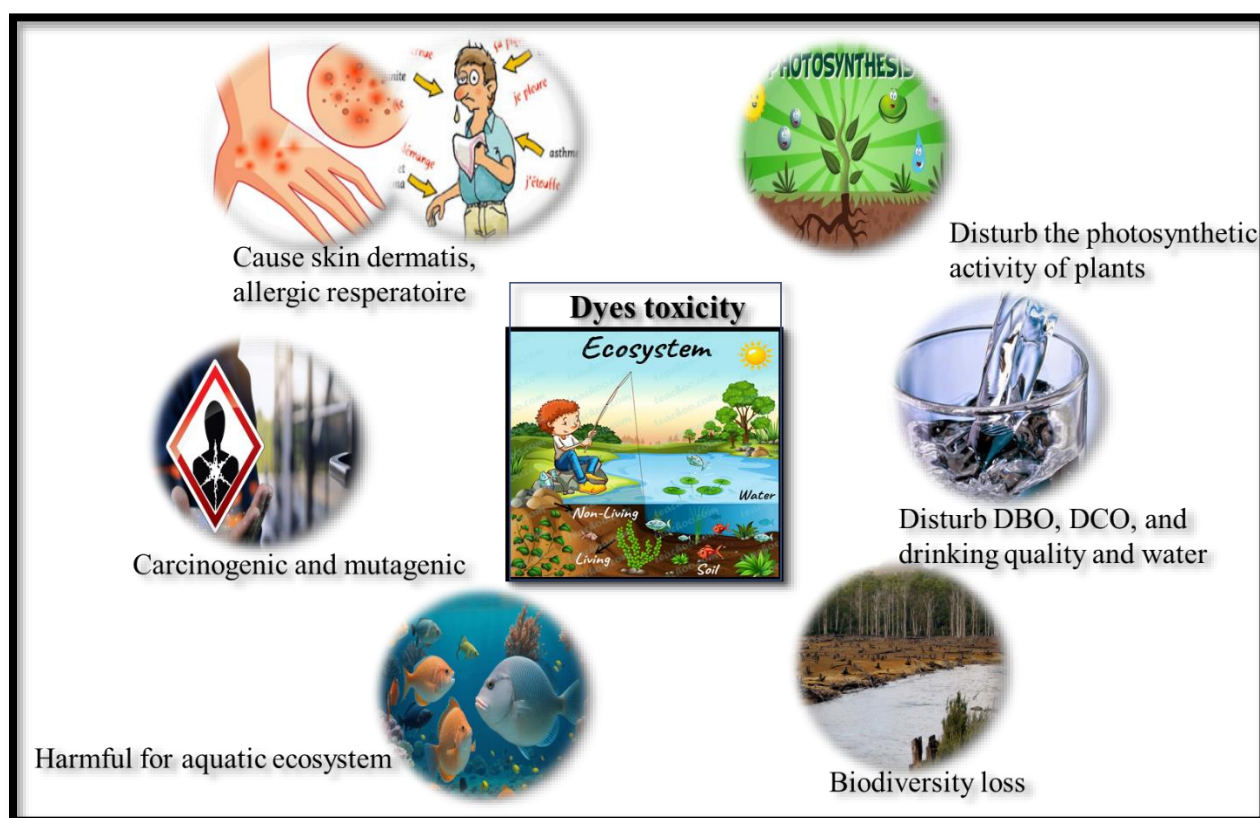
Figure I. 3: The effect of dyes on both human health and ecosystems.

I.4.   Dye classification

The idea of dyes is currently prevalent in practically every aspect of our everyday lives. Their category is based on the **chemical nature** (according to the auxochrome vs the chromophore) and the **source of the materials** (natural or manufactured dyes).

I.4.1. Natural Dyes

The human race has been using dyes for thousands of years. They were originally manufactured from plants and animals using straightforward procedures like grinding or heating. There are two groups of all these dyes: vat dyes and mordant dyes.

➢ Insoluble in water substances known as **mordant dyes** are created when metal ions, which have been deposited following an initial treatment on the fiber, combine with the functional groups found in the colored molecule [7].

➢ **Vat dyes** have at least two ketone functionalities and are initially insoluble in water. Leuco-soluble, an alkaline enolic form, is the result of an alkaline reduction procedure that allows for their dissolution. When enolate groups are substituted, the dissolved dye exhibits a preference for cellulosic fibers [8].

I.4.2. Synthetic dyes

Dye made from either inorganic or organic materials is known as synthetic dye. The overall chemical of these dyes for clothing serves as the foundation for their division into many groups it shown in the **Figure I.4**: [8], [9]
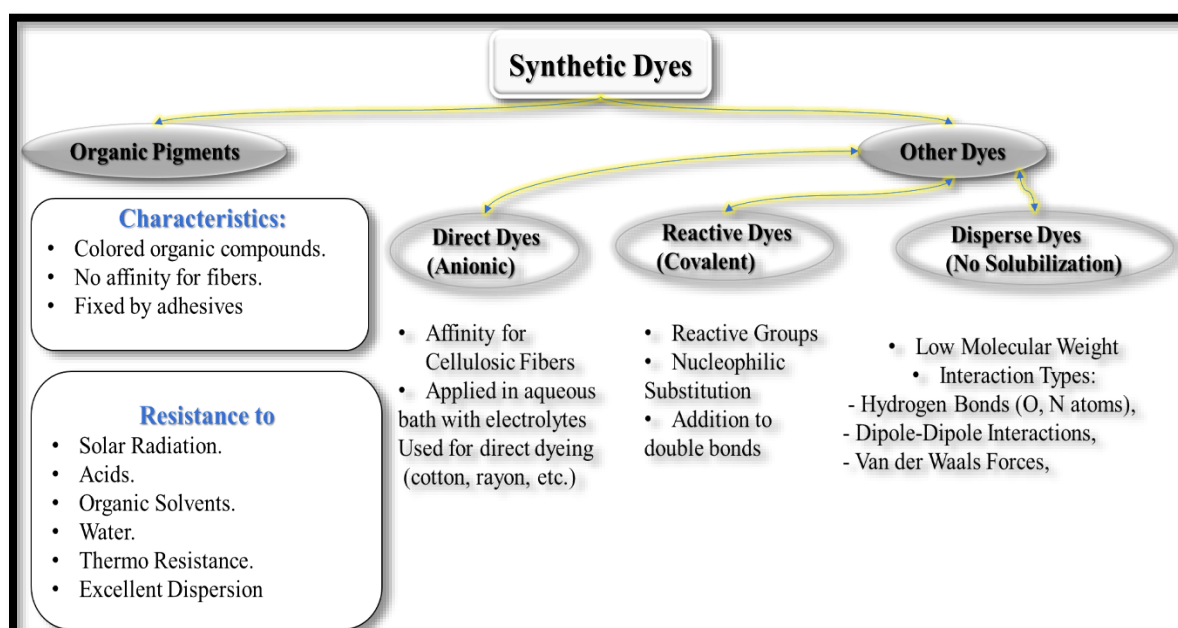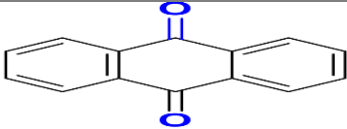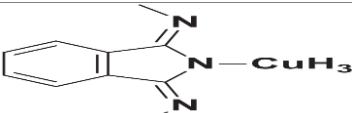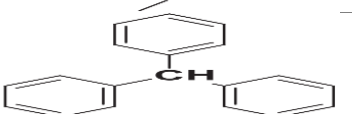
Figure I. 4: Synthetics dyes types.

I.4.3. Chemical classification of dyes

Depending on their chemical structures, the primary basis for categorizing dyes is whether they are **auxochromes** or **chromophores**.

➤ **Chromophores** are the parts of the dye molecule responsible for its color; they absorb specific wavelengths of light, leading to the perception of color. **Table I.2** represents the chromophors groups.

➤ **auxochromes** are functional groups that do not possess color alone but enhance chromophores' color properties when attached. They can increase the dye's ability to absorb light, thus intensifying its color. The table below shows the auxochroms groups. This classification is essential for understanding the behavior and properties of dyes, enabling manipulation for various applications. It includes vat dyes, direct dyes, mordant dyes, reactive dyes, azo dyes, dispersion dyes, basic or cationic dyes, and acid or anionic dyes.

Table I. 2: *Represents Chromophoric and auxochromic groups of dyes[8].*

Groups chromophoric		Groups auxochromic	
Azo	$(-N=N-)$	Amino	$(-NH_2)$
Nitroso	(-NO or -N-OH)	Methylamino	$(-NHCH_3)$
Carbonyl	$(>C=O)$	Dimethylamino	$(-N(CH_3)_2)$
Ethylenic	$(>C=C<)$	Hydroxyl	(-OH)
Nitro	$(-NO_2$ or $=NO-OH)$	Alkoxyl	(-OR)
Sulphide	(C=S)	Electron donor	$(-NO_2)$
Ketone-imine	$(>C=NH)$	Groups	$(-CO_2H)$, $(-SO_3H)$
Polymethine	(=CH-CH =CH-CH=)		$(-OCH_3)$Cl, Br, I, At
Anthraquinone			
Phthalocyanine			
Triphenylmethane			

I.4.4. Classification according to their charge

This approach of classifying dyes into two groups is shown in **Figure I.5**. This is not particularly common, but it may be done nonetheless [8], [10], [11]:
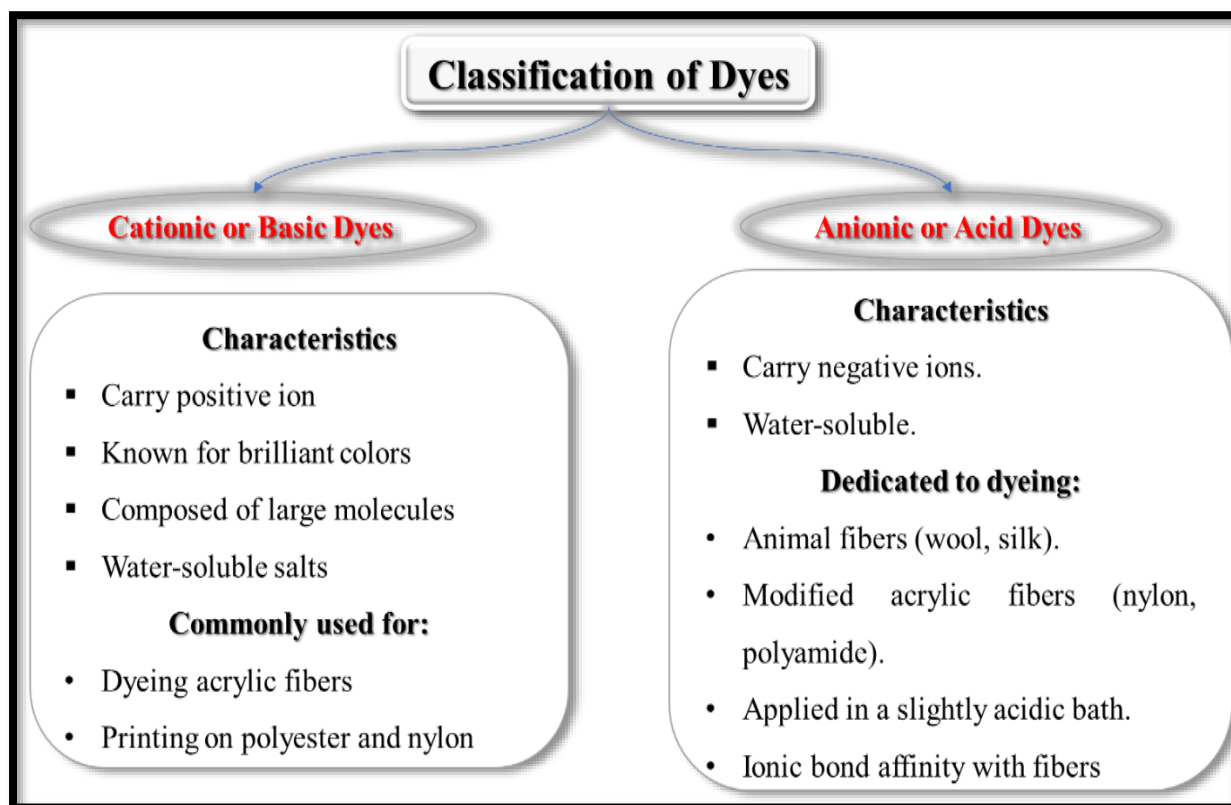
Figure I. 5: Characteristics of cationic and anionic color.

I.5.　　Example of dyes:

Molaire mass: 696,665 g/mol	Molaire mass: 327,33 g/mol	Molaire mass: 465,598 g/mol
Formula: $C_{32}H_{22}N_6Na_2O_6S_2$	Formula: $C_{14}H_{14}N_3Na\,O_3S$	Formula: $C_{31}H_{31}NO_3$
Congo Red	Methyl orange	Vat Green 3
Molaire mass: 319,85 g/mol	Molaire mass: 566,5 g/mol	Molaire mass: 424,4 g/mol
Formula: $C_{16}H_{18}N_3ClS$	Formula: $C_{20}H_{16}N_4Na_2O_9S_2$	Formula: $C_{18}H_8N_4O_5S_2$
Methylene Blue	Acid Violet 7	Sulfur Black 1

Figure I. 6: *Basic characteristics of some dyes mentioned in litterature.*

I.6.　　Investigating Treatment Methods for Effective Dye Removal

A wide array of methods is available for the treatment of dye-bearing effluents. Although various techniques exist for the removal of dye contaminants from wastewater including coagulation, chemical oxidation, membrane separation processes, electrochemical treatment, and both aerobic and anaerobic microbial degradation each method possesses specific limitations. These technologies can be classified into three principal categories: physical, chemical, and biological methods. Each of these approaches has its own set of advantages and disadvantages. **Figure I.7** provides a comparative analysis of the benefits and limitations associated with different dye removal methods [12].
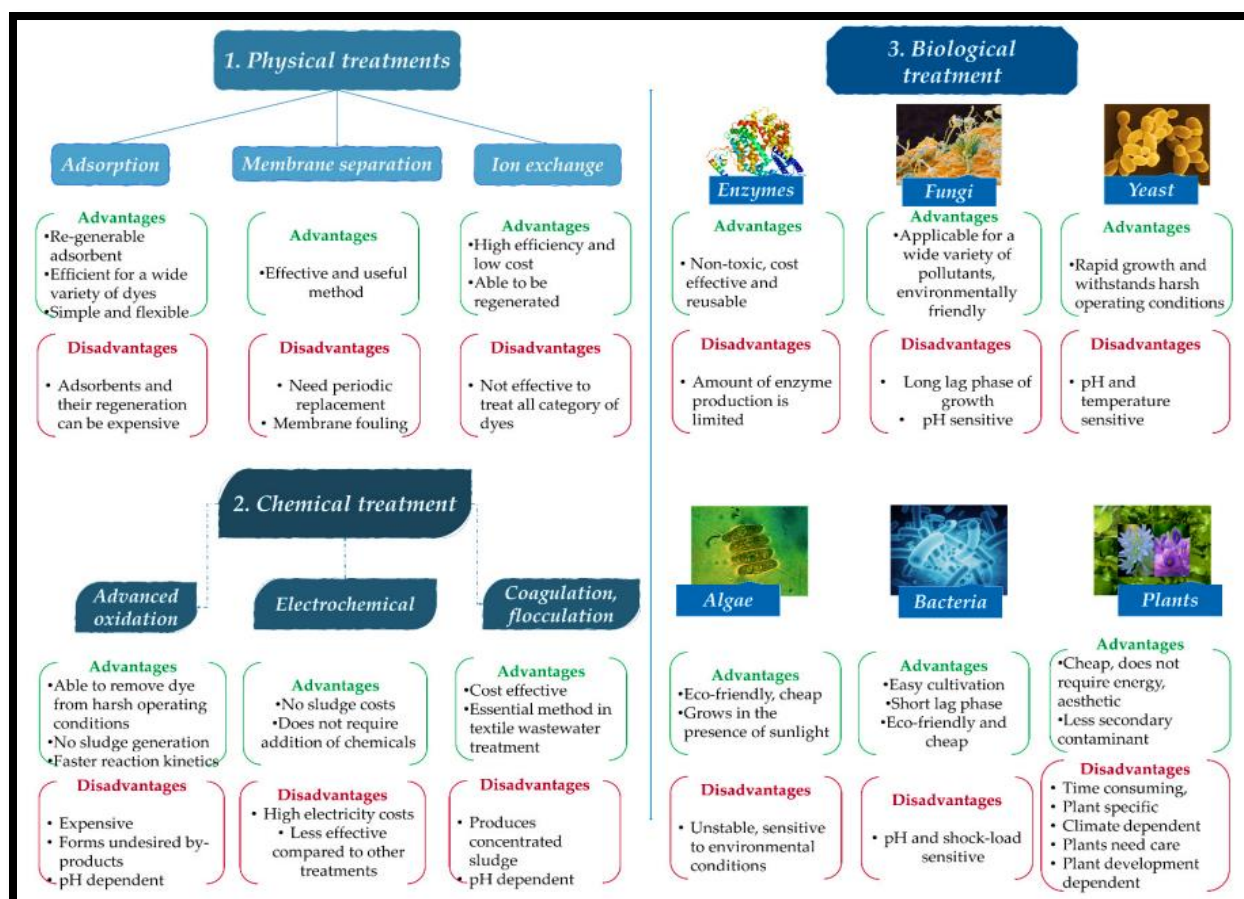
Figure I. 7: *Techniques for removing dye and their benefits and drawbacks.*

Part three:

Adsorption process

I.7.   Introduction:

Adsorption involves the interaction of synthetic compounds with solid phases. The primary distinction between adsorption and absorption is their dimensional engagement. In adsorption, molecules attach to the surface of a material, forming a two-dimensional layer. In contrast, in absorption, the molecules are taken up into the material's interior, occupying a three-dimensional space [13]. Adsorption is typically categorized as either physisorption or chemisorption, depending on the strength of the interaction between the adsorbate and the adsorbent (see **Figure I.8**).
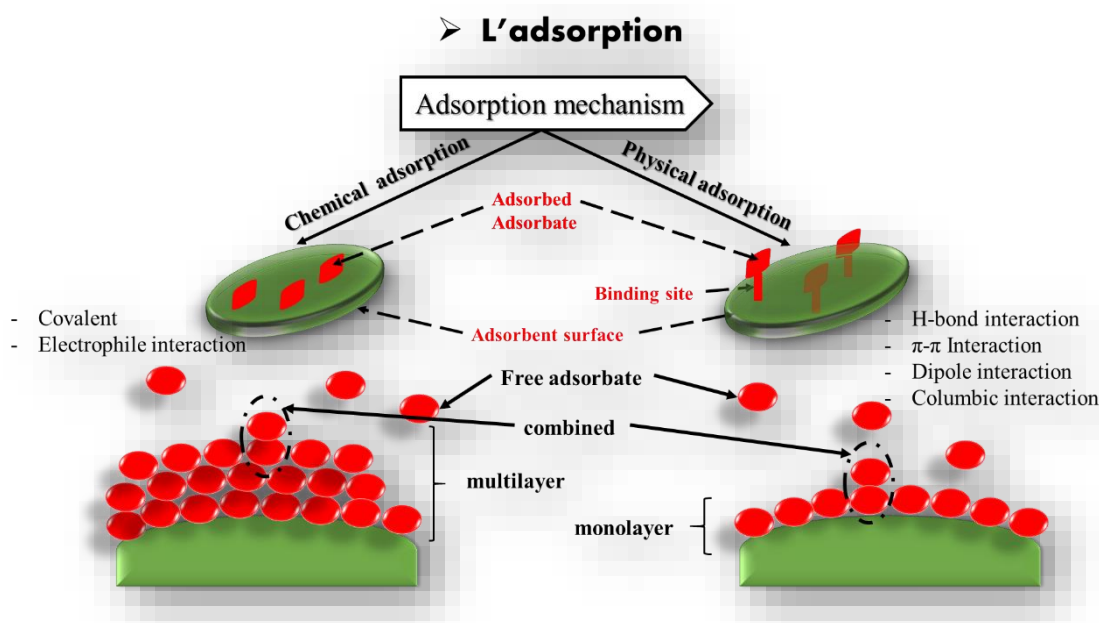
***Figure I. 8:** Physical, chemical adsorption characterization.*

Physical adsorption, or physisorption, is characterized by weak intermolecular forces, such as van der Waals interactions, making it a reversible process. It generally takes place at low temperatures and is exothermic [14]. In contrast, chemical adsorption, or chemisorption,

involves the formation of strong chemical bonds between the adsorbate and the adsorbent. This process occurs at higher temperatures, requires a significant activation energy, and is typically irreversible, releasing a considerable amount of heat due to the energy generated during the chemical bonding [15].

Because of the forces of attraction, the solute will be deposited on the surface of the adsorbent during the adsorption process [16]. It may eventually form a monolayer or multilayer (see **Figure I.8**), depending on the experiment's outcomes.

I.8.   Factors Affecting Adsorption Capacity

Adsorption refers to the process in which molecules of a liquid, known as the "adsorbate," are attracted to and held on the surface of a solid, called the "adsorbent," resulting in a higher concentration of molecules at the surface. The conventional adsorption mechanism occurs in three phases: f**irst**, the adsorbate diffuses onto the adsorbent's surface due to intermolecular forces between the two; **second**, the adsorbate migrates into the pores of the adsorbent; and **finally**, a monolayer form as adsorbate particles settle on the surface, filling the pore spaces. In this stage, molecules, ions, or atoms in the adsorbate bind to the active sites on the adsorbent [17]. When treating this water before releasing it into the natural world, the latter approach is one of the more popular ones. Three physicochemical factors control the transfer of pollutants in aqueous media: the competition between the various colors, the kinetics of adsorption, and the thermodynamic equilibrium between the two phases, which represents the process limit. As a result, a number of variables, including particle size, adsorbent mass, pH, solution temperature, and starting dye concentration, will affect these chemical processes [12], [18].
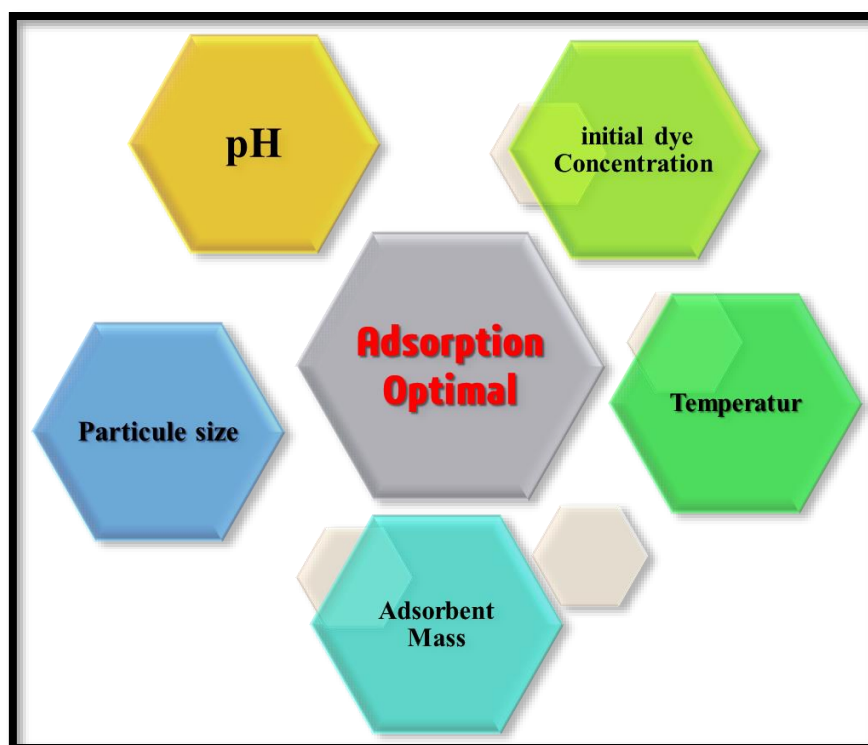
Figure I. 9: Variables Influencing the Adsorption Process.

❖ **Initial dye concentration:** The quantity of chemical adsorbed per unit mass of adsorbent is known as the ability to adsorb, and it increases with increasing dye concentration in the solution for each cationic and anionic color [19].

❖ **Solution pH:** Anionic dyes exhibit higher adsorption efficiency under acidic conditions, while cationic dyes are more effectively adsorbed in alkaline solutions [20].

❖ **Solution temperature:** Adsorption is classified as exothermic if it is enhanced at lower temperatures, whereas higher temperatures indicate an endothermic process [21].

❖ **Adsorbent mass:** A decrease in adsorbent capacity is implied by an increase in adsorbent mass for cationic dyes. This result might be explained by the dye's cations' easy access to the adsorption sites as long as there is little adsorbent added to the dye solution [22]. When it comes to anionic dyes, the potential for adsorption decreases as the adsorbent mass increases. Such a pattern might be predicted from the number

constancy of the adsorbate molecules due to the increasing quantity of vacant active sites on the adsorbent surface with a higher adsorbent dosage [23].

❖ The adsorbent **size of the particle**, or **granulometry**, is a characteristic that is directly related to the specific adsorption surface area. Smaller particles outperform large ones because they have a larger specific adsorption surface [24].

I.9. Adsorbent

The adsorbent is a sponge-like, porous, and insoluble material that can capture and hold adsorbate particles on its surface [25]. Isn't exclusively composed of solid raw materials; it can also be made from other types of materials deemed suitable for the adsorption process. This means that various materials, such as polymers, gels, fibers, or even liquids, can serve as adsorbents, depending on their ability to interact with the adsorbent molecules. the process of adsorption employing several kinds of adsorbents. To be more precise, a variety of adsorbents are used extensively for the adsorption of dye from contaminated water, notably active carbon, metal oxide-based, carbon-based, bio-adsorbent, metal–organic framework (MOF), and polymer-based materials (see **Figure I.9**) [26], [27]. The benefits of using these adsorbents to treat resistant chemicals include ease of **manufacture**, **high effective surface area**, **multifunctionality**, **high surface volume ratio**, **high reactivity**, **numerous active sites**, **reusability**, **cheap cost**, and **high efficiency** [28].
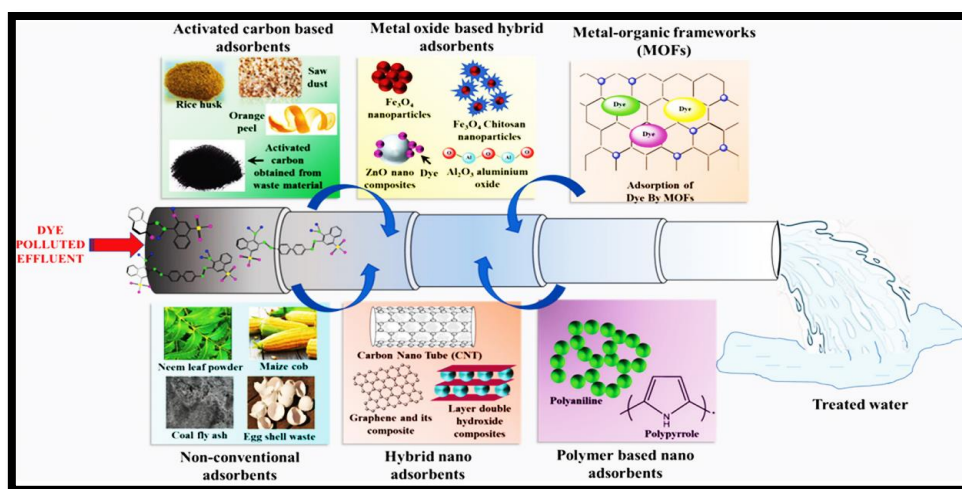
Figure I. 10: *Schematic shown of categories adsorbent.*

I.10.　　Affordable Adsorbents for Efficient Dye Elimination

Many considerations go into choosing the precursor for the creation of inexpensive adsorbents. The precursor should be readily available, in-expensive, and non-hazardous. Recently, there has been a lot of discussion on several natural solids that can inexpensively remove pollutants from contaminated water. When contrasting the sorbent materials, cost is a crucial factor to consider. A sorbent is often considered the lowest price if it is abundant in nature, requires little processing, or is waste material from another business that has lost its economic value or is a product of further processing. Numerous inexpensive adsorbents have been employed to remove dyes (see **Figure I.11**). [10]
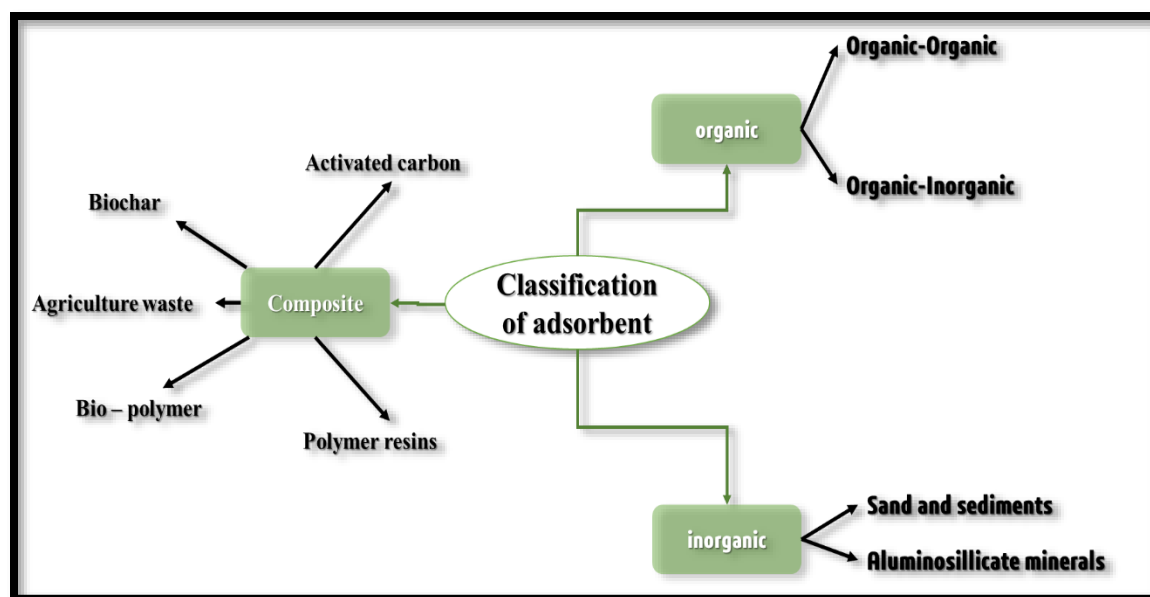
Figure I. 11: Adsorbent Categories for Dye Elimination.

I.10.1. Activated carbon

A lot of activated carbon is used to remove colors from water released. Coal, sawdust, and charcoal are sources of activated carbon; these materials undergo fractional oxidation as a pretreatment to create a porous surface that can function as an adsorbent. There are two kinds of activated carbons: hydrophilic, which is water-loving, and hydrophobic, which is water-repelling. Granular activated carbon, powdered activated carbon, and activated carbon tablets are the three kinds of activated carbon that are most efficient in preventing effluent removal [29].

I.10.2. Metal-organic framework (MOF)

Because of their highly adjustable pore widths and remarkably large surface areas—which sometimes exceed 6000 m^2/g—metal-organic frameworks, or MOFs—are recognized for their porous and crystalline structure. As such, they have been extensively used in the separation of diverse compounds. Because of their large surface area, homogeneous pore distribution, and multidimensional structure, MOFs are excellent choices for adsorption in chemical separation and catalysis applications. Furthermore, MOFs show a robust ability to self-assemble, which

improves their capacity to adsorb bigger molecules like dye molecules. Several studies in the scientific field demonstrate how well MOFs remove colors, such as methyl orange, xylenol orange, methylene blue, malachite green, and Rhodamine B.

I.10.3. Nanomaterials and composites

Because they have superior pore volume and surface capabilities, a variety of nanomaterials and composites, such as metal nanoparticles, carbon nanomaterials (composites and nanotubes), biologically produced nanomaterials, and bio-chitosan, are frequently employed in dye removal. Although carbon nanotubes (CNTs) and nanomaterials in general exhibit high dye removal efficiency, their handling is a challenge. This has led to the utilization of these materials in composite forms, such as cyclodextrin, graphene oxides (GOs), and magnetic nanoparticles. Magnetic nanocomposites have been successfully used to remove dyes in many experiments published in the literature. These investigations include the removal of methylene blue utilizing cyclodextrin- and Fe_3O_4-loaded nanoparticles that contain carbon nanotubes [30].

I.10.4. Adsorbents Derived from Agricultural Waste

Adsorbents derived from agricultural waste are becoming popular alternatives to conventional methods for water treatment due to their cost-effectiveness, high efficiency, and eco-friendly nature. They generate less chemical or biological sludge, require no additional nutrients, allow for biosorbent regeneration, and facilitate potential metal recovery. Functional groups such as carboxyl, amine, and hydroxyl provide adsorption binding sites. The main components of agricultural waste biomass include hemicellulose, proteins, simple sugars, lignin, lipids, starch, aqueous hydrocarbons, and extractives, all of which contain functional groups that can form complexes with metals. Researchers have also explored functionalizing these adsorbents to enhance their adsorption capacity. Given the high cost of coal-based activated carbon, efforts have been made to produce activated carbon from various agricultural sources [31]. The selection of agricultural waste-based adsorbents is driven by factors like local

availability, ease of desorption, high regeneration capacity, strong binding and selectivity for heavy metals, cost-effectiveness, and minimal release of unwanted substances into water. **Table I.3** represents the same literature on biomass for the elimination of dye.

Table I. 3: *Adsorption capacities Q_m (mg/g) of waste materials from raw agricultural by-products.*

Biomass	dyes	Adsorption capacity (mg/g)
Green peas peels [32]	Methylene blue	207.52
Pine sawdust [33]	Acid Blue 256	280.3
Tree fern 13 [34]	Basic Red	408
Grapefruit peel [35]	Crystal violet	254.16
Lemon peel [36]	Malachite green	112
Coconut shell [37]	Malachite Green	214.63
Pine fruit shell-carbon [38]	Methylene blue	529.00

I.11.   Activated or optimization of adsorbents

Factors like (a) big surface area, (b) high penetrability with small-sized pores, (c) thermal and chemical stability, and (d) superior mechanical strength are what define an adsorbent's performance and efficacy. Each of these elements contributes favorably to the effectiveness of adsorbents. A few surface-modifying methods that alter the chemical, biological, and physical properties of substances are also in use to increase the adsorption capacity of substances that absorb.

➢ **Acid treatment**: also known as wet oxidation modification, is the process of enhancing a material's adsorbent behavior by adding mineral acids and oxidizing agents, such as HCl, H_3PO_4, and HNO_3. Because less mineral matter is present, this treatment improves the hydrophilic quality and acidic surface of adsorbents. By enhancing polar O-containing functional moieties like carbonyl, carboxyl, and lactone, it enhances the

porosity of the surface. Furthermore, the buildup of H^+ on the surface of the adsorbent facilitates the absorption of negatively charged wastewater. When H_2SO_4 is used to modify brown algae, trapped gases are released, increasing the adsorbent's porosity and improving its adsorption capacity. This results in the creation of cylindrical porous structures on the adsorbent surface. [39], [40]

➤ **Alkali treatment**. The adsorbent surface becomes more non-polar when reducing agents like KOH and adding NaOH oxides. The alkali-treated fuller's earth surface is more absorbed by the toluidine blue dye due to the dispersion of negatively charged particles on the adsorbent's area. Because fewer functional moieties containing O are present, activated carbon treated with alkali (NaOH) has improved surface area and pore volume [41], [42].

➤ **The process of becoming pregnant**. Or **Impregnation** is the uniform dispersion of chemical materials onto the porous adsorbent material, such as metals, carbonates, and chlorides.The stability, adsorption capacity, and regeneration of adsorbents are enhanced by impregnation [43].

➤ **Solvents that are organic**. Alcohols and other organic solvents can be used to improve adsorption and introduce additional functional moieties. However, organic solvents have few uses in the adsorption process due to their expensive nature and unstable character. additional than the components listed above, a variety of additional chemicals are also utilized in the modification of adsorbents, such as oxidants and neutral solutions [44]. The KMnO4-modified wood biochar produced a porous surface covered with MnOx that was more oxygen-containing and shown improved absorption of Pb (II) and Cd (II) [45].

I.12. Desorption Dynamics Study

Desorption, the reverse process of adsorption, involves the removal of previously adsorbed molecules from the adsorbent surface through the application of various desorbing agents (**Figure I.12**). The percentage of dye desorbed (%) is determined using Eq. I.1.

$$\boldsymbol{Desorption\ rate}\ (\%) = \frac{C_d}{C_a} * 100 \dots\dots\dots\dots\dots\dots\dots\dots\dots\dots\dots\dots\dots\dots\ (I.1)$$

where C_a (mg/L) is the concentration of adsorbed and C_d (mg/L) is the concentration of desorbed dye.

A desorption study plays a crucial role in reducing waste, recovering adsorbed substances, and lowering operational costs. Adsorbent regeneration is achieved by washing and mixing it with an appropriate desorbing solution. The desorbing agent must be cost-efficient, effective, and environmentally benign, and should preserve the structural integrity of the adsorbent. Common desorption techniques include thermal treatment and chemical methods such as acid treatments with H_2SO_4 [46], HNO_3, HCl, EDTA, and H_3PO_4 [47], or base treatment with KOH [48]and NaOH. Furthermore, organic solvents like methanol and ethanol can be employed to restore adsorbents, as organic pollutants readily dissolve in these solvents.
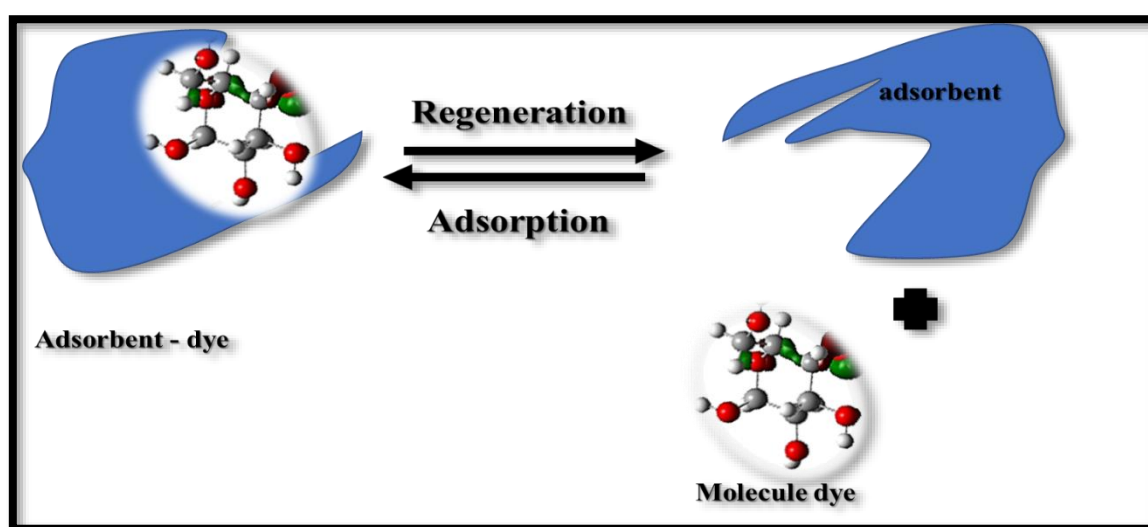
Figure I. 12: Dye Adsorption and Desorption Processes on Loaded Adsorbent.

Chapter I reference

[1]   Aruna, N. Bagotia, A. K. Sharma, et S. Kumar, « A review on modified sugarcane bagasse biosorbent for removal of dyes », *Chemosphere*, vol. 268, p. 129309, avr. 2021, doi: 10.1016/j.chemosphere.2020.129309.

[2]   C. Fn et M. Mf, « Factors Affecting Water Pollution: A Review », *J. Ecosyst. Ecography*, vol. 07, nᵒ 01, 2017, doi: 10.4172/2157-7625.1000225.

[3]   J. K. Summers, *Water Quality: Science, Assessments and Policy*. BoD – Books on Demand, 2020.

[4]   V. Katheresan, J. Kansedo, et S. Y. Lau, « Efficiency of various recent wastewater dye removal methods: A review », *J. Environ. Chem. Eng.*, vol. 6, nᵒ 4, p. 4676-4697, août 2018, doi: 10.1016/j.jece.2018.06.060.

[5]   M. A. M. Salleh, D. K. Mahmoud, W. A. W. A. Karim, et A. Idris, « Cationic and anionic dye adsorption by agricultural solid wastes: A comprehensive review », *Desalination*, vol. 280, nᵒ 1-3, p. 1-13, oct. 2011, doi: 10.1016/j.desal.2011.07.019.

[6]   M. Shabir *et al.*, « A review on recent advances in the treatment of dye-polluted wastewater », *J. Ind. Eng. Chem.*, vol. 112, p. 1-19, août 2022, doi: 10.1016/j.jiec.2022.05.013.

[7]   Ö. E. İşmal et L. Yıldırım, « 3 - Metal mordants and biomordants », in *The Impact and Prospects of Green Chemistry for Textile Technology*, Shahid-ul-Islam et B. S. Butola, Éd., in The Textile Institute Book Series. , Woodhead Publishing, 2019, p. 57-82. doi: 10.1016/B978-0-08-102491-1.00003-4.

[8]   M. Berradi *et al.*, « Textile finishing dyes and their impact on aquatic environs », *Heliyon*, vol. 5, nᵒ 11, p. e02711, nov. 2019, doi: 10.1016/j.heliyon.2019.e02711.

[9]   M. Benjelloun, Y. Miyah, G. Akdemir Evrendilek, F. Zerrouq, et S. Lairini, « Recent Advances in Adsorption Kinetic Models: Their Application to Dye Types », *Arab. J. Chem.*, vol. 14, nᵒ 4, p. 103031, avr. 2021, doi: 10.1016/j.arabjc.2021.103031.

[10]   M. T. Yagub, T. K. Sen, S. Afroze, et H. M. Ang, « Dye and its removal from aqueous solution by adsorption: A review », *Adv. Colloid Interface Sci.*, vol. 209, p. 172-184, juill. 2014, doi: 10.1016/j.cis.2014.04.002.

[11]   Y. Zhou, J. Lu, Y. Zhou, et Y. Liu, « Recent advances for dyes removal using novel adsorbents: a review », *Environ. Pollut.*, vol. 252, p. 352-365, 2019.

[12]   E. Rápó et S. Tonk, « Factors Affecting Synthetic Dye Adsorption; Desorption Studies: A Review of Results from the Last Five Years (2017–2021) », *Molecules*, vol. 26, nᵒ 17, Art. nᵒ 17, janv. 2021, doi: 10.3390/molecules26175419.

[13]   A. H. Jawad, A. S. Waheeb, R. A. Rashid, W. I. Nawawi, et E. Yousif, « Equilibrium isotherms, kinetics, and thermodynamics studies of methylene blue adsorption on pomegranate (*Punica granatum*) peels as a natural low-cost biosorbent », *Desalination Water Treat.*, vol. 105, p. 322-331, févr. 2018, doi: 10.5004/dwt.2018.22021.

[14]   F. E. Titchou, H. Zazou, H. Afanga, J. El Gaayda, R. A. Akbour, et M. Hamdani, « Removal of Persistent Organic Pollutants (POPs) from water and wastewater by adsorption and electrocoagulation process », *Groundw. Sustain. Dev.*, vol. 13, p. 100575, mai 2021, doi: 10.1016/j.gsd.2021.100575.

[15] F. E. Titchou, H. Zazou, H. Afanga, J. El Gaayda, R. A. Akbour, et M. Hamdani, « Removal of Persistent Organic Pollutants (POPs) from water and wastewater by adsorption and electrocoagulation process », *Groundw. Sustain. Dev.*, vol. 13, p. 100575, mai 2021, doi: 10.1016/j.gsd.2021.100575.

[16] A. B. D. Nandiyanto, « Isotherm Adsorption of Carbon Microparticles Prepared from Pumpkin (Cucurbita maxima) Seeds Using Two-Parameter Monolayer Adsorption Models and Equations », *Moroc. J. Chem.*, vol. 8, nᵒ 3, Art. nᵒ 3, juill. 2020, doi: 10.48317/IMIST.PRSM/morjchem-v8i3.21636.

[17] D. R. Kammerer, J. Kammerer, et R. Carle, « Chapter 19 - Adsorption and Ion Exchange for the Recovery and Fractionation of Polyphenols: Principles and Applications », in *Polyphenols in Plants (Second Edition)*, R. R. Watson, Éd., Academic Press, 2019, p. 327-339. doi: 10.1016/B978-0-12-813768-0.00018-9.

[18] M. T. Yagub, T. K. Sen, S. Afroze, et H. M. Ang, « Dye and its removal from aqueous solution by adsorption: A review », *Adv. Colloid Interface Sci.*, vol. 209, p. 172-184, juill. 2014, doi: 10.1016/j.cis.2014.04.002.

[19] M. Sulyman, J. Namiesnik, et A. Gierak, « Low-cost Adsorbents Derived from Agricultural By-products/Wastes for Enhancing Contaminant Uptakes from Wastewater: A Review », doi: 10.15244/pjoes/66769.

[20] X. Zhao, X. Wang, et T. Lou, « Preparation of fibrous chitosan/sodium alginate composite foams for the adsorption of cationic and anionic dyes », *J. Hazard. Mater.*, vol. 403, p. 124054, févr. 2021, doi: 10.1016/j.jhazmat.2020.124054.

[21] S. Wong *et al.*, « Effective removal of anionic textile dyes using adsorbent synthesized from coffee waste », *Sci. Rep.*, vol. 10, nᵒ 1, p. 2928, 2020.

[22] A. N. Alene, G. Y. Abate, et A. T. Habte, « Bioadsorption of basic blue dye from aqueous solution onto raw and modified waste ash as economical alternative bioadsorbent », *J. Chem.*, vol. 2020, nᵒ 1, p. 8746035, 2020.

[23] Syieluing Wong et Nawal Abd Ghafar, « Effective removal of anionic textile dyes using adsorbent synthesized from coffee waste | Scientific Reports ». Consulté le: 3 mai 2025. [En ligne]. Disponible sur: https://www.nature.com/articles/s41598-020-60021-6

[24] J. N. Wekoye, W. C. Wanyonyi, P. T. Wangila, et M. K. Tonui, « Kinetic and equilibrium studies of Congo red dye adsorption on cabbage waste powder », *Environ. Chem. Ecotoxicol.*, vol. 2, p. 24-31, janv. 2020, doi: 10.1016/j.enceco.2020.01.004.

[25] N. A. Khan, B. N. Bhadra, et S. H. Jhung, « Heteropoly acid-loaded ionic liquid@metal-organic frameworks: Effective and reusable adsorbents for the desulfurization of a liquid model fuel », *Chem. Eng. J.*, vol. 334, p. 2215-2221, févr. 2018, doi: 10.1016/j.cej.2017.11.159.

[26] S. Dutta, B. Gupta, S. K. Srivastava, et A. K. Gupta, « Recent advances on the removal of dyes from wastewater using various adsorbents: A critical review », *Mater. Adv.*, vol. 2, nᵒ 14, p. 4497-4531, 2021.

[27] S. Senapati, S. K. Srivastava, S. B. Singh, et A. R. Kulkarni, « SERS active Ag encapsulated Fe@SiO2 nanorods in electromagnetic wave absorption and crystal violet detection », *Environ. Res.*, vol. 135, p. 95-104, nov. 2014, doi: 10.1016/j.envres.2014.08.026.

[28] S. Dutta, B. Gupta, S. K. Srivastava, et A. K. Gupta, « Recent advances on the removal of dyes from wastewater using various adsorbents: A critical review », *Mater. Adv.*, vol. 2, nᵒ 14, p. 4497-4531, 2021.

[29] T. Maneerung, J. Liew, Y. Dai, S. Kawi, C. Chong, et C.-H. Wang, « Activated carbon derived from carbon residue from biomass gasification and its application for dye adsorption: Kinetics, isotherms and thermodynamic studies », *Bioresour. Technol.*, vol. 200, p. 350-359, janv. 2016, doi: 10.1016/j.biortech.2015.10.047.

[30] N. T. Abdel-Ghani, G. A. El-Chaghaby, E.-S. A. Rawash, et E. C. Lima, « Magnetic activated carbon nanocomposite from Nigella sativa L. waste (MNSA) for the removal of Coomassie brilliant blue dye from aqueous solution: Statistical design of experiments for optimization of the adsorption conditions », *J. Adv. Res.*, vol. 17, p. 55-63, mai 2019, doi: 10.1016/j.jare.2018.12.004.

[31] I. Anastopoulos et G. Z. Kyzas, « Agricultural peels for dye adsorption: A review of recent literature », *J. Mol. Liq.*, vol. 200, p. 381-389, déc. 2014, doi: 10.1016/j.molliq.2014.11.006.

[32] O. R. Benkouachi *et al.*, « Advanced green peel utilization for efficient methylene blue removal: Integrated analysis and predictive modeling », *J. Mol. Liq.*, p. 125951, 2024.

[33] M. Özacar et İ. A. Şengil, « Adsorption of metal complex dyes from aqueous solutions by pine sawdust », *Bioresour. Technol.*, vol. 96, nᵒ 7, p. 791-795, mai 2005, doi: 10.1016/j.biortech.2004.07.011.

[34] Y.-S. Ho, T.-H. Chiang, et Y.-M. Hsueh, « Removal of basic dye from aqueous solution using tree fern as a biosorbent », *Process Biochem.*, vol. 40, nᵒ 1, p. 119-124, janv. 2005, doi: 10.1016/j.procbio.2003.11.035.

[35] A. Saeed, M. Sharif, et M. Iqbal, « Application potential of grapefruit peel as dye sorbent: Kinetics, equilibrium and mechanism of crystal violet adsorption », *J. Hazard. Mater.*, vol. 179, nᵒ 1, p. 564-572, juill. 2010, doi: 10.1016/j.jhazmat.2010.03.041.

[36] K. V. Kumar, « Optimum sorption isotherm by linear and non-linear methods for malachite green onto lemon peel », *Dyes Pigments*, vol. 74, nᵒ 3, p. 595-597, janv. 2007, doi: 10.1016/j.dyepig.2006.03.026.

[37] Olugbenga Solomon Bello, « Coconut (Cocos nucifera) Shell Based Activated Carbon for the Removal of Malachite Green Dye from Aqueous Solutions: Separation Science and Technology: Vol 47, No 6 ». Consulté le: 3 mai 2025. [En ligne]. Disponible sur: https://www.tandfonline.com/doi/abs/10.1080/01496395.2011.630335

[38] B. Royer *et al.*, « Applications of Brazilian pine-fruit shell in natural and carbonized forms as adsorbents to removal of methylene blue from aqueous solutions—Kinetic and equilibrium study », *J. Hazard. Mater.*, vol. 164, nᵒ 2-3, p. 1213-1222, 2009.

[39] B. Huang, G. Liu, P. Wang, X. Zhao, et H. Xu, « Effect of nitric acid modification on characteristics and adsorption properties of lignite », *Processes*, vol. 7, nᵒ 3, p. 167, 2019.

[40] P. M. Godwin, Y. Pan, H. Xiao, et M. T. Afzal, « Progress in preparation and application of modified biochar for improving heavy metal ion removal from wastewater », *J. Bioresour. Bioprod.*, vol. 4, nᵒ 1, p. 31-42, 2019.

[41] C. Zheng, L. Zhao, X. Zhou, Z. Fu, et A. Li, « Treatment technologies for organic wastewater », *Water Treat.*, vol. 11, p. 250-286, 2013.

[42] G. Hisarli, « The effects of acid and alkali modification on the adsorption performance of fuller's earth for basic dye », *J. Colloid Interface Sci.*, vol. 281, nᵒ 1, p. 18-26, 2005.

[43] A. Rehman, M. Park, et S.-J. Park, « Current progress on the surface chemical modification of carbonaceous materials », *Coatings*, vol. 9, nᵒ 2, p. 103, 2019.

[44] S. Sonal, P. Prakash, B. K. Mishra, et G. C. Nayak, « Synthesis, characterization and sorption studies of a zirconium (iv) impregnated highly functionalized mesoporous activated carbons », *RSC Adv.*, vol. 10, nᵒ 23, p. 13783-13798, 2020.

[45] H. Wang, B. Gao, S. Wang, J. Fang, Y. Xue, et K. Yang, « Removal of Pb (II), Cu (II), and Cd (II) from aqueous solutions by biochar derived from KMnO4 treated hickory wood », *Bioresour. Technol.*, vol. 197, p. 356-362, 2015.

[46] A. Guediri, A. Bouguettoucha, D. Chebli, N. Chafai, et A. Amrane, « Molecular dynamic simulation and DFT computational studies on the adsorption performances of methylene blue in aqueous solutions by orange peel-modified phosphoric acid », *J. Mol. Struct.*, vol. 1202, p. 127290, févr. 2020, doi: 10.1016/j.molstruc.2019.127290.

[47] A. Guediri, A. Bouguettoucha, D. Chebli, et A. Amrane, « The use of encapsulation as a proposed solution to avoid problems encountered with conventional materials in powder form: Application in methylene blue removal from aqueous solutions », *J. Mol. Liq.*, vol. 316, p. 113841, oct. 2020, doi: 10.1016/j.molliq.2020.113841.

[48] W. Chen *et al.*, « Insight into KOH activation mechanism during biomass pyrolysis: Chemical reactions between O-containing groups and KOH », *Appl. Energy*, vol. 278, p. 115730, nov. 2020, doi: 10.1016/j.apenergy.2020.115730.

CHAPTER II

Chapter II:

Experimental Protocols and Analytical Techniques

II.1   Introduction

This chapter outlines the procedures for synthesizing adsorbent materials and the characterization techniques employed in this thesis. Additionally, all of the procedures needed to carry out the adsorption tests with different parameters are included in this chapter. The quantum chemical computations used in this work will consist of density functional theory and molecular dynamics simulations. Furthermore, this chapter will discuss statistical physical modeling based on the grand canonical ensemble, including Artificial Intelligence.

II.2   Product and materials used

II.2.1 Investigated Substrates

The product property used is summarized in the following **Table II.1**:

Table II. 1: *Some characteristics of Methylene blue (MB) dye.*

Methylene Blue dye (MB)	
Category	Basic cationic dye
Brute formula	$C_{16}H_{18}N_3SCl$
Chemical name	Tetramethylthionine hydrochloride
Vapor pressure	Weak
Molar mass (g /mol)	319.90
Diameter (A°)	15
Maximum wavelength (nm)	654
pKa	3.8
Solubility at 20 °C (g/L)	High 50 g.l^{-1} in water 10 g.l^{-1} in ethanol
Structure	

II.2.2 Reagents used

In addition to the molecules mentioned in **Table II.1**, we used Hydrochloric acid HCl (98%), sodium hydroxide NaOH, and KOH.

II.2.3 Comprehensive Characterization of the Adsorbent

In this thesis, three biomass materials—GP (Green Pea Peels), MWA (Mixed Waste Agriculture), and CR (Cupule of Oak)—were prepared following a multi-stage process involving drying, grinding, sieving, and washing. Approximately 1 kg of each precursor was collected and dried to a constant mass at 60°C using an oven. This drying step served to remove both moisture and impurities. The materials were then ground to achieve a uniform consistency.

The biosorbents GP and CR were used in the case raw. An additional treatment step was included for the second biosorbent, MWA. The powder was washed with tap and distilled water to enhance its surface area. Following this, the material was dried again at 60°C. The figure below shows the protocol for preparing these biosorbents.
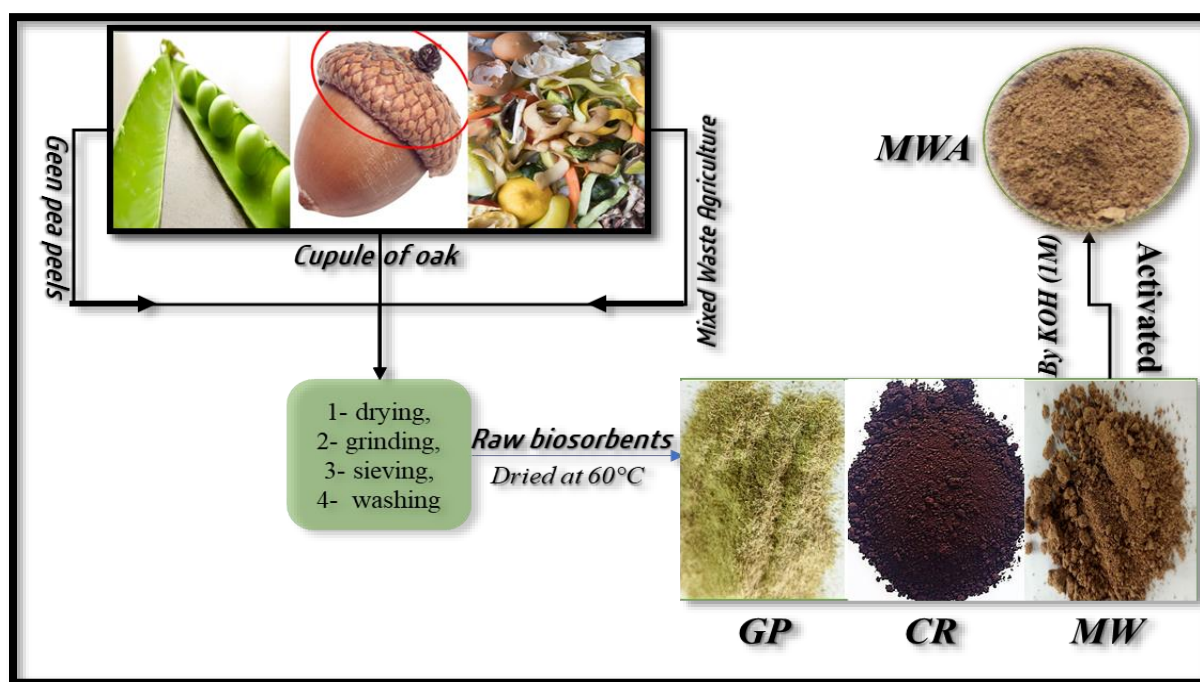
Figure II. 1: Schematic Representation of Biosorbent Preparation Process.

II.3 Materials characterization

Each adsorbent was subjected to a surface chemical analysis using a Fourier transform spectrophotometer (FTIR) (SHIMADZU brand, specifically an IRAffinity-1S model), whose infrared spectra varied from 4000 cm to 500 cm^{-1}. In conjunction with potassium bromide (KBr) discs.

The utilization of the scanning electron microscope (SEM) emerges as an invaluable tool for the meticulous examination and analysis of microstructural morphology. In the context of this investigation, the technique was applied to scrutinize the surface characteristics and morphological attributes exhibited by GP, MWA, and CR.

Additionally, SDT Q600 V20.9 Build 20 thermal gravimetric was used to perform thermogravimetric analysis (TGA) on the produced materials at a heating flow rate of 10 °C/minute and temperatures ranging from 35 to 1000 °C.

X-ray diffraction (XRD) diagrams were created with an incremental step of 0.02 degrees and an acquisition period of 6.985 seconds per step, covering a 2θ angle range of 4 to 90 degrees.

The concept of zero-point charge is fundamental to physics because it clarifies the conditions under which a particle's neutral electrical charge state arises. In order to find the point of zero charge (pHpzc), an experimental approach was adopted. This involved adding 50 mL of sodium chloride (NaCl) solution to sealed vials. The pH values of these solutions were systematically adjusted between [2, 4, 6, and 12] using a 0.1 M sodium hydroxide (NaOH) or hydrochloric acid (HCl) solution. Each vial received an additional 50 mg of MWA material. After allowing the suspensions to agitate for approximately a day at room temperature, the final pH values were determined.

II.4 Kinetic studies

The kinetic studies of adsorption with relation to rate constants evaluate the refining of the adsorption process. The speed of adsorption contributes to a more effective selection of materials used as adsorbents based on adsorption capacity.

The kinetics of MB adsorption were investigated at their normal state using a range of starting dye concentrations (50–250 mg L^{-1}) and a continuous 250 rpm mixing rate until equilibrium was attained. **Equation (II.1)** was utilized to ascertain the adsorbed quantities of MB [1].

$$Q_e = \frac{(C_0 - C_t)\, V}{m} \dots\dots\dots\dots\dots\dots\dots\dots\dots\dots\dots\dots\dots\dots\dots\dots (II.1)$$

Where C_0 (mg.L^{-1}) is the first concentration of colorant, C_t (mg.L^{-1}) is the remaining concentration of dye at the time t, V (mL) is the volume of the solution, and m(g) is the mass of the adsorbent.

For the study of rate kinetics, the pseudo-first-order and pseudo-second-order models are typically employed. In this paper search use several kinetic models, represented in the following **Table II.2.**

Table II. 2: Mathematical Equations and Key Parameters of These Kinetic Models. [2], [3], [4]

Equation number	Equation name	Equation formed	Parameters
(II.2)	pseudo-first-order (PFO)	$Q_t = Q_e\,(1 - e^{k_1\,t})$	Q_e (mg g^{-1}) and Q_t (mg g^{-1}) refer to the amount of dye adsorbed at equilibrium and at time t (min). respectively. k_1(L min^{-1}) is the equilibrium rate constant of the pseudo-first-order equation
(II.3)	pseudo-first-order (PSO)	$Q_t = (\dfrac{K_2\,Q_e^2\,t}{K_2\,Q_e\,t + 1})$	k_2 (L min^{-1}) is the equilibrium rate constant of the pseudo-second-order equation
(II.4)	pseudo-nth-order (PNO)	$Q_t = Q_e - \big[(n-1)K_n\,t + Q_e^{(n-1)}\big]^{1/(1-n)}$	k_n is a constant and n is the biosorption reaction order.
(II.5)	Elovich	$Q_t = \dfrac{1}{\beta}\ln(\alpha\beta) + \dfrac{1}{\beta}\ln t$	α is the constant of the initial sorption rate (mg/(g·min)). β is the constant of desorption (g/mg).
(II.6)	the intraparticle diffusion	$Qt = K_{id}\,t^{0.5} + C$	k_{id} (mg.g^{-1} $min^{-0.5}$) is the rate constant of intraparticle diffusion. **C** is the intercept.

II.5   Isotherms study

This research report employed a few isothermal tests, which are listed in **Table II.3**, to investigate the adsorption ability and behavior of adsorbates towards adsorbents. These models aid in identifying the monolayer or multilayer kind of surface phase.

Furthermore, we assessed the interactions between Methylene Blue (MB) and the GP composite. The adsorption isotherm experiments were conducted by exposing Methylene Blue (MB) solutions at varying concentrations (ranging from 50 to 800 mg/L for powder and from 15 to 1000 mg/L for biomass) to specific masses of adsorbent, maintaining a mass-to-volume ratio of 1. These mixtures were continuously stirred at a rate of 250 rpm for 24 hours (48 hours for beads) under precisely controlled temperatures of 10, 20, 30, and 40 °C. Upon reaching equilibrium, the solutions were separated and analyzed, and the quantities adsorbed were calculated using Eq.2.

Table II. 3: shows the equations and parameters of such models. [5], [6]

Equation number	Equation name	Equation formed	Parameters
(II.7)	Langmuir	$\dfrac{Q_e}{Q_m} = \dfrac{K_L C_e}{1 + K_L C_e}$	Q_e (mg g^{-1}) is the amount of MB adsorbed per unit mass of adsorbent. Q_m (mg.g^{-1}) is the monolayer capacity of the adsorbent. C_e (mg.L^{-1}) is the equilibrium dye concentration in the solution. K_L the Langmuir constant.
(II.8)	Freundlich	$Q_e = K_F C_e^{1/n}$	K_F and n^{-1} are empirical constants indicative of sorption capacity and sorption intensity, respectively.
(II.9)	Sips	$\dfrac{Q_e}{Q_m} = \dfrac{(K_S C_e)^m}{1 + (K_S C_e)^m}$	K_S is (L mg^{-1}) the Sips constant m the exponent of the Sips model

II.6   Modeling Based on Statistical Physics

Physical modeling was explored utilizing statistical physics models based on employing the grand canonical partition function in statistical physics to give more in-depth and reliable

explanations for the MB adsorption mechanism on adsorbents [7]. The next part provides specifics about the three models that were used.

II.6.1 Monolayer model with single energy: ME_1

This model assumes that the adsorption occurred in a monolayer with only one energy [8]. The demonstration of the applied physical models needs to go through the use of the grand canonical partition function in statistical physics; for this purpose, the grand canonical partition function of one site is given as follows (Eq. 11) [5] :

$$Z_{gc} = 1 + e^{\beta_s(\varepsilon_1 + \mu)} \ldots\ldots\ldots\ldots.\ldots\ldots\ldots.\ldots\ldots\ldots.\ldots\ldots\ldots.\ldots\ldots\ldots.\ldots\ldots\ldots..(II.10)$$

Where μ is the chemical potential of the adsorbed molecule, and β is the Boltzmann factor.

Furthermore, the adsorbed quantity at saturation is given by Eq. II.11 [9], [10]:

$$Q_{sat} = n_{im}N_{iS} \ldots\ldots\ldots\ldots.\ldots\ldots\ldots.\ldots\ldots\ldots.\ldots\ldots\ldots.\ldots\ldots\ldots.\ldots\ldots\ldots\ldots(II.11)$$

After accounting for all preceding equations, Eq. II.12 in **Table II.4** provides the monolayer model with single energy (ME1) [9], [10]:

It is noteworthy that on a single adsorption site, MMSE can yield a number of adsorbates equal to or more than unity. [11].

II.6.2 Monolayer model with two energies: MMTE

The Monolayer Two-Energy (MMTE) model suggests that adsorption takes place on a single molecular layer, where two types of receptor sites are involved, each associated with distinct energy values (ΔE1 and ΔE2). These receptor sites are capable of capturing a variable number of adsorbate molecules. The relationship between the adsorbed quantity and the equilibrium concentration is mathematically represented by **Equation II.13** in **Table II.4** [3]:

II.6.3 Monolayer model with triple energy: TE_1

This model is the last model utilized in this section. This model assumes that adsorption takes place in multilayers, with molecules in the first layer having larger adsorption energy than those

in the second, and so on. The following equation in **Table II.4** describes how the adsorbed

quantity changes in this scenario [12], [13].

Table II. 4: *The Advanced statistical physics models ME$_1$, ME$_2$ and ME$_3$.* *[7], [14]. [15]*

model	Equation	Parameters
Single-energy single-layer model eq (II.12)	$$Q = \frac{Q_0}{1 + \left(\frac{C_{1/2}}{C_e}\right)^n} = \frac{n.N_m}{1 + \left(\frac{C_{1/2}}{C_e}\right)^n}$$	Q (mg.g^{-1}): adsorbed quantity.
Double-energy single-layer model eq (II.13)	$$Q = n.N_m \cdot \frac{\left(\frac{C_e}{C_{1/2}}\right)^n + 2.\left(\frac{C_e}{C_{1/2}}\right)^{2n}}{1 + \left(\frac{C_e}{C_{1/2}1}\right)^n + \left(\frac{C_e}{C_{1/2}}\right)^{2n}}$$	n : number of ions per site. N_m (mg.g^{-1}) : sites receptor density. Q_0 (mg.g^{-1}); adsorbed quantity at saturation
Multilayer model eq (II.14)	$$Q = n.N_m \cdot \frac{F_1(C_e) + F_2(C_e) + F_3(C_e) + F_4(C_e)}{G(C_e)}$$ **with** $$F_1(C_e) = \frac{\left(-2.\left(\frac{C_e}{C_1}\right)^{2n}\right)}{\left(1 - \left(\frac{C_e}{C_1}\right)^n\right)} + \frac{\left(\frac{C_e}{C_1}\right)^n\left(1 - \left(\frac{C_e}{C_1}\right)^{2n}\right)}{\left(1 - \left(\frac{C_e}{C_1}\right)^n\right)^2}$$ $$F_2(C_e) = \frac{2.\left(\frac{C_e}{C_1}\right)^n\left(\frac{C_e}{C_2}\right)^n\left(1 - \left(\frac{C_e}{C_2}\right)^{(nN_2)}\right)}{\left(1 - \left(\frac{C_e}{C_2}\right)^n\right)}$$ $$F_3(C_e) = \frac{-\left(\frac{C_e}{C_1}\right)^n\left(\frac{C_e}{C_2}\right)^n\left(\frac{C_e}{C_2}\right)^{(nN_2)}N_2}{\left(1 - \left(\frac{C_e}{C_2}\right)^n\right)}$$ $$G(C) = \frac{\left(1 - \left(\frac{C_e}{C_1}\right)^{(2n)}\right)}{\left(1 - \left(\frac{C_e}{C_1}\right)^n\right)} + \frac{\left(\frac{C_e}{C_1}\right)^n\left(\frac{C_e}{C_2}\right)^n\left(1 - \left(\frac{C_e}{C_2}\right)^{(nN_2)}\right)}{\left(1 - \left(\frac{C_e}{C_2}\right)^n\right)}$$	$C_{1/2}$(mg .L^{-1}) : the concentration at half–saturation C_1 and C_2 (mg.L^{-1}) : concentrations at half saturation for the first and the second active sites respectively. n_1 and n_2 : number of ions per site for the first and the second sites receptor respectively.

II.7 Functionality of the MB adsorption method

II.7.1 Temperature Influence and Associated Thermodynamic Parameters

The temperature impact was measured between 10 and 40°C, and the tests were conducted in a manner akin to that of adsorption isotherms. Consequently, the viability of the MB adsorption method was examined while taking **Eqs. II.15** and II.**16** into account [16].

$$ln\left(\frac{Q_e}{C_e} * 1000\right) = \Delta S° - \frac{\Delta H°}{T} \dots\dots\dots\dots\dots\dots\dots\dots\dots\dots\dots\dots\dots\dots\dots\dots\dots\dots(II.15)$$

$$\Delta G° = \Delta H° - T * \Delta S° \dots\dots\dots\dots\dots\dots\dots\dots\dots\dots\dots\dots\dots\dots\dots\dots\dots(II.16)$$

II.7.2 Effect of pH

In adsorption research, the surface charge of the adsorbent is a key factor that must be considered, as pH influences both the material's surface charge and the distribution of anions and cations within the solution. This pH dependency plays a pivotal role in the adsorption of MB. To assess the impact of pH on MB adsorption, 20 mL of MB solution at an initial concentration of 100 mg/L was combined with 15-20 mg of adsorbent in a 0.05 L beaker at room temperature. The system was stirred at 250 rpm, with an initial pH range of 2 to 12. pH adjustments were achieved using sodium hydroxide or hydrochloric acid. After 24 hours of shaking, the samples were centrifuged and analyzed by UV-visible spectrophotometry.

II.7.3 Effect of adsorbent dose

The quantity of adsorbent employed plays a critical role in shaping adsorption dynamics, impacting the equilibrium between the adsorbent and the adsorbate in the system. Adsorbent dosages of 0.2, 0.4, 0.6, 0.8, and 1 g/L were tested at an initial dye concentration of 100 mg/L to examine the impact of the initial biosorbent dosage on the MB dye.

II.7.4 Effect of ionic force

A particular salt, such as $NaNO_3$, Na_2SO_4, NaCl, and KCl, can have an impact on the adsorption capacity of biosorbents, Uniform concentrations of the employed agents,

specifically 0.1 mol/L for salts, were maintained while varying concentrations of the dye ranging from 20 to 100 mg/L were employed. After the dissolution of salts in 50 ml of the MB dye, 50 mg of MWA adsorbent was introduced at 20°C under ambient pH conditions. The resultant mixtures underwent stirring using a multi-post magnetic stirrer for 24 hours, followed by centrifugation and subsequent analysis. The effectiveness of elimination of cationic pollutants from aqueous solutions is often significantly reduced when salt is available.

II.8 Theoretical study

II.8.1 Specifics of the Density Function Theory

The characterization of the systems under investigation is substantially contingent on the frontier molecular orbitals (FMOs), specifically the Highest Occupied Molecular Orbital (HOMO) and the Lowest Unoccupied Molecular Orbital (LUMO), which are determined utilizing the Density Functional Theory (DFT) with the DMOl$_3$ technique. The energies associated with HOMO and LUMO play a pivotal role in quantum chemical computations, as they furnish crucial insights into the microscopic interactions occurring within adsorption systems. These parameters are integral to quantum chemistry simulations, and the computed energy values for E_{HOMO}, E_{LUMO}, and E_o are presented in the formulae below [17].

The following formulas are employed to determine potential (μ), electronegativity (χ), global hardness (η), global softness (S), global electrophilicity index (ω), softness (σ), and the maximum amount of electronic charge (ΔN_{max}).

$$\mu = E_{HOMO} + E_{LUMO} \ldots\ldots\ldots\ldots\ldots\ldots\ldots\ldots\ldots\ldots\ldots\ldots\ldots\ldots\ldots\ldots\ldots\ldots\ldots\ldots.(II.17)$$

$$\chi = -\mu \ldots\ldots\ldots\ldots\ldots\ldots\ldots\ldots\ldots\ldots\ldots\ldots\ldots\ldots\ldots\ldots\ldots\ldots\ldots.(II.18)$$

$$\eta = \frac{E_{LIMO} - E_{HOMO}}{2} \ldots\ldots\ldots\ldots\ldots\ldots\ldots\ldots\ldots\ldots\ldots\ldots\ldots\ldots\ldots\ldots.(II.19)$$

$$S = \frac{1}{2\eta} \ldots\ldots\ldots\ldots\ldots\ldots\ldots\ldots\ldots\ldots\ldots\ldots\ldots\ldots\ldots\ldots\ldots.(II.20)$$

$$\omega = \frac{\chi^2}{2\eta} \ldots\ldots\ldots\ldots\ldots\ldots\ldots\ldots\ldots\ldots\ldots\ldots\ldots\ldots\ldots\ldots.(II.21)$$

$$\sigma = \frac{1}{\eta} \ldots \ldots \ldots \ldots \ldots . \ldots \ldots \ldots . \ldots \ldots \ldots . \ldots \ldots \ldots . \ldots \ldots \ldots . \ldots \ldots \ldots . \ldots \ldots \ldots . \ldots \ldots \ldots . \ldots \ldots (II.22)$$

$$\Delta N_{max} = \frac{-\mu}{\eta} \ldots \ldots \ldots \ldots . \ldots \ldots \ldots . \ldots \ldots \ldots . \ldots \ldots \ldots . \ldots \ldots \ldots . \ldots \ldots \ldots . \ldots \ldots \ldots . \ldots \ldots (II.23)$$

II.8.2   Description of Molecular Dynamic Simulation

All molecular dynamic simulations (MDS) conducted in this study were executed utilizing the BIOVIA MATERIALS STUDIO 2020 software. In these simulations, the GP (-1 0 0) surface was employed as the substrate for investigating the adsorption of MB onto the GP surface. The application of periodic boundary conditions defined a simulation box with dimensions of (27 Å × 27 Å × 15 Å), encompassing the GP slab, the MB molecule, and a vacuum slab. Geometrical refinement of the MB molecular structure and the GP (-1 0 0) surface was achieved by energy minimization. Employing a time step of 0.1 femtoseconds (fs) and a simulation duration of 50 picoseconds (ps), the COMPASS force field model was applied under the NVT ensemble during the molecular dynamic simulations. The objective of this computational work is to identify low-energy adsorption sites and explore the species' preferred adsorption on the surface of cellulose. Based on an initial evaluation of the possible interaction energy of the adsorbate–substrate system, the adsorption research of the molecules, or molecules set, is conducted. Typically, the calculation of this energy involves adding together the following three factors: [18]

- The equilibrium surface and the total interaction energy (E_{Tot}) between the molecule and the surface.
- The surface's total internal energy, marked $E_{Tot\,(surface)}$, in the absence of the molecule and after any potential relaxation.
- Without the surface, the molecule's total energy relaxes, as shown by $E_{Tot\,(molecule)}$. Accordingly, the surface molecule system's adsorption energy has the following form:

$$E_{ads} = E_{Tot\,(molecule/surface)} - \left(E_{Tot\,(surface)} + E_{Tot\,(molecule)} \right) \ldots \ldots \ldots \ldots \ldots . \ldots \ldots \textbf{(II.24)}$$

Chapter II Reference:

[1] T. Bohli, A. Ouederni, N. Fiol, et I. Villaescusa, « Evaluation of an activated carbon from olive stones used as an adsorbent for heavy metal removal from aqueous phases », *Comptes Rendus Chimie*, vol. 18, nᵒ 1, p. 88-99, janv. 2015, doi: 10.1016/j.crci.2014.05.009.

[2] C. Aharoni, D. L. Sparks, S. Levinson, et I. Ravina, « Kinetics of Soil Chemical Reactions: Relationships between Empirical Equations and Diffusion Models », *Soil Science Society of America Journal*, vol. 55, nᵒ 5, p. 1307-1312, sept. 1991, doi: 10.2136/sssaj1991.03615995005500050019x.

[3] F. Dhaouadi, L. Sellaoui, G. L. Dotto, A. Bonilla-Petriciolet, A. Erto, et A. B. Lamine, « Adsorption of methylene blue on comminuted raw avocado seeds: Interpretation of the effect of salts via physical monolayer model », *Journal of Molecular Liquids*, vol. 305, p. 112815, mai 2020, doi: 10.1016/j.molliq.2020.112815.

[4] H. Ait Ahsaine *et al.*, « Cationic dyes adsorption onto high surface area 'almond shell' activated carbon: Kinetics, equilibrium isotherms and surface statistical modeling », *Materials Today Chemistry*, vol. 8, p. 121-132, juin 2018, doi: 10.1016/j.mtchem.2018.03.004.

[5] A. H. Almuqrin, S. Wjihi, F. Aouaini, et A. B. Lamine, « New insights on physico-chemical investigation of bisphosphonate adsorption isotherm into apatite substrate using statistical physics treatment », *Journal of Molecular Liquids*, vol. 310, p. 113230, juill. 2020, doi: 10.1016/j.molliq.2020.113230.

[6] S. T. Al-Asadi, F. F. Al-Qaim, H. F. S. Al-Saedi, I. F. Deyab, H. Kamyab, et S. Chelliapan, « Adsorption of methylene blue dye from aqueous solution using low-cost adsorbent: kinetic, isotherm adsorption, and thermodynamic studies », *Environ Monit Assess*, vol. 195, nᵒ 6, p. 676, juin 2023, doi: 10.1007/s10661-023-11334-2.

[7] L. Sellaoui *et al.*, « Implementation of a multilayer statistical physics model to interpret the adsorption of food dyes on a chitosan film », *Journal of Environmental Chemical Engineering*, vol. 9, nᵒ 4, p. 105516, août 2021, doi: 10.1016/j.jece.2021.105516.

[8] A. Yazidi, L. Sellaoui, G. L. Dotto, A. Bonilla-Petriciolet, A. C. Fröhlich, et A. B. Lamine, « Monolayer and multilayer adsorption of pharmaceuticals on activated carbon: Application of advanced statistical physics models », *Journal of Molecular Liquids*, vol. 283, p. 276-286, juin 2019, doi: 10.1016/j.molliq.2019.03.101.

[9] F. Dhaouadi *et al.*, « Adsorption mechanism of Zn2+, Ni2+, Cd2+, and Cu2+ ions by carbon-based adsorbents: interpretation of the adsorption isotherms via physical modelling », *Environ Sci Pollut Res*, vol. 28, nº 24, p. 30943-30954, juin 2021, doi: 10.1007/s11356-021-12832-x.

[10] A. Gómez-Avilés, L. Sellaoui, M. Badawi, A. Bonilla-Petriciolet, J. Bedia, et C. Belver, « Simultaneous adsorption of acetaminophen, diclofenac and tetracycline by organo-sepiolite: Experiments and statistical physics modelling », *Chemical Engineering Journal*, vol. 404, p. 126601, janv. 2021, doi: 10.1016/j.cej.2020.126601.

[11] S. Wjihi, F. Aouaini, A. H. Almuqrin, et A. B. Lamine, « Physicochemical assessment of prednisone adsorption on two molecular composites using statistical physics formalism in cosmetics », *Arabian Journal of Chemistry*, vol. 13, nº 8, p. 6876-6886, août 2020, doi: 10.1016/j.arabjc.2020.06.040.

[12] F. Aouaini, S. Knani, M. B. Yahia, N. Bahloul, N. Kechaou, et A. B. Lamine, « Application of Statistical Physics on the Modeling of Water Vapor Desorption Isotherms », *Drying Technology*, vol. 32, nº 16, p. 1905-1922, déc. 2014, doi: 10.1080/07373937.2014.924131.

[13] L. Sellaoui, H. Guedidi, S. Knani, L. Reinert, L. Duclaux, et A. Ben Lamine, « Application of statistical physics formalism to the modeling of adsorption isotherms of ibuprofen on activated carbon », *Fluid Phase Equilibria*, vol. 387, p. 103-110, févr. 2015, doi: 10.1016/j.fluid.2014.12.018.

[14] H. Xue *et al.*, « Efficient adsorption of anionic azo dyes on porous heterostructured MXene/biomass activated carbon composites: Experiments, characterization, and theoretical analysis via advanced statistical physics models », *Chemical Engineering Journal*, vol. 451, p. 138735, janv. 2023, doi: 10.1016/j.cej.2022.138735.

[15] A. H. Almuqrin, S. Wjihi, F. Aouaini, et A. B. Lamine, « New insights on physico-chemical investigation of bisphosphonate adsorption isotherm into apatite substrate using statistical physics treatment », *Journal of Molecular Liquids*, vol. 310, p. 113230, juill. 2020, doi: 10.1016/j.molliq.2020.113230.

[16] T. Benhalima et H. Ferfera-Harrar, « Eco-friendly porous carboxymethyl cellulose/dextran sulfate composite beads as reusable and efficient adsorbents of cationic dye methylene blue », *International Journal of Biological Macromolecules*, vol. 132, p. 126-141, juill. 2019, doi: 10.1016/j.ijbiomac.2019.03.164.

[17] A. Geies, G. S. Gomaa, S. M. Ibrahim, A. F. Al-Hossainy, et F. K. Abdelwadoud, « Experimental and simulated TD-DFT study of malachite green dye and

tetrahydroquinoxaline hybrid blend: Its application removal from wastewater », *Journal of Molecular Structure*, vol. 1291, p. 136050, nov. 2023, doi: 10.1016/j.molstruc.2023.136050.

[18] M. Khnifira *et al.*, « Combined DFT and MD simulation approach for the study of SO2 and CO2 adsorption on graphite (111) surface in aqueous medium », *Current Research in Green and Sustainable Chemistry*, vol. 4, p. 100085, 2021, doi: 10.1016/j.crgsc.2021.100085.
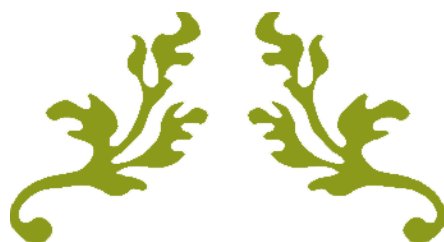
CHAPTER III

III.1 **Introduction**

Industrial effluents from various industrial sectors, including textiles, dyeing, food processing, pharmaceuticals, paper manufacturing, leather production, and cosmetics, serve as a prominent source of environmental pollution and are notable generators of chromatic wastewater emissions [1], [2], [3]. Among these sectors, the dye industry plays a notably pivotal role in this environmental context. [4], [5]. The presence of dye compounds in water leads to a decrease in sunlight penetration, potentially disrupting the photosynthesis of aquatic plants, This toxicity is due to the presence of various components, including aromatics and amines [6], [7]. dyes effect all living organisms with mutagenic, carcinogenic, or teratogenic risks, and they can affect the human body by harmfully disrupting the functions of the kidney, liver, reproductive system, and central nervous system [8], [9]. Among these colorants, Methylene Blue stands out as a cationic dye extensively used in the textile industry for dyeing wool and cotton [10], [11]. It boasts high visibility at ambient temperatures and exhibits remarkable water stability [12], [13]. However, owing to its resistance to biodegradation and toxic characteristics, significant attention has recently been focused on eliminating dyes from aqueous effluents. Additionally, Methylene Blue serves as a pigment in paper production [14]. Despite its industrial applications, Methylene Blue is also employed in the cosmetics industry for synthetic hair coloring. Yet, prolonged and high-level exposure to it poses significant environmental and human health risks. A significant amount of this dye is released into the environment, causing serious concerns, such as effects potential adverse effects include nausea, vomiting, respiratory complications, allergic reactions, cardiac arrhythmias, tissue necrosis, dermal irritation, cognitive impairment, and, in severe cases, a heightened risk of carcinogenicity and mutagenic effects, dysfunction in vital physiological systems, such as the brain, liver, and central nervous system [14], [15]. Additionally, it leads to aesthetic pollution and eutrophication, which disrupts aquatic life [16].

Throughout the years, researchers have effectively devised a diverse array of methodologies for the eradication of methylene blue in industrial effluent, including electrochemical treatment, ion exchange, photocatalytic degradation [17], membrane filtration, coagulation-flocculation [18], and the Fenton process [19], [20]. Among these techniques, the adsorption method is an important process for improving the quality of water and protecting the environment [4], [21]. Due to its good performance, simplicity of use, ability to regenerate, and environmental friendliness, adsorption stands out as a highly efficient advanced wastewater treatment process employed by industries for the mitigation of hazardous inorganic/organic pollutants inherent in the effluent [22], [23].

Numerous adsorbents are at one's disposal for the purpose of dye removal, are distinguished by their straightforward application, and exhibit a distinct advantage by making use of agricultural and industrial byproducts. Utilizing adsorbents in their raw form serves to mitigate waste disposal expenses and presents an eco-friendly solution to environmental challenges. However, to optimize practical applicability, it is imperative to implement modifications aimed at augmenting adsorption efficacy, durability, and reusability [9]. Different modifying reagents, such as base solutions (sodium hydroxide, calcium hydroxide, and sodium carbonate) and mineral and organic acids (hydrochloric acid, sulphuric acid, nitric acid, tartaric acid, thioglycolic acid, citric acid, etc.), are used in the chemical modification of adsorbents [24].

Researchers have conducted extensive examinations and assessments of prospective biosorbents in order to successfully extract colors from water pollution.

In recent years, notable advancements have included the utilization of materials such as orange peel [25], Ziziphus jujube [26], Pinus pinaster [27], almond shell [28], Acorus calamus [29], green macroalgae [30], the prickly pear [31], corn cob [32], and other similar substances for various successful applications in dye removal processes.

Despite advancements in adsorption methods, several limitations persist [11]. The limited adsorption capacity of traditional adsorbents can be quickly exhausted, hindering their long-term effectiveness [33]. Additionally, the efficiency of adsorption can be compromised by inefficient processes, suboptimal conditions, and sometimes inadequate selectivity, leading to the adsorption of non-targeted components [33]. The development of new, efficient adsorbents remains a challenge, as does the optimization of operational conditions to ensure effective adsorption in variable environments [11].

In the context of this chapter, the utilization of green peel (GP) was meticulously investigated as an adsorbent for the effective removal of methylene blue (MB) dye from solution-made water. In the early stages, scanning electron microscopy (SEM) and Fourier-transform infrared spectroscopy (FT-IR) were judiciously employed to confirm the dye adsorption process of GP. Conversely, X-ray diffraction (XRD) was specifically utilized to elucidate the crystalline structure of GP, offering crucial insights into the structural properties of the adsorbent material.

A systematic exploration of parameters influencing MB removal, including adsorbent mass, pH, initial concentration, and temperature, was conducted. Detailed analysis of isotherm data, accompanied by steric parameters, particularly 'n,' provided insights into the geometry and adsorption mechanisms. Thermodynamic analysis underscored the exothermic nature of MB adsorption on GP, indicating a decrease in adsorption capacity at elevated temperatures. Furthermore, a comprehensive investigation into the reactivity and stability of MB and GP was undertaken, shedding light on potential electron transfer phenomena during the adsorption process. In the context of MB adsorption onto cellulose-based materials like green peel, diverse mechanisms contribute to the overall adsorption process. Notably, electrostatic attraction between positively charged MB molecules and negatively charged functional groups on the adsorbent surface plays a significant role. Additionally, van der Waals forces aid in bringing MB molecules into proximity with the adsorbent surface. Hydrogen bonding, especially

between polar functional groups on the adsorbent surface and MB molecules, facilitates the attachment of MB to the adsorbent material. Under certain conditions, covalent bonding may occur, forming chemical bonds between MB molecules and reactive sites on the adsorbent surface. Moreover, precipitation of MB onto the adsorbent surface can occur, particularly when MB concentration exceeds its solubility limit. This phenomenon results in the physical deposition of MB particles onto the adsorbent surface, contributing to overall adsorption. The relative contribution of each interaction mechanism varies based on factors such as pH, temperature, and the specific chemical composition of the adsorbate and adsorbent. While electron transfer may be one aspect of the adsorption process, it is just one component within a broader array of interactions influencing MB adsorption onto green peel. The recyclable properties of GP were also carefully examined, using a 0.1 M ethanol solution. Post adsorption, the concentration of MB in the solution was quantified, and subsequently, removal efficiency and adsorption capacity were computed. A dive into the stable adsorption configuration of MB on the GP surface through molecular dynamics simulation was undertaken.

This chapter is groundbreaking as it delves into an unexplored research area. The primary innovation of this study lies in the thorough exploration of the usage of GP material as an adsorbent in order to extract MB from solutions water. This represents a significant advancement, providing an environmentally friendly and economically viable solution for treating water contaminated with cationic dyes. Moreover, the study stands out for its meticulous characterization of GP, employing techniques such as XRD to elucidate its crystalline structure and FT-IR to demonstrate the presence of hydroxyl and phenolic functional groups on its surface, thereby understanding MB adsorption process. This in-depth characterization improves our understanding of GP's structural and chemical properties as an adsorbent. Additionally, the study innovates by exploring the complex mechanisms of adsorption between GP and MB, using kinetic and adsorption models, as well as techniques

like molecular mechanics and Density Functional Theory (DFT) simulation to provide critical insights into the underlying interactions.

III.2 **Results and discussion**

III.2.1 Characterizations

Figure III.1 illustrates the diffraction pattern of GP, manifesting a distinct prominent peak at $2\theta = 22°$ attributed to the (0 0 2) crystallographic plane, alongside a minor peak at $2\theta = 15°$ corresponding to the (1 0 1) plane [34], [35]. The XRD spectrum shows that for the 2 theta analysis range above 40°, there are no distinct diffraction peaks of crystalline cellulose. Instead, there are mainly amorphous peaks. This implies that the predominant components of the native pulp are non-cellulosic substances, such as hemicellulose and lignin [34], [35]. These observations collectively signify the characteristic structural features associated with cellulose I.

FT-IR characterization was employed to quantitatively appraise the functional categories that are identifiable on the pure green peel (GP) samples. Both acid-activated (OP-H_3PO_4) and alkali-activated (OP-KOH) samples were analyzed for comparative purposes. The outcomes, as depicted in **Figure III.2**, reveal the presence of distinct absorption bands. Notably, the surface of GP exhibited a higher concentration of alcoholic and phenolic -OH functional groups in comparison to cellulose, as evidenced by a broad absorption band at 3341 cm^{-1} [36]. Additional spectral features included weak bands at 2924 cm^{-1}, indicative of hydrophobic CH_2 asymmetrical and symmetrical stretching vibrations, and a band at 1623 cm^{-1}, corresponding to C=O and N-H functionalities, potentially associated with amide I groups [37]. Furthermore, the band at 1320 cm^{-1} was attributed to the C-H group, and at 1030 cm^{-1}, stretching vibrations corresponding to O-H and C-OH were identified, indicative of the presence of polysaccharides within cell walls, such as arabinan and cellulose [38].

Figure III.3 indicates that the pHpzc (point of zero charge) of the adsorbent was determined to be 5.5. This implies that the GP surface exhibited a positive charge when the solution's pH was lower than 5.5 and a negative charge when the solution's pH exceeded 5.5.

Within this pH range, MB is found in both cationic (tri-protonated, or MBH_2^+) and undissociated (MB°) forms. The cationic forms mono-protonated (MBH) and di-protonated (MBH_2^+) occur for pH values higher than 6, with the latter form species predominating [39]. However, with pKa values greater than 8.33, the nitrogen atom in the MB molecule's core cycle is completely deprotonated, leaving the MB dye negatively charged (MB-). Because our biomaterial has a negative charge as a result (pH>5.5), we chose the cationic dye (MB).

Figure III.4 depicts the scanning electron microscope (SEM) analysis of the surface morphology of GP biomass during the adsorption process of MB dye, conducted at varying magnifications ranging from 100 to 5 μm and at an accelerating voltage of 5 kV. Furthermore, the raw green peel exhibits a distinct structural characteristic. The SEM imagery reveals the presence of abundant pores and an irregular surface structure within the fibers of the GP [40]. It is clearly illustrated that the enhanced adsorption potential can be attributed to this specific surface feature of the fiber material.
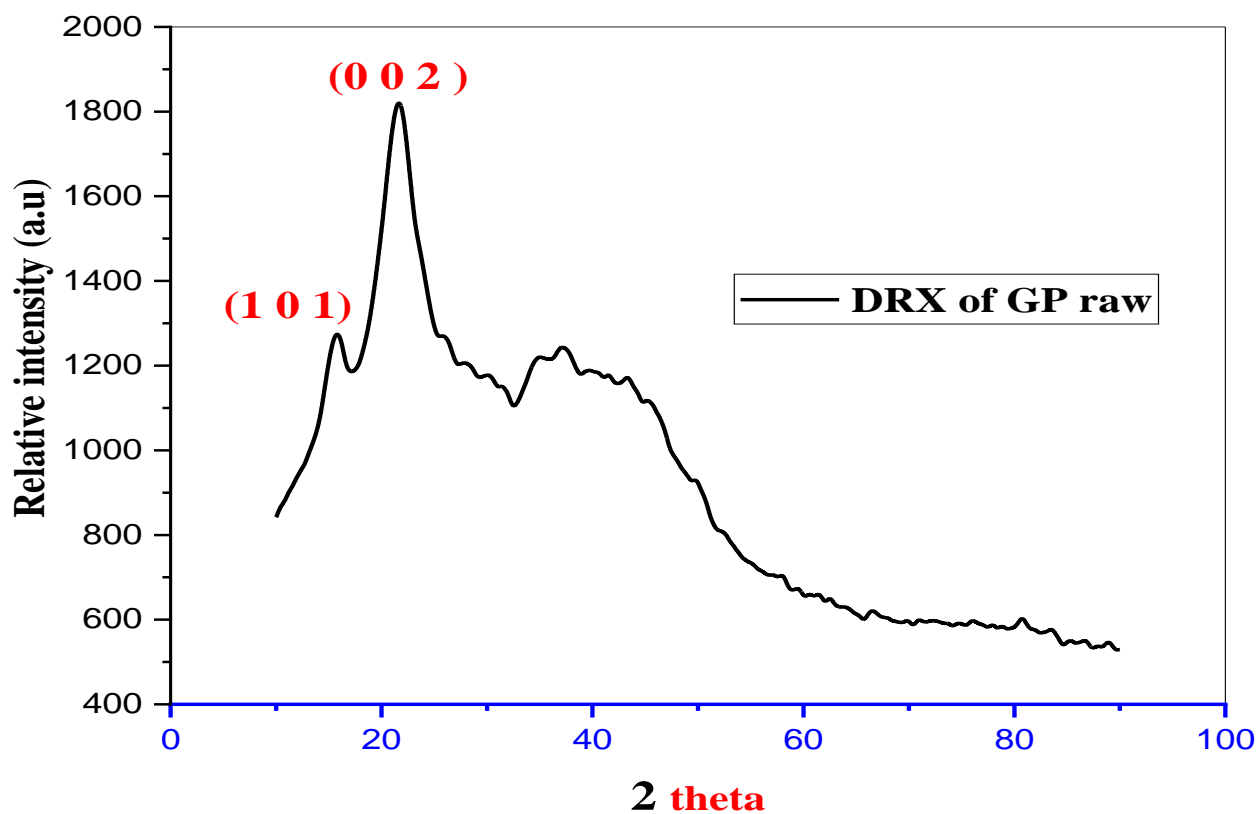
Figure III. 1: XRD pattern of green peel raw (GP).
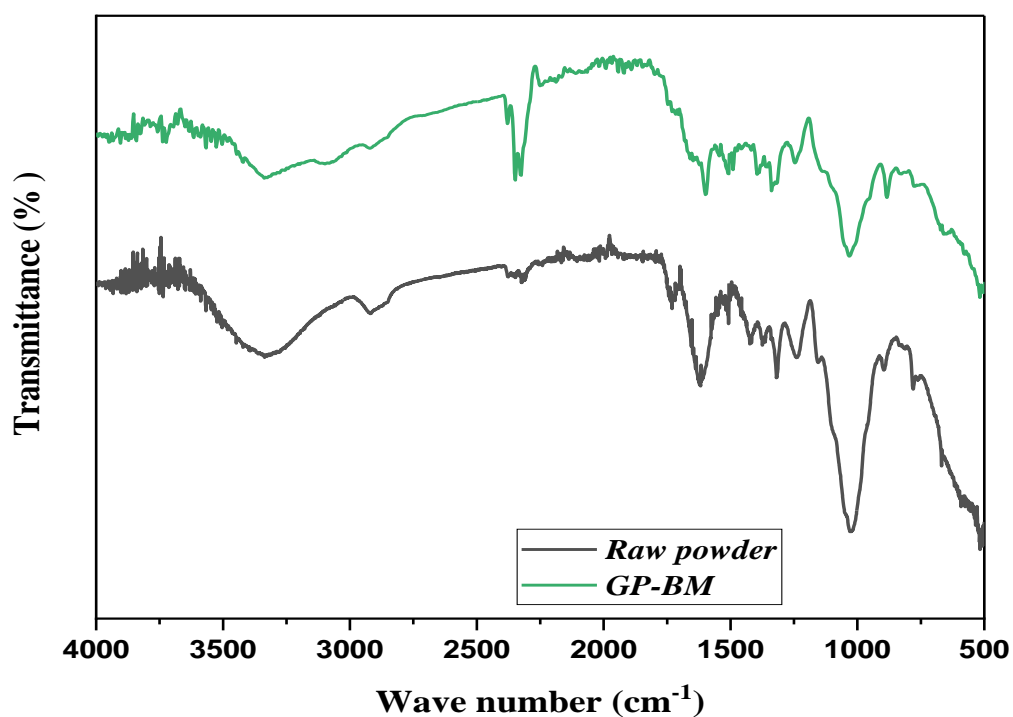
Figure III. 2: FTIR characterization of biomass (raw and GP-BM).
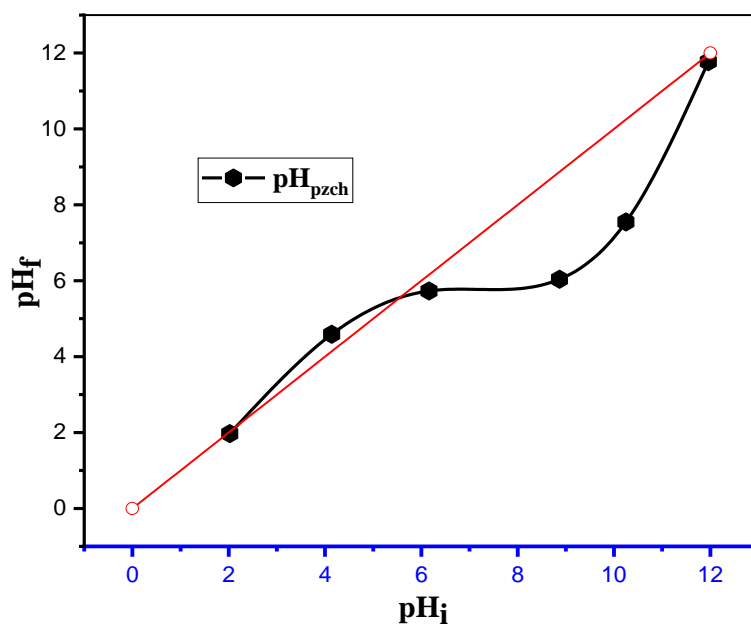
Figure III. 3: *Determination of the zero charge point of GP raw.*
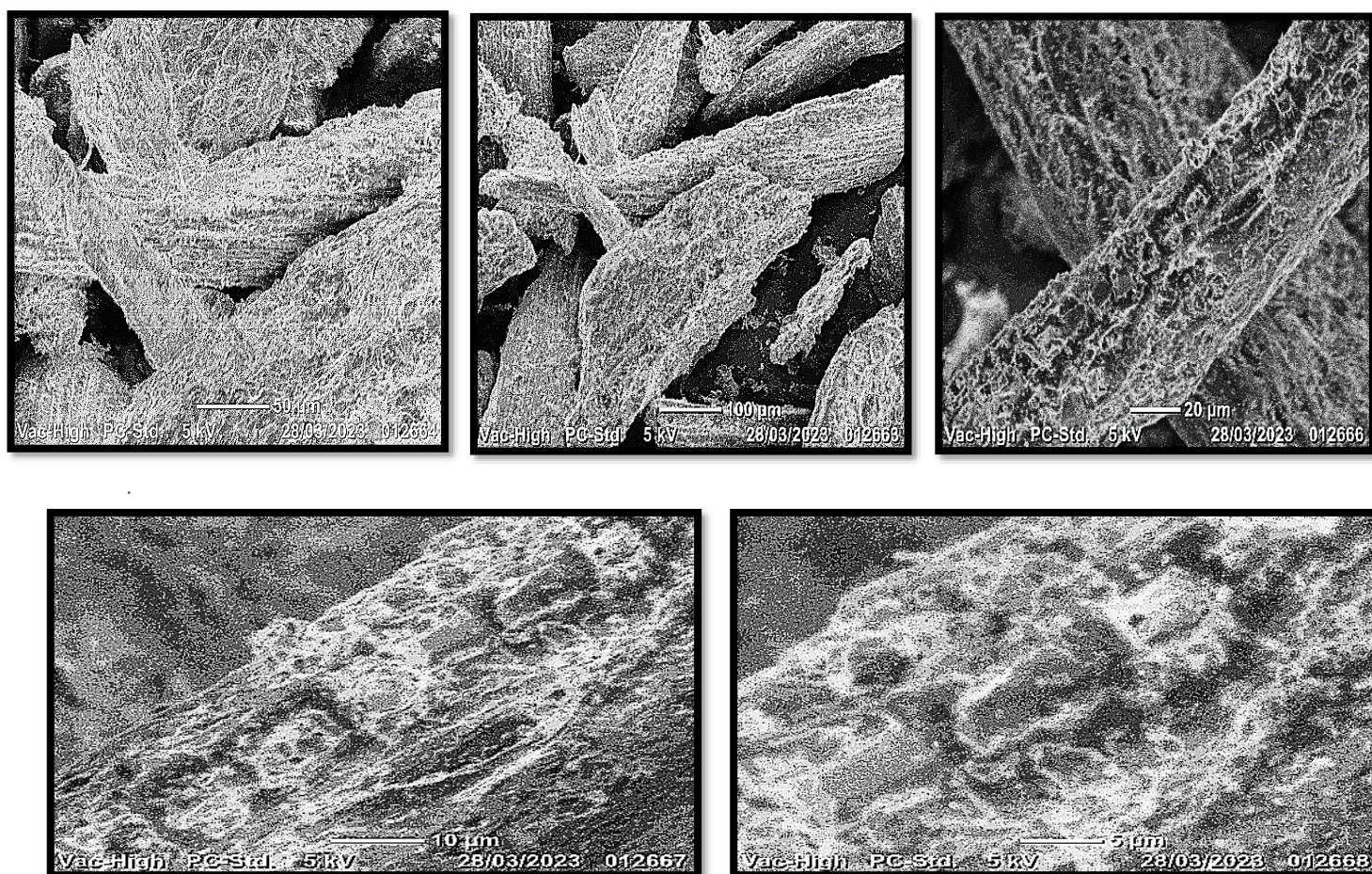
Figure III. 4: SEM images of a GP raw.

III.2.2 Effect of adsorbent dose

Figure III.5 illustrates the impact of the mass of adsorbent on the binding of MB. It reveals a reduction in the adsorption capacity per unit mass of adsorbent as the adsorbent mass increases. This reduction is accompanied by an increase in the absorption rate, leading to enhanced pollutant removal. This phenomenon may be attributed to an increase in the available surface area and the number of active sites on the surface of GP material[29].
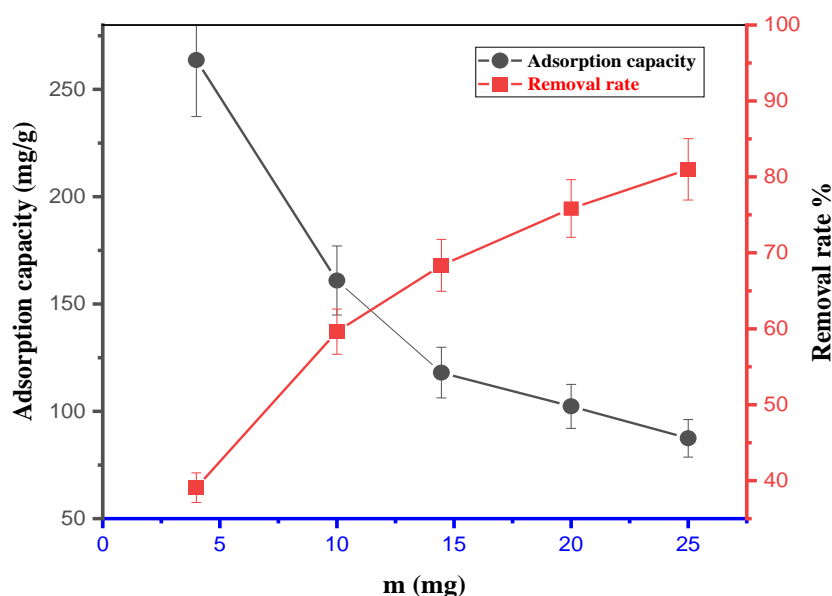
Figure III. 5: *Effect of adsorbent dose on the adsorption of MB on GP (Co: 100 mg. L-1, Contact time: 30 min).*

III.2.3 Effect of pH

Figure III.6 indicates how the pH of an aqueous solution affects the MB adsorption on GP material. The findings illustrate that under acidic conditions (pH < 6), the adsorption capacity of (GP) exhibits an augmentation from 10.6 to 111.22 mg/g. Conversely, under alkaline conditions (pH > 6), there is a reduction in adsorption capacity to 107.56 mg/g. At very low starting pH levels, there is relatively little MB absorption. This is brought on by the protonation of the adsorbate (MB) in an acidic environment and the competition with excess H^+ ions and dye cations for active sites. Because of electrostatic attraction, there are fewer strongly charged sites and more less charged sites when the pH of the solution rises. The negatively charged

adsorbent surface at greater pH values changes the polarity of the adsorbent by forming an electric double layer, resulting in dye adsorption [41].
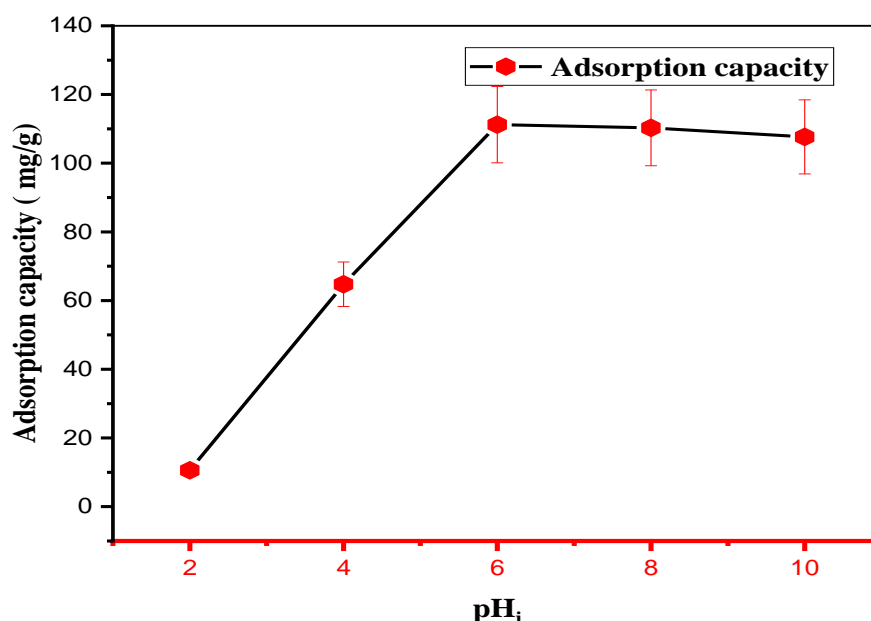
Figure III. 6: *Influence of pH on the adsorption of BM on GP (m_{GP}: 0.015 g, Co: 0.1 g/L, Contact time: 30 min).*

III.2.4 Removal Kinetics in Relation to Contact Duration

In **Figure III.7**, the impact of contact duration on the adsorption capability of the biosorbent under investigation is depicted for dye concentrations ranging from 50 to 250 mg/L. The dye solution was allowed to come into contact with the biosorbents for 24 hours in order to calculate the adsorption capacity at equilibrium, Qe_{exp}, **(Table II.4)**. However, the data points shown in **Figure III.7** are only for the first 30 minutes because there were no noticeable changes in the adsorption capacity of the biosorbent under study after that point. Due to the presence of multiple functional groups on the surface of all biosorbents during the first stages of adsorption, which led to highly attractive interactions between dye molecules and adsorbent, the adsorption capacity of MB dye rose fast in the first 15 min. The concentration of adsorbed dye grew slowly during prolonged contact durations, converging after 30 minutes to a value close to equilibrium.
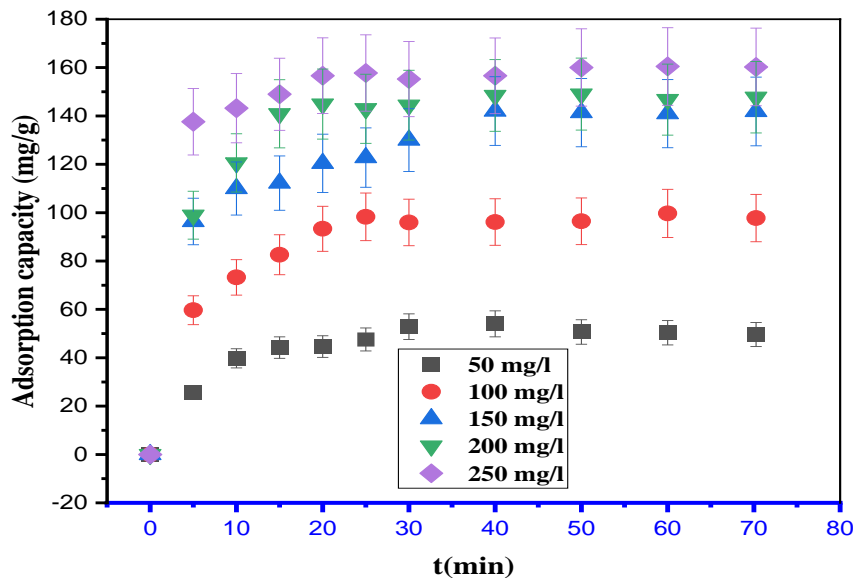
Figure III. 7*: Experimental MB adsorption kinetics on GP biosorbant (m = 30 mg, v = 50 ml, stirring = 250 ppm, T ambient).*

The outcomes of the nonlinear regression of the PFO, PSO, and PNO equations are shown in **Figure III.8**. **Table III.1** summarizes the parameters they were able to gather. At the beginning and for the first five concentrations (50, 100, 150, 200, and 250 mg L^{-1}), respectively. The PFO-derived curves are flatter than the experimental data from adsorption. They surpass the experimental results for the latter step of adsorption, on the other hand. Given a little variation in the beginning stage time, the same observation for the PSO-derived curves. Because of this, there is another order n besides 1 and 2 that offers the least amount of variation throughout the adsorption process [42]. The Elovich model's poor R^2 values **(Table III.1)** showed that pore diffusion was not the primary factor influencing MB adsorption onto GP.

The PNO-derived curves that deviate the least from the experimental data support this assertion, and all of this was supported by **Table III.1** normalized standard deviation (ΔQ%) and the correlation coefficient R^2 values. The correlation coefficients of the pseudo-nth-order kinetic model exhibit strong correlation coefficients and low average percentage error values. This model performs better than the pseudo-first and pseudo-second-order equations and matches the experimental data nicely. For concentrations of 50, 100, 150, 200, and 250 mg L^{-1}, the order

of the adsorption reaction n was discovered to be between 1.09, 1.41, 5.14, 1.26, and 2.98, respectively.

The rate-controlling step is intraparticle diffusion, and the plot of (qt) vs ($t^{1/2}$) should be linear and pass through the origin. The correlation coefficients in this study ($0.978 < R^2 < 0.989$) show that the adsorption closely resembles the intra-particle diffusion model. However, the intercept does not pass through the origin, indicating that intra-particle diffusion is not the rate-limiting step. This shows that there are three unique zones, with the first being curved, the second being linear, and the third being horizontal lines. The first area is swift and is a result of the outward diffusion of MB molecules from their exterior surface. The diffusion of MB molecules in the pores is regulated by intra-particle diffusion (inner diffusion) during the progressive adsorption stage, which causes the second area. The intraparticle diffusion is beginning to slow down in the third area, which is the last equilibrium stage, as a result of the low concentration of MB in the solution. Further observations show that the boundary layer thickens as Co is increased from 50 to 250 mg L^{-1}, which is explained by a decrease in the likelihood of external mass transfer and an increase in the likelihood of internal mass transfer.

Additionally, it was discovered that the intra-particle-diffusion rate constant, k_p, increased as the initial MB concentration increased, indicating that the boundary layer may have played a role in the growing driving force for the mass transfer between the solution and GP surface [43]. As shown by the positive and less than 1 value of v in the fractional power model, this model should explain the mechanism. However, the poor values of the correlation coefficient (R^2) along with the capacity calculated using this model are not close to the experimentally obtained value, indicating that this model is also not applicable (**Figure III.8**).

Table III. 1: *Kinetic Parameters for nonlinear regression of BM Adsorption onto GP.*

models	Parameters	50 mg.L^{-1}	100 mg.L^{-1}	150 mg.L^{-1}	200 mg.L^{-1}	250 mg.L^{-1}
	Q_{exp}	45.54	96.49	143.26	196.98	238.09
	Qe	50.94	97.94	133.41	146.54	156.18
PFO	K_1	0.138	0.159	0.197	0.205	0.394
	R^2	0.989	0.988	0.948	0.994	0.990
	ΔQ%	**0.140**	**0.002**	**0.047**	**0.692**	**1.183**
PSO	Qe	56.68	106.46	146.10	157.50	161.95
	K_2	0.003	0.002	0.002	0.002	0.006
	R^2	0.976	0.989	0.983	0.992	0.997
	ΔQ%	**0.598**	**0.106**	**0.003**	**0.433**	**1.022**
PNO	Qe	51.27	100.06	202.007	148.52	170.18
	K_n	0.004	0.005	$1.09*10^{-10}$	0.007	$4.42*10^{-5}$
	n	1.09	1.41	5.14	1.26	2.98
	R^2	0.986	0.992	0.992	0.996	0.998
	ΔQ%	0.158	0.013	1.681	0.641	0.813
Elovich	a	65.73	264.51	585.78	2352.44	$1.751*10^7$
	B	0.114	0.058	0.052	0.058	0.112
	R^2	0.945	0.971	0.993	0.973	0.997
Intraparticule	Kp	18.845	35.504	49.532	52.137	53.097
	C	2.723	7.655	11.763	17.894	29.727
	R^2	0.914	0.932	0.959	0.899	0.838

(a)

(b)

(c)

(d)

(e)
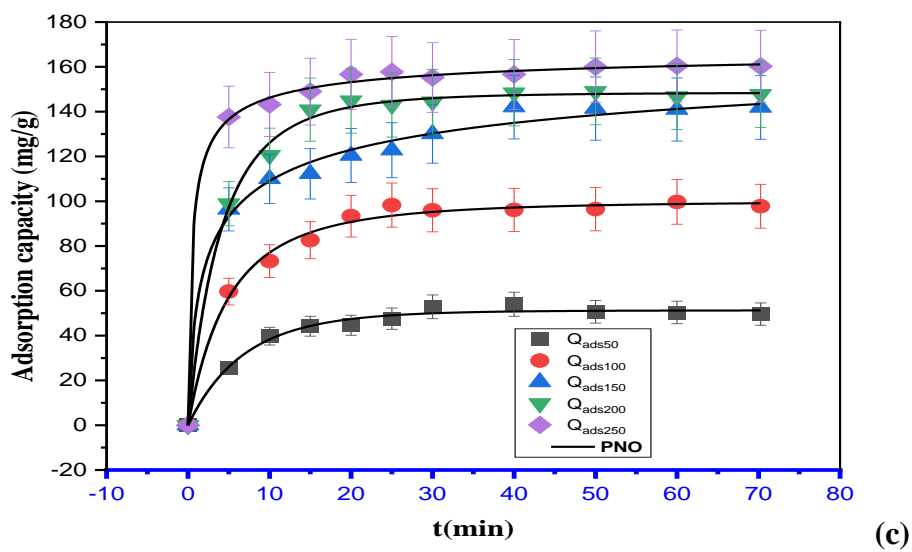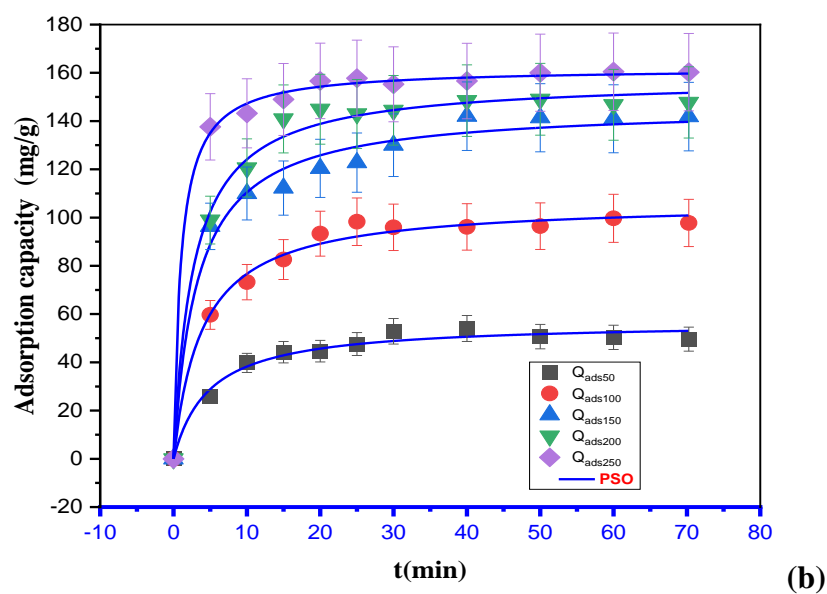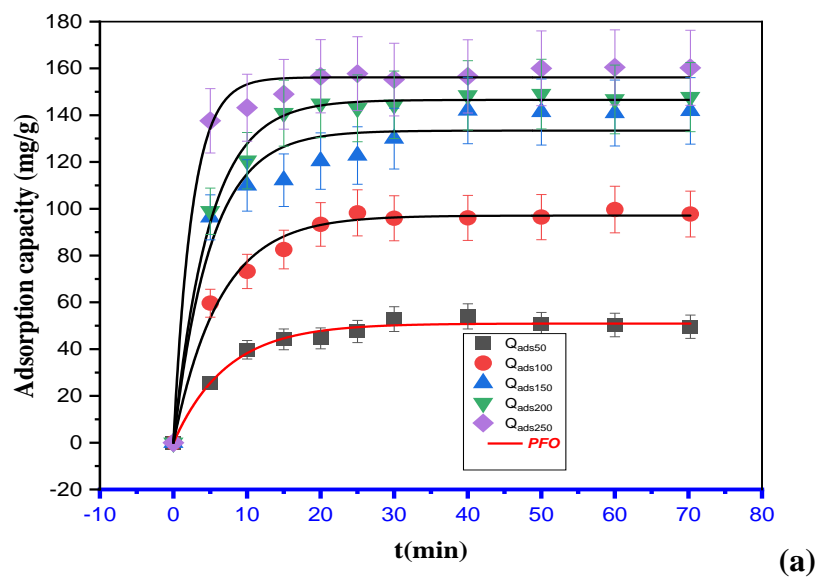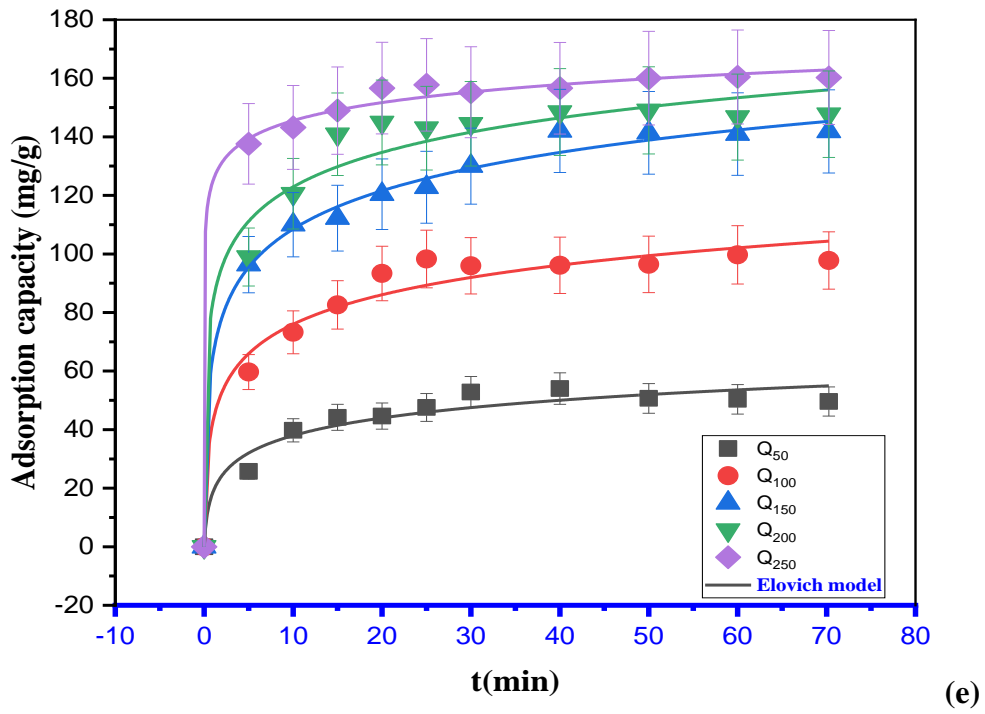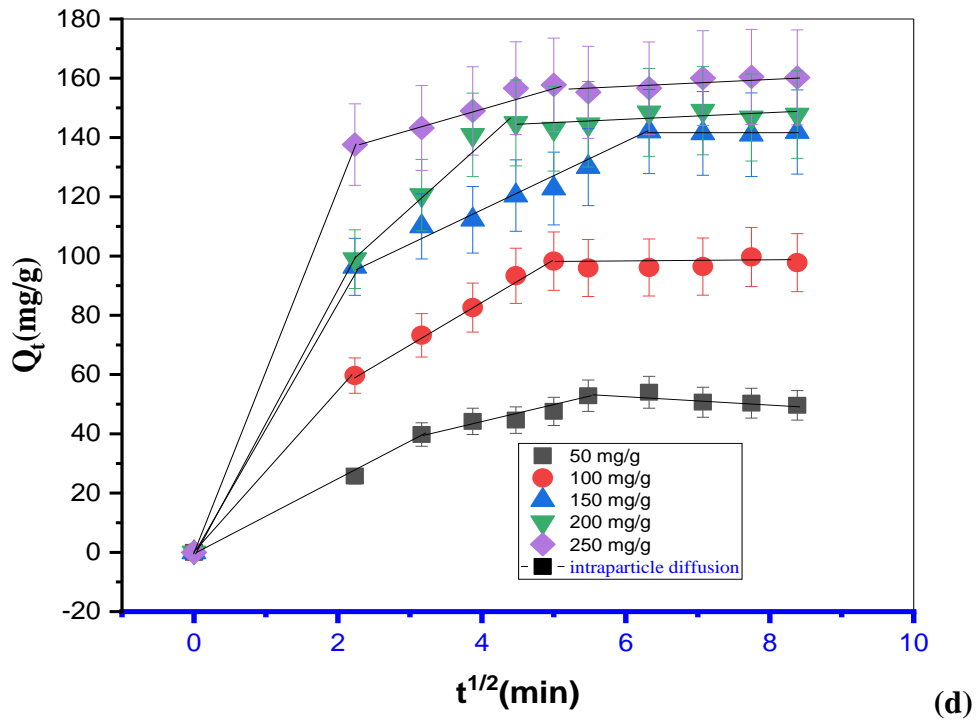
Figure III. 8: *graph representative of Nonlinear simulation of the pseudo-first-order (a),
pseudo-second-order (b), pseudo-nth-order (c), intraparticle (d), and Elovich kinetic models
(e). (m = 30 mg, v = 50 ml, stirring = 250 ppm, T = ambient temperature).*

III.2.5 Adsorption isotherm study
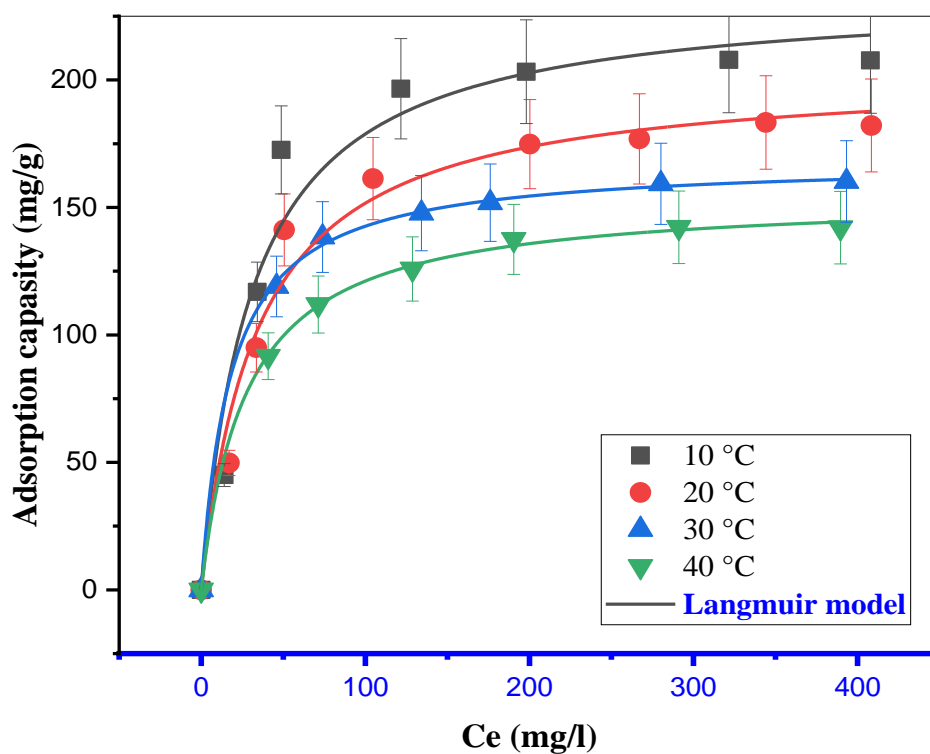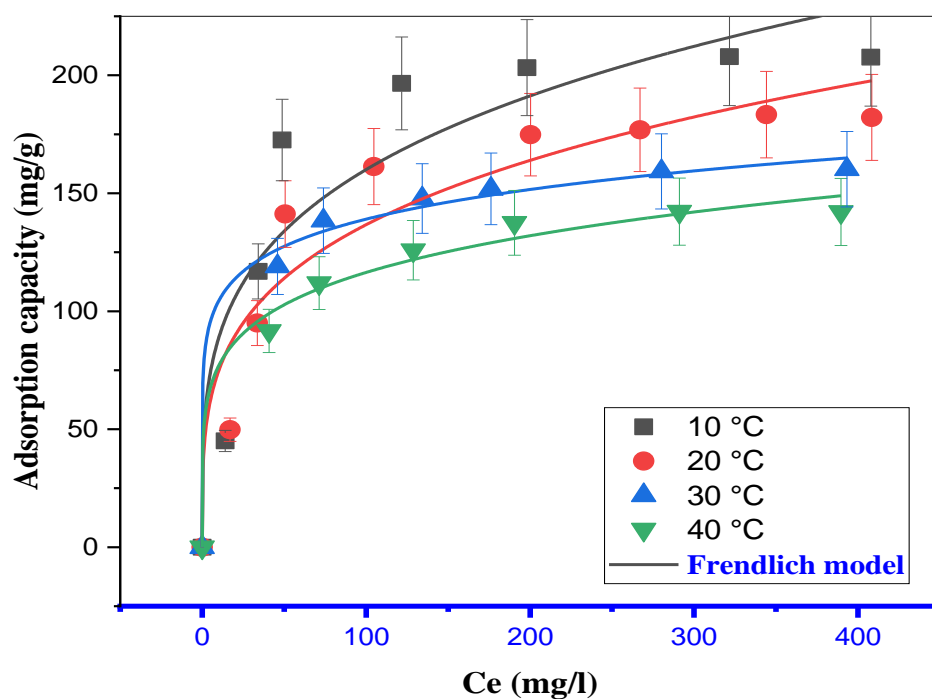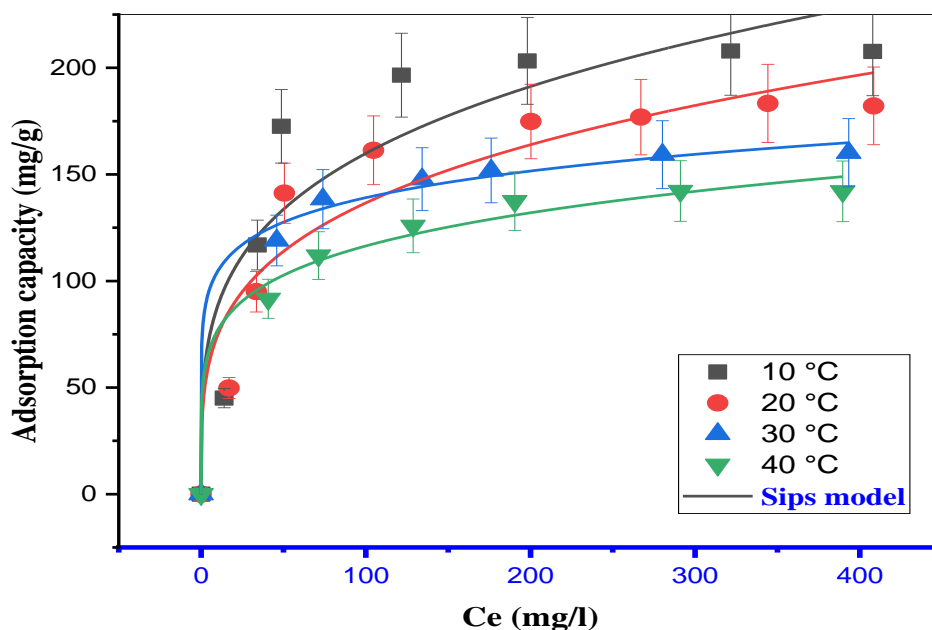
Figure III. 9: *Result of fitting isotherms data of MB adsorption onto GP with Langmuir, Freundlich and Sips models. (m = 15 mg. v = 25 ml. stirring = 250 ppm. pHnatural).*

The hybrid error function (HYBRID) and fitting parameters are displayed in **Table III.2**. By contrasting the (HYBRID) and R^2 scores for data fit. The high coefficients ($R^2 > 0.99$) and the lower HYBRID levels demonstrate that the Langmuir model provides the best applicability to the equilibrium adsorption data with a monolayer of MB attributed to a homogeneous distribution of active sites on the surface of the GP. The maximum monolayer adsorption of MB on GP was observed to be 207.33 mg/g at 10 °C, decreasing to 148.52 mg/g at 40 °C. This reduction at higher temperatures is attributed to desorption, facilitated by the formation of more hydrophobic bonds between the MB molecules in water. These bonds decrease the contact between the molecules and the adsorbent surface [43], as molecules in water tend to detach from the surface to which they adhere as temperature rises. This phenomenon occurs because, with increased temperature, molecules in water exhibit a tendency to form stronger bonds with each other, thereby diminishing their affinity for the surface. A high tendency for the adsorption of the MB on the GP is indicated by values of 1/n for the Freundlich isotherm between 0 and 1, whereas lower R^2 values imply that the model is inadequate for adjusting experimental data.

The three conventional models that were utilized to build the MB uptake dynamic are inadequate. The setup and regulation of the MB-GP interaction are therefore considered as requiring the help of theoretical treatment using sophisticated models.

Table III. 2: Different Isotherm model parameters for the adsorption of MB onto GP.

Models	Parameters	10 °C	20 °C	30 °C	40°C
Langmuir	**$Q_{exp}(mg \bullet g^{-1})$**	**203.333**	**192.187**	**179.380**	**147.828**
	$Q_m(mg \bullet g^{-1})$	234.161	203.351	168.405	154.527
	$K_L (L \bullet mg^{-1})$	0.032	0.029	0.055	0.036
	R^2	**0.997**	**0.997**	**0.999**	**0.999**
	HYPRID	**3.887**	**8.649**	**7.677**	**0.014**
Freundlich	N	3.890	3.813	8.006	5.526
	$K_F(mg \bullet g^{-1})(L/mg)^{1/n}$	48.993	40.853	78.215	50.609
	R^2	**0.876**	**0.915**	**0.994**	**0.989**
	HYPRID	**19.850**	**1.055**	**11.734**	**1.066**
Sips	$Q_m(mg \bullet g^{-1})$	126.71	115.05	99.60	71.41
	$K_S (L \bullet mg^{-1})$	0.05276	0.09661	0.062117	1.4016
	M	1.05426	1.03999	1.1606	1.108
	R^2	**0.92913**	**0.90737**	**0.98158**	**0.91354**
	HYPRID	481.237	**516.00**	519.374	658.377

III.2.6 Sophisticated statistical physics models

Our trial isotherm information was subjected to simulation applying ORIGIN software (version 2018). In **Figure III.10**, we determined the most suitable model or models for comprehending MB adsorption onto GP material by assessing the correlation coefficient R^2 as detailed in **Table III.2**. The optimal model from advanced statistical physics for describing the MB adsorption onto the GP adsorbent was identified as the double-energy single-layer model.

III.2.6.1 Steric parameters

> **Parameter n**

The adsorption geometry (vertical or horizontal) and uptake method (multi-docking or multi-interactions) of the studied dye MB on GP adsorbent may both be explained by the steric n parameter, where n is the number of dye molecules adsorbed per active site of the adsorbent

(GP). Based on the n parameter, three primary situations are often recognized when defining the adsorption shape and mechanism: Si $(n > 1)$ MB adsorption can occur in a vertical geometry via a multi-interaction process, when $(n < 1)$ MB adsorption takes place horizontally via a multi-docking process (multiple GP functional groups can bind to a single molecule of the under-studied dye), and when $(n=1)$ this condition signifies the attachment of the adsorbed species to an adsorption site in a non-parallel configuration, indicative of a mono-adsorbate process leading to the formation of a monomer [44].

Figure III.11 shows the n values at four temperatures, 283, 293, 303, and 313 K, and the obtained values of this parameter are given in **Table III.3.** The n1 values corresponding to the four temperatures were found as 2.7, 3.058, 2.342 and 2.721, while the n2 values are 0.452, 0.966, 7.411and 5.126 at 283, 293, 303 and 313, respectively. The MB–GP interaction revealed a vertical (non-parallel) arrangement with a multimolecular manner mechanism for the n_1. In addition, in the 2nd variable n_2 a vertical setting presented, a multimolecular mode for temperatures 283 and 293, the adsorbed MB attitude was changed to horizontal placement, and the molecule acquired a parallel (horizontal) orientation with a multi–docking mode by increasing the solution temperature to 303 and 313 K.

➢ **Parameter N_m**

The density of the receptor site N_m parameter functions as a steric indicator, specifying the number of occupied adsorption sites within a unit mass of the adsorbent. Moreover, it denotes the number of available adsorption sites for species adsorbed at the state of equilibrium [45].

In **Figure III.11**, the temperature-dependent variation in receptor site density (N_m) is depicted. The densities of the GP receptor sites, specifically N_{m1} and N_{m2}, exhibited a decreasing trend with the temperature rise. This phenomenon is correlated with an elevation in the quantity of

captured molecules (n_1 and n_2 per site), indicative of a heightened tendency toward aggregation as the temperature rises.

➢ **Parameter Q_{sat}**

The saturation adsorption quantity, Q_{sat}, serves as a steric parameter interdependent with other steric factors ($Q_{sat,i}=N_{mi}*n_i$). In accordance with the most appropriate statistical physics model, Q_{sat} can be expressed in terms of the number of species adsorbed per adsorption site, the density of adsorption sites, and/or the formation of layers. This metric enables an assessment of the effectiveness of the adsorbent utilized in the adsorption process [46].

In **Figure III.11**, the temperature-dependent variation of the overall saturation adsorption quantity was graphically represented. The total adsorbed amount at saturation exhibited a notable sensitivity to temperature fluctuations. Specifically, an elevation in temperature led to a decrease in the adsorbed quantity, attributable to the exothermic nature of the adsorption process a characteristic feature in conventional adsorption phenomena.
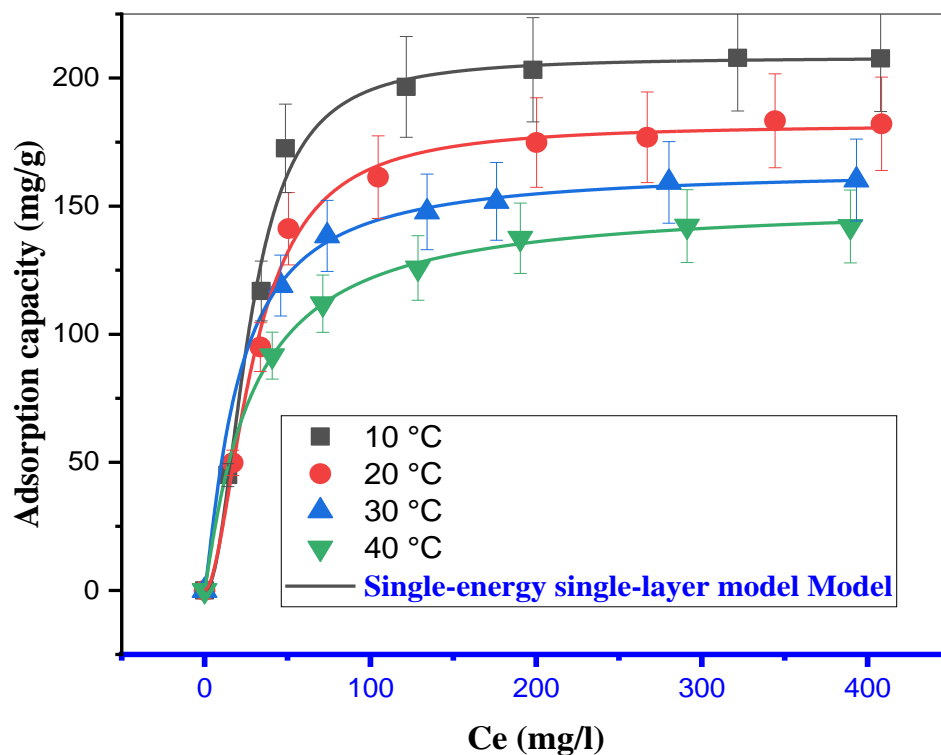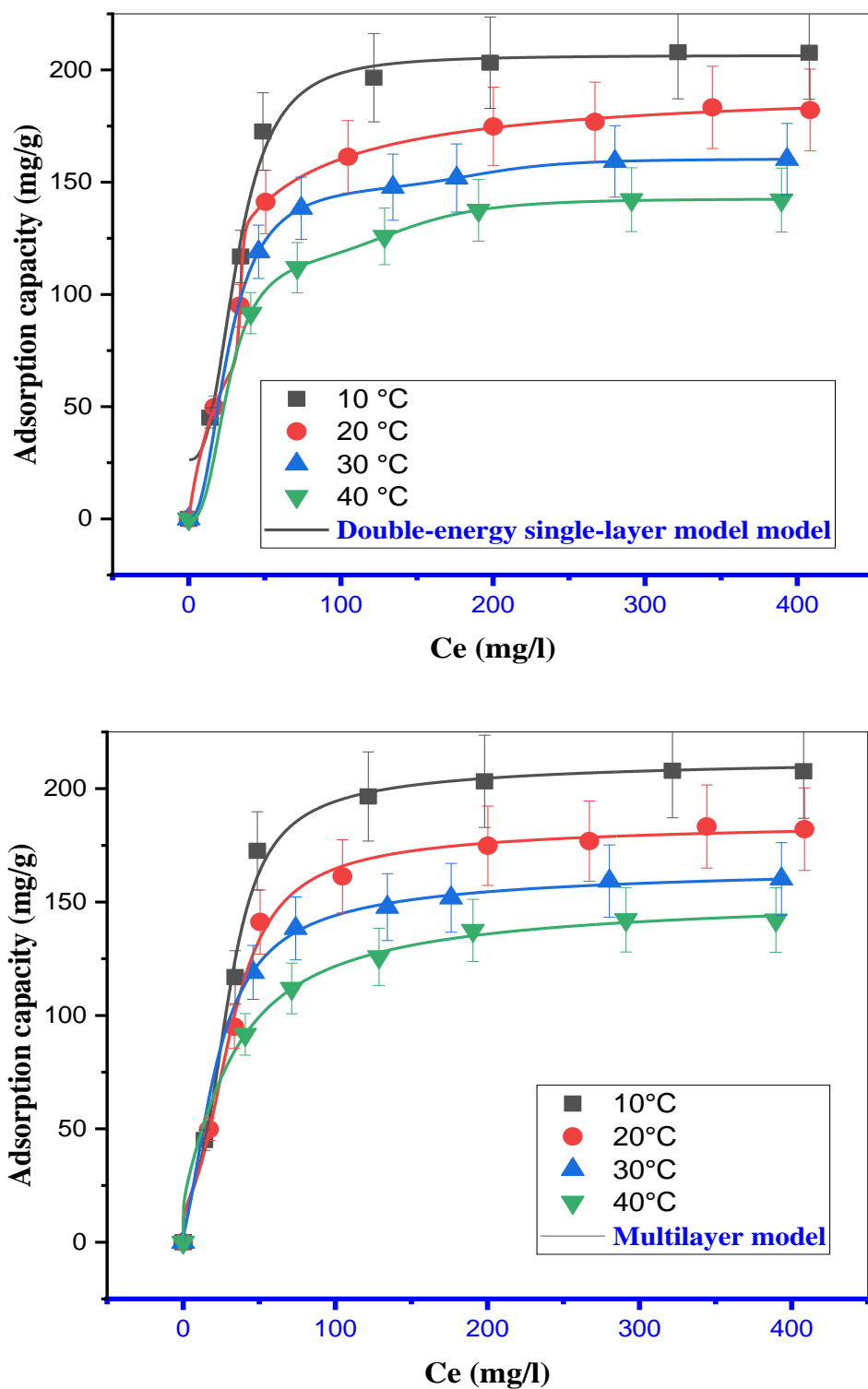
Figure III. 10: *The outcome of fitting isotherm data pertaining to the adsorption of MB onto a GP adsorbent with M1, M2, and M3 models (m = 15 mg. v = 25 ml. stirring = 250 ppm. pH=6.6).*

Table III. 3: *The determined parameter values for advanced models in the context of the adsorption process of MB onto GP biomass.*

Models	Parametrs	T = 283 K	T = 293 K	T = 303 K	313 K
M1	n	2.102	1.844	1.209	1.101
	N_m	98.981	98.642	135.976	137.628
	$C_{1/2}$	27.381	29.598	20.277	27.866
	R^2	**0.993**	**0.995**	**0.999**	**0.999**
M2	n_1	2.700	3.058	2.342	2.721
	n_2	0.452	0.966	7.411	5.126
	N_{m1}	66.716	64.158	43.494	1.861
	N_{m2}	142.174	58.234	4.727	1.377
	C_1	32.101	34.024	25.945	25.944
	C_2	$6.569*10^{-16}$	30.487	195.439	143.787
	R^2	**0.995**	**0.999**	**1**	**0.999**
M3	n	0.178	0.164	0.095	0.117
	N_{m1}	36.423	33.872	30.501	23.634
	N_{m2}	32.784	33.399	58.987	56.983
	C_1	$1.151*10^{-32}$	$3.737*10^{-34}$	$4.91*10^{11}$	$6.848*10^{-35}$
	C_2	30.957	33.193	18.847	34.896
	R^2	**0.995**	**0.996**	**0.999**	**0.999**
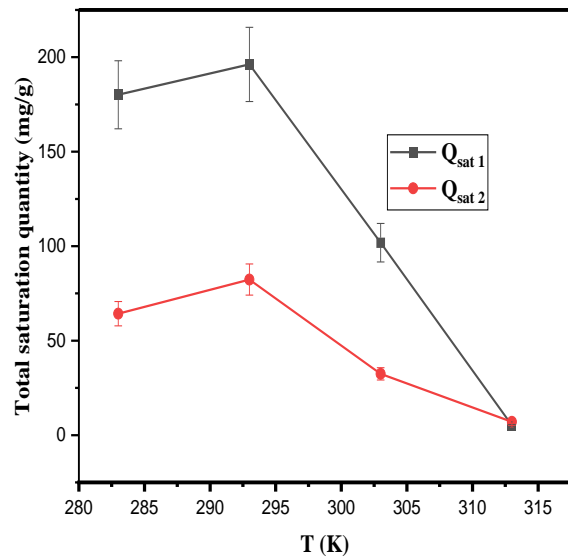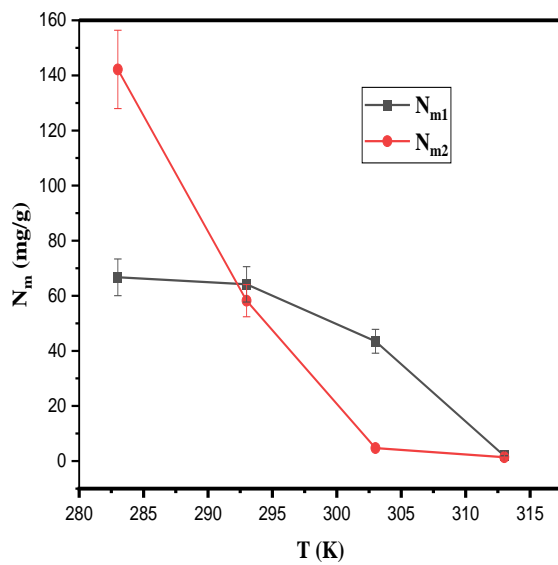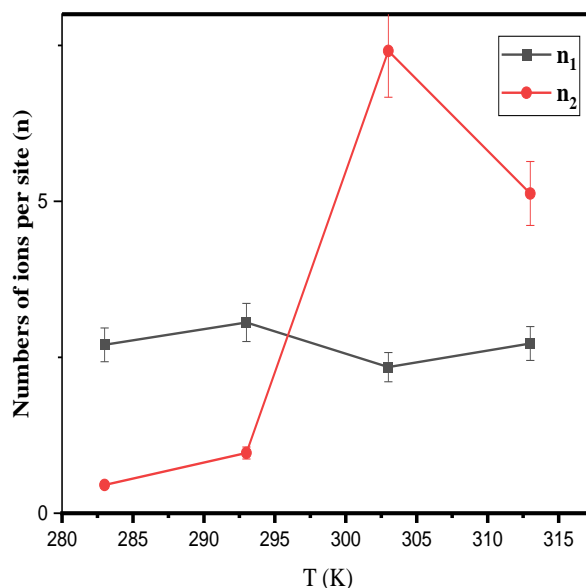
Figure III. 11: Changes in Nm, n, and Qsat with temperature during the adsorption process of MB-GP.

III.2.7 Thermodynamic

From **Table III.4**, it is clear that the sorption of MB onto GP is exothermic, as shown by the negative value of H, supporting the findings on the temperature impact, which shows that the adsorption capacity falls as temperature rises. From 10 to 40 °C, $\Delta G°$ is positive and augmented, indicating that adsorption is viable at higher temperatures. At the solid-liquid interface during adsorption, the positive entropy $\Delta S°$ indicates an increase in randomness as indicated in **Table III.4**.

Table III. 4: Thermodynamic characteristics ($\Delta H°$, $\Delta S°$ and $\Delta G°$) of MB on GP at various temperatures.

Adsorbent	Temp (K)	K_L	$\Delta G°$ (KJ.mol^{-1})	$\Delta H°$ (KJ.mol^{-1})	$\Delta S°$ (KJ.mol^{-1})	R^2 (KJ.mol^{-1})
	283	0.055	6.824292			
MB	293	0.036	8.097846	-15.40584	78.395.5	0.984
	303	0.032	8.670935			
	313	0.029	9.213273			

The application of the advanced Double-energy single-layer model (M2) enables the computation of thermodynamic parameters, encompassing entropy, Gibbs free energy, and internal energy [47], [48].

Table III. 5: The function of entropy, free enthalpy, and internal energy as related to the M2 model.

Function	Equation	Number
Entropy	$\frac{S_a}{K_B} = N_1\left[ln\left(1+\left(\frac{C_e}{C_1}\right)^{n_1 m}\right)+\frac{n_1 ln\left(\frac{C_1}{C_e}\right)}{1+\left(\frac{C_1}{C_e}\right)^{n_1 m}}\right]+N_2\left[ln\left(1+\left(\frac{C_e}{C_2}\right)^{n_2}\right)+\frac{n_2 ln\left(\frac{C_2}{C_e}\right)}{1+\left(\frac{C_2}{C_e}\right)^{n_2}}\right]$	**(III.1)**
Gibbs free enthalpy	$G = K_B T ln\left(\frac{C_e}{Z_v}\right)\left[\frac{Q_{sat1}}{1+(\frac{C_1}{C_e})^{n_1 m}}+\frac{Q_{sat2}}{1+(\frac{C_2}{C_e})^{mn_2}}\right]$ $Z_v = \frac{Z_{gtr}}{V}=\left(\frac{2\pi m K_B T}{h^2}\right)^{3/2}$	**(III.2)**
Internal energy	$E_{int} = K_B T\left[N_{1s}\frac{ln(\frac{C_e}{Z_v})+n_{1m}ln(\frac{C_1}{C_e})}{1+(\frac{C_1}{C_e})^{n_1 m}}+N_{2s}\frac{ln(\frac{C_e}{Z_v})+n_2 m ln(\frac{C_2}{C_e})}{1+(\frac{C_2}{C_e})^{n_2 m}}\right]$	**(III.3)**

The computation of the Gibbs free enthalpy involves the utilization of **Equation (III.1)** as outlined in **Table III.5**, relying on the M2. Subsequently, the Gibbs free enthalpy is graphically represented against adsorbate concentrations across diverse temperatures for the GP adsorbent, as illustrated in **Figure III.12**. The observation in **Figure III.12** indicates the negativity of the Gibbs free energy, signifying the spontaneous nature of the adsorption process. Furthermore, an increase in temperature is correlated with a diminishing free enthalpy, indicating a consequential reduction in the viability of the adsorption process [49].

The assessment of internal energy serves as a comprehensive means to evaluate all energy contributions to the MB adsorption system [48], [50]. The general expression for internal energy is represented by **Equation (III.2)**. The depicted values for this thermodynamic parameter in the examined adsorption system are presented in **Figure III.12**. Notably, all

recorded internal energy values manifest as negative, indicative of the spontaneous occurrence of the Methylene Blue adsorption systems and the concurrent release of energy.

The entropy variation for M2 model given by **Equation (III.3)**, exhibits two distinct behaviors discernible in terms of concentration. At lower concentrations ($C_{1/2} > C$), there is an observed increase in entropy, indicating a rise in molecular disorder. This implies that MB molecules undergo random movement across the biosorbent (GP) surfaces, facilitated by the abundant active sites provided by GP at low concentrations, enhancing the adsorption process. Conversely, at higher concentrations ($C_{1/2} < C$), an opposite phenomenon is evident. The elevation in concentration results in a reduction of entropy. This decline is attributed to a plausible decrease in the number of receptor sites available on GP for adsorption as the concentration increases [48], [49].
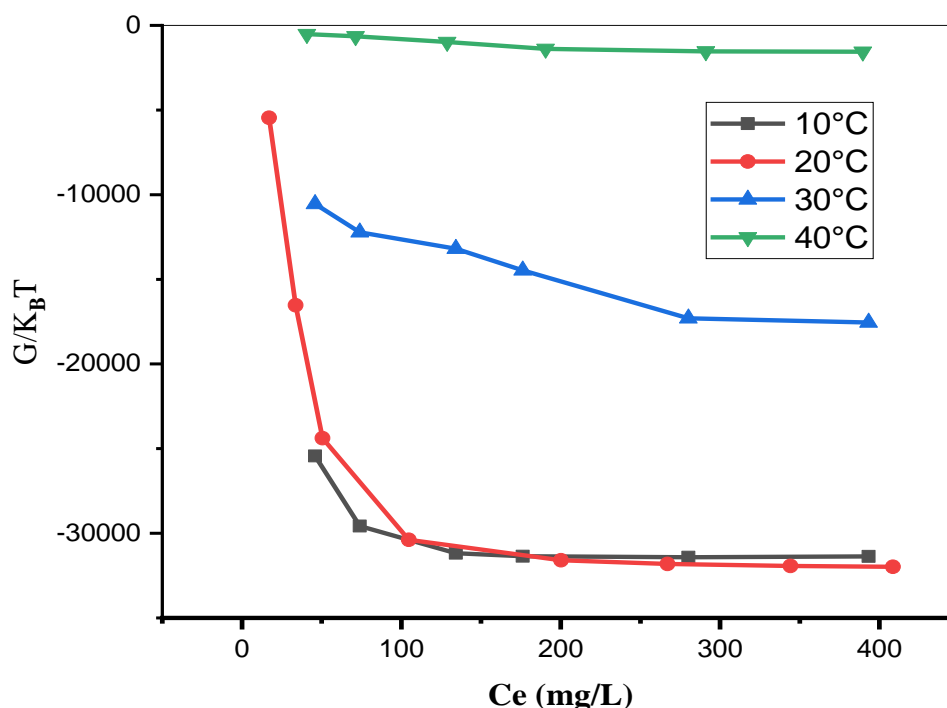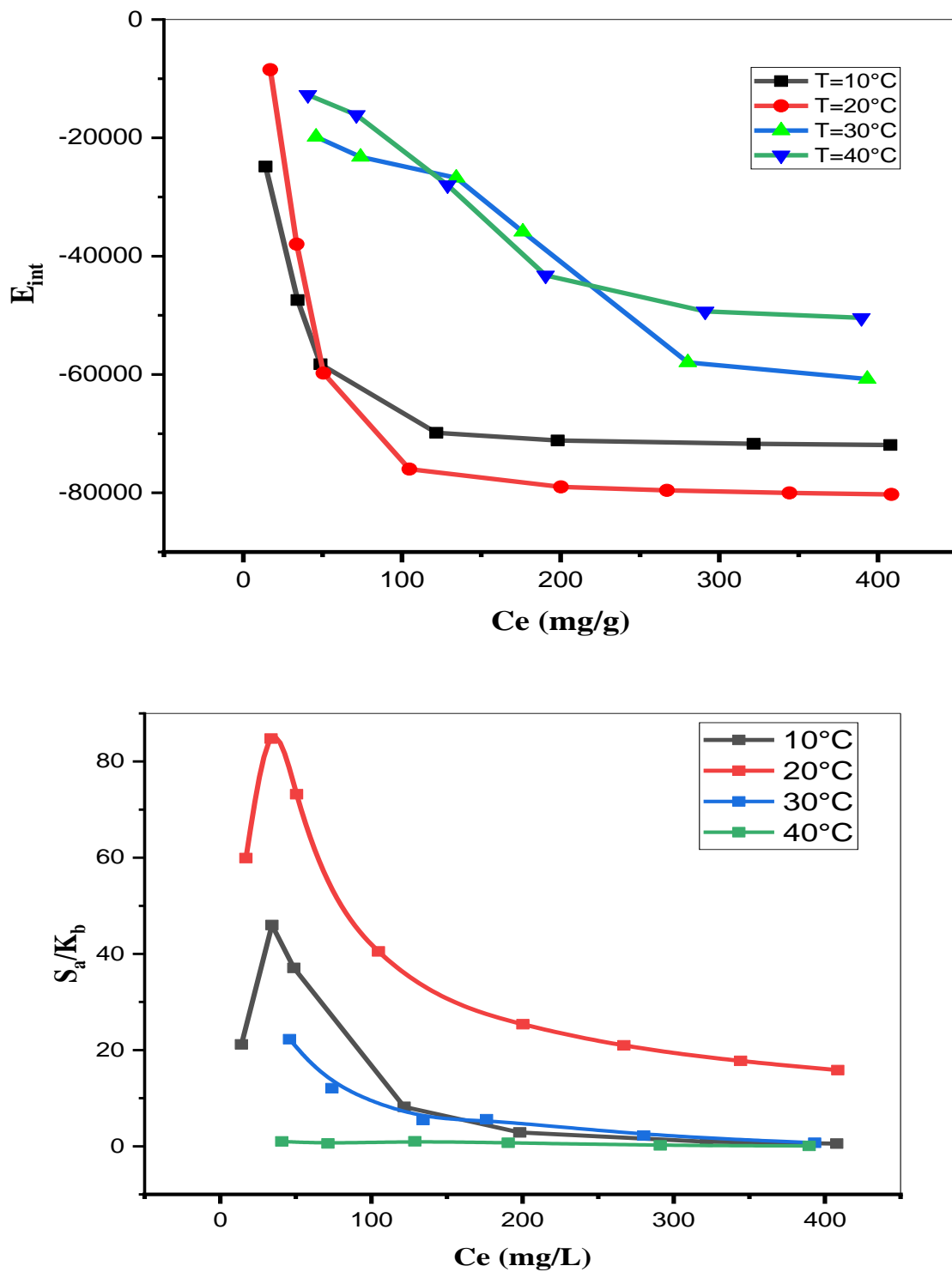
Figure III. 12: *Evolution of entropy, free enthalpy, and internal energy as a function of concentration during the absorption of MB by GP adsorbent at distinct temperatures.*

III.2.8 Density Function Theory (DFT) study

Quantum chemical parameters	MB	GP
E_{Tot} (ev)	-1181.86	-4104.31
E_{HOMO} (ev)	-3.870	0.423
E_{LUMO} (ev)	-2.684	0.268
ΔE^{Gap} (ev)	1.186	-0.155
η (ev)	-0.593	0.07751
X (ev)	6.554	-0.691
S (ev)	-0.843	6.4516
ω (ev)	-36.218	3.0805
σ (ev)	-1.686	12.903
ΔN_{max} (ev)	-11.05	-8.916

As widely recognized, the propensity of a molecule to undergo electron loss is frequently associated with its highest occupied molecular orbital energy (E_{HOMO}), whereas the molecule's capacity to accept electrons, as well as its lowest unoccupied molecular orbital energy (E_{LUMO}), are closely tied to its electron affinity [51], [52].

Furthermore, a diminutive energy gap (E_{GAP}) signifies heightened reactivity within the molecule, thereby enhancing the efficacy of MB adsorption onto the GP surface, thereby manifesting a notably stable adsorption process.

The concept of global hardness encapsulates a molecule's resistance to deformations or polarization when subjected to minor perturbations in chemical reactions. In general, molecules characterized by low global hardness values and elevated global softness values exhibit greater ease in adhering to suitable surfaces. The capacity of molecules to attract electrons is also demonstrated by the electrophilicity index, which can rise with falling values.

MB	GP
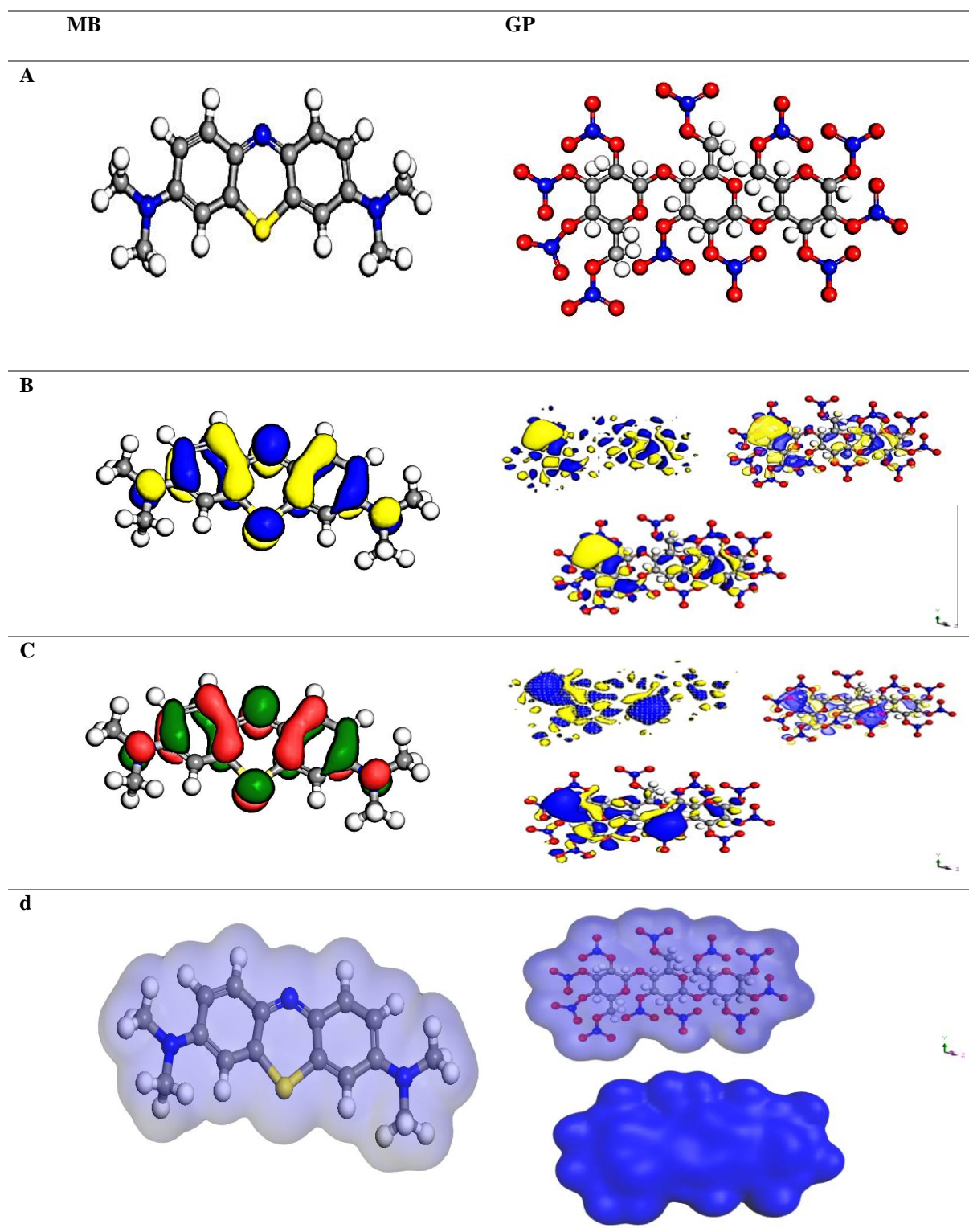
Figure III. 13: *(a) Optimized molecular structure, (b) HOMO, (c) LUMO and (d) electron density.*

III.2.9 Molecular Dynamic Simulation study

A pivotal approach for elucidating the intricate interactions between MB molecules and the adsorbent (GP) surface involves leveraging molecular dynamic simulations (MDS). The MDS-based investigation reveals that the equilibrium configuration of MB adsorption onto the GP (-1 0 0) surface, as illustrated in **Figure III.14**, corresponds to the most thermodynamically stable state. **Figure III.14** depicts the parallel adsorption mode of MB molecules on the GP (-1 0 0) surface, which underscores the strong intermolecular contacts between MB and the GP surface atoms. The chemical adsorption of MB onto the GP surface can be attributed to the contribution of electron-rich atoms, specifically sulfur, nitrogen, and oxygen, as inferred from a comprehensive analysis of the molecular structures of both MB and GP. Furthermore, Van der Waals dispersion is crucial in enabling and facilitating the capture of MB molecules onto the cellulose surface, which aligns with the outcomes obtained during the isoelectric point characterization, confirming physical adsorption. The computational assessment of various adsorption energy parameters for MB onto the GP surface is concisely presented in **Table III.6**. The observed negative adsorption energy value (-75.821 kcal/mol) underscores the fact that the adsorption procedure is spontaneous. The notably elevated binding energy value (37.117 kcal/mol) can be attributed to a superior and highly stable adsorption process. It is noteworthy that the deformation energy associated with the molecular rearrangements induced by MB adsorption implies a reduction in the stability of both the MB molecules and the GP surface.

In summary, molecular dynamic simulations serve as a pivotal tool for gaining a comprehensive understanding of the complex interplay between MB molecules and the GP surface [53]. The adsorption process is primarily governed by chemical interactions involving electron-rich atoms, and it is further enhanced by Van der Waals forces, culminating in a stable adsorption configuration. Thermodynamic analysis, as succinctly conveyed in **Table III.6**, underscores the

spontaneity and favorability of the adsorption process, with the deformation energy indicating the stability implications arising from MB-induced conformational changes.

Table III. 6: *Energies derived from computational calculations pertaining to the adsorption of MB molecules onto the GP surface.*

Adsorption energy, Kcal/mol	Rigid adsorption energy, Kcal/mol	Deformation energy, Kcal/mol	BM: d Fad/dNi	Total energy, Kcal/mol
-75.821	-85.69	9.868	-75.821	-143.212
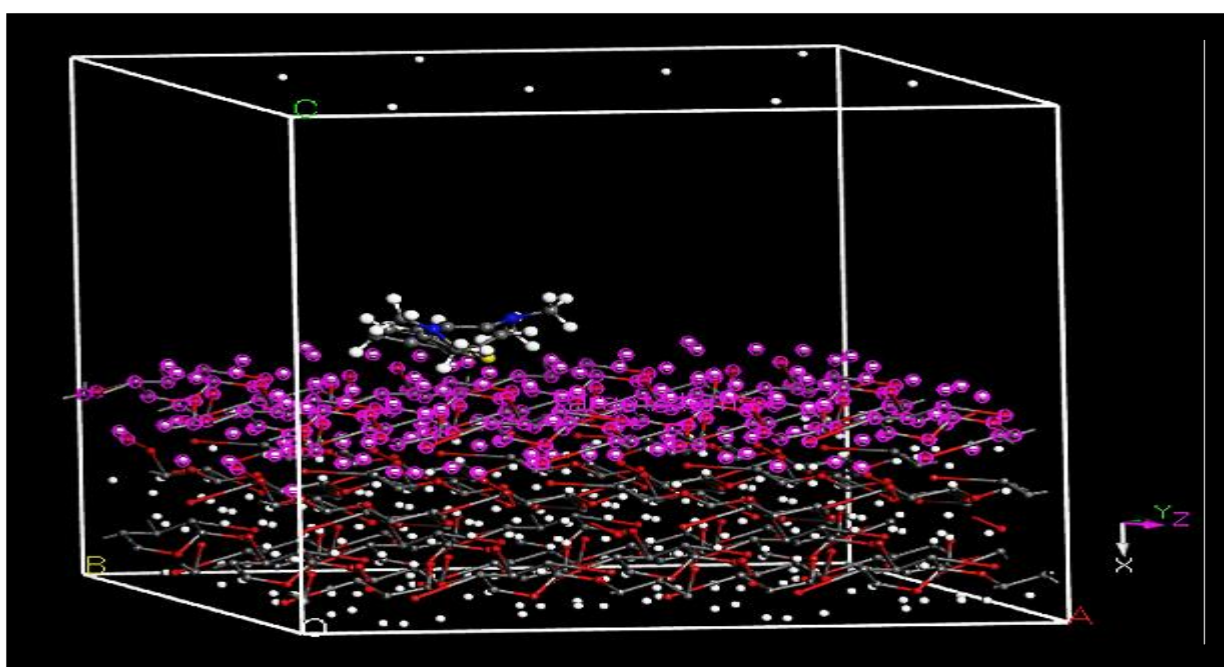
Figure III. 14: *The arrangement of MB's equilibrium adsorption onto the GP surface.*

III.2.10   Regenerative Characteristics

The recyclable properties of the adsorbent material played a pivotal role in the assessment of its applicability. The regenerative performance of GP in the context of MB adsorption is depicted in **Figure III.15**. It is obvious that both have the ability for adsorption and desorption efficiency exhibited a diminishing trend with an increasing number of usage cycles. During the first four cycles, GP retained substantial adsorption efficacy, demonstrating adsorption capacities (mg/g) and removal rates (%) of 80.92, 60.84, 43, and 35.75 mg/g for cycles 1 to 4

respectively, constituting 78.75%, 59.20%, 41.84%, and 34.78% of the initial values. Nonetheless, after five cycles, the adsorption capacity of the adsorbent decreased to 13.26 mg/g. This decline is related to the incomplete desorption of MB from the adsorption sites, when MB molecules are not fully released from these sites, they continue to occupy space on the biosorbent surface, limiting its capacity to adsorb more MB molecules, resulting in a decrease in the adsorption capability of the GP. Consequently, the optimal usage cycle for GP was determined to be five cycles.
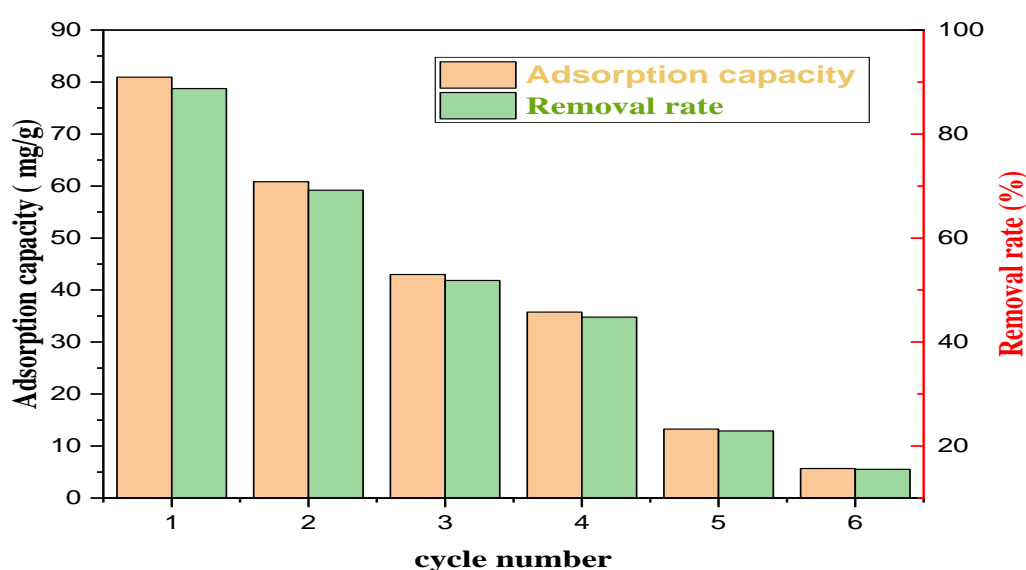
Figure III. 15: Assessment of the Durability and Reusability of GP for MB Adsorption. Experimental Parameters: MB Solution (100 mg/L), T= Room Temperature, GP Mass= 50 mg, Time: 1 hour.

III.2.11   Comparison with Published Results: A Comparative Analysis

The Table III.10 provides a comparison of the maximum adsorption capacities of various adsorbents, expressed in milligrams per gram (mg/g). Among the listed adsorbents, the biocomposite film derived from cellulose demonstrates a maximum adsorption capacity of 146.81 mg/g. This highlights the adsorption capabilities of this material, indicating its potential for water contaminant removal. The tea-derived activated material (AST) shows a slightly lower adsorption capacity, at 104.2 mg/g. Although this value is lower than that of the biocomposite film of cellulose, it remains significant, suggesting the effectiveness of AST as

an adsorbent. On the other hand, the sludge-rice husk biochar exhibits a more modest adsorption capacity, at 22.59 mg/g. However, it still serves as a potentially useful adsorbent, especially considering its biological origin and availability. The jute stick biomass stands out with an impressive adsorption capacity of 198.86 mg/g, making it one of the most efficient adsorbents on the list. This high adsorption capacity underscores the effectiveness of jute stick biomass for water contaminant removal. The banana stem-activated carbon shows an adsorption capacity of 64.66 mg/g, making it a reasonable choice for various water purification applications, although it is less efficient than jute stick biomass. Macore fruit shells exhibit the lowest adsorption capacity among the listed adsorbents, with a value of 10.61 mg/g. While this is the lowest value listed, it remains significant in certain application contexts. Lastly, the "GP" developed in this study stands out with a remarkable adsorption capacity of 207.89 mg/g, the highest among all the mentioned adsorbents. This high value suggests that the "GP" could be a highly effective adsorbent for water contaminant removal, offering new prospects for treating contaminated water.

Table III. 7: Comparative Assessment of Adsorption Capacities for MB Dye among Various Adsorbents.

Adsorbent name	Capacity maximum (mg/g)	Reference
Biocomposite film derived from cellulose	146.81	[54]
Tea-derived activated material (AST)	104.2	[55]
Sludge-rice husk biochar	22.59	[56]
Jute stick biomass	198.86	[57]
Banana stem-activated carbon	64.66	[58]
Macore fruit shells	10.61	[59]
GP	207.89	This work

In conclusion, the data from the table reveal that the "GP" exhibits the highest adsorption capacity among all listed adsorbents. This remarkable performance suggests that the "GP" could

be an extremely effective adsorbent for treating contaminated water, thereby providing new opportunities to enhance water purification technologies. These findings underscore the importance of research on advanced materials such as the "GP" in seeking sustainable solutions to challenges related to access to clean water.

III.2.12 Proposal for an adsorption mechanism

Figure 21 provides a visual representation of the interactions involved in the adsorption process of cationic methylene blue dye onto the biosorbent. Understanding the mechanism behind the adsorption of organic compounds onto the adsorbent requires a comprehensive analysis, typically involving a comparison of the FTIR spectra of the adsorbent before and after the adsorption process. This analysis is often supplemented by studies conducted under various conditions such as pH, temperature, and initial dye concentration, as well as desorption experiments. These investigations, combined with FTIR analysis and MDS results, allow researchers to propose the primary adsorption mechanisms. The identified mechanisms typically include electrostatic attraction, dipole-dipole interactions, Yoshida hydrogen bonding formations, and n-π interactions. Specifically, the primary adsorption process for various aromatic contaminants on carbonaceous materials is often attributed to the n-π electron interaction. In this process, the aromatic rings of pollutant molecules act as electron acceptors, while carbonyl oxygen ions on the biochar surface serve as electron donors. Through spectral analysis, researchers observe a significant reduction in the intensity of the band at 1623 cm^{-1}, associated with C=O functional groups, after adsorption, indicating the involvement of n-π interactions in the adsorption process. Hydrogen bonding interactions also play a crucial role in adsorption and can be classified into two types. Firstly, dipole-dipole hydrogen bonds frequently form between appropriate atoms (e.g., oxygen or nitrogen) of the aromatic adsorbates and surface hydrogen atoms of hydroxyl groups on the carbonaceous material. Secondly, Yoshida hydrogen bonding connections typically occur between the aromatic rings of adsorbate molecules and the surface hydroxyl groups of the carbonaceous material. Spectral analysis post-adsorption shows a slight decrease in the intensity of bands associated with C-O and -OH groups, suggesting the presence of dipole-dipole and Yoshida hydrogen bonding interactions. Overall, understanding these complex interactions is essential for elucidating the adsorption mechanisms and optimizing the adsorption process for efficient removal of contaminants from water sources.
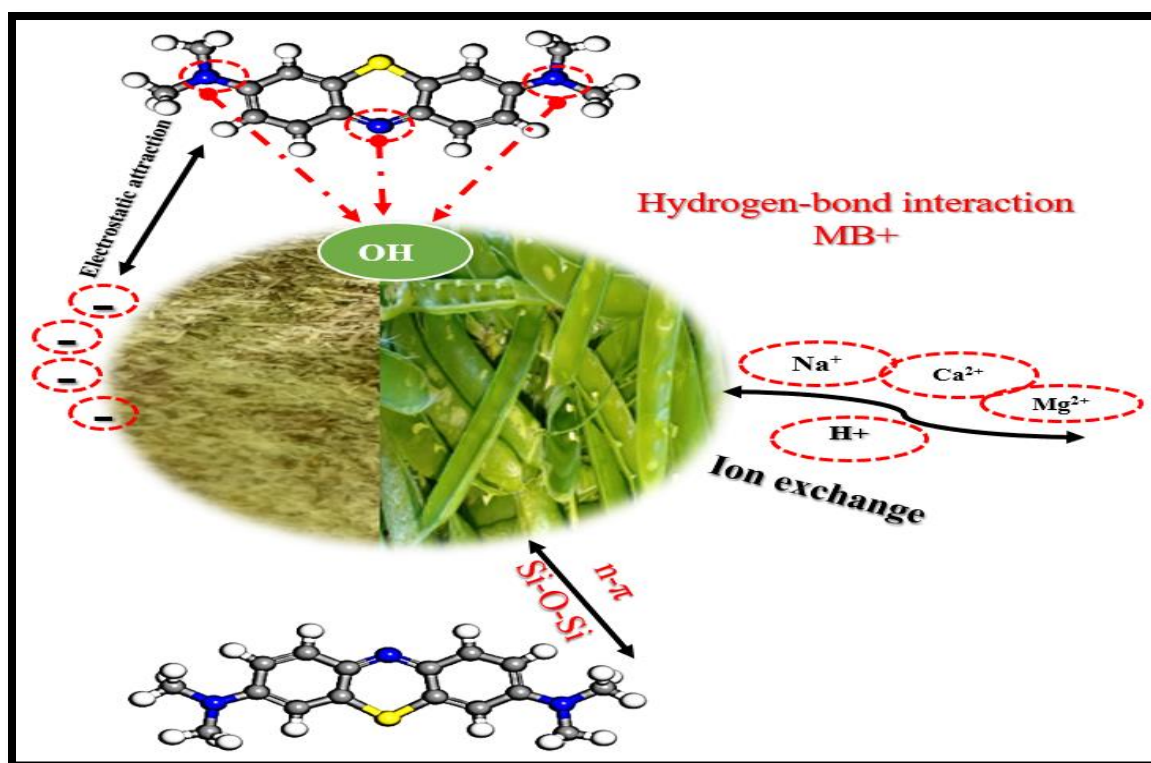
Figure III. 16: Adsorption mechanism of MB onto GP absorbent.

III.2.13   Cost Analysis for natural GP biosorbent Synthesis

The Energy and Cost Estimate section provides a meticulous breakdown of the financial aspects associated with the production of natural green pea peels (GP) biosorbent. This analysis aims to offer a comprehensive prediction of the anticipated production costs involved in generating one kilogram of GP biosorbent. Table 15 in the section presents a detailed cost estimation of the various stages involved in the production process. The first item listed is the "Cost of peels collection," which is intriguingly noted as 0.00 USD. This indicates that there are no direct expenses incurred in collecting the pea peels, suggesting that they are obtained as a byproduct, potentially from food processing industries or agricultural activities. This approach not only minimizes production costs but also underscores the sustainability of utilizing agricultural waste for value-added purposes. Moving on, the "Cost of drying of adsorbent" is also listed as 0.00 USD, with a note specifying that the drying process utilizes natural sunlight. By leveraging solar energy for drying, the production process avoids the need for energy-intensive methods,

significantly reducing operational expenses. This environmentally friendly approach not only contributes to cost-effectiveness but also aligns with sustainable practices. The final cost item in Table 15 is "Milling and sieving," which incurs a total cost of 100 w. The cost is expressed in terms of power consumption, with 1 kW/h equivalent to 0.035 USD in Algeria. This cost likely represents the electricity consumption associated with milling and sieving equipment used to process the pea peels into the desired biosorbent form. Despite this expense, the overall cost remains relatively low, further enhancing the economic viability of the production process.

In summary, the cost estimation provided in Table 15 offers valuable insights into the financial aspects of GP biosorbent production. The absence of expenses for peels collection and drying, coupled with the utilization of solar energy and relatively low milling and sieving costs, highlights the cost-effectiveness and sustainability of the production process. This comprehensive cost analysis serves as a valuable tool for decision-makers and stakeholders, facilitating informed decisions regarding resource allocation and investment in GP biosorbent production for efficient and environmentally friendly water treatment solutions.

Table III. 8: cost estimation of GP biosorbent.

unit	Total cost
Cost of peels collection	0.00 USD
Cost of drying of adsorbent	0.00 USD (dried using the sun)
Milling and sieving	100 w (1KW/h = 0.035 USD in Algeria)

References chapter III

[1] A. Mammeri *et al.*, « Assessment of surface water quality using water quality index and discriminant analysis method », *Water*, vol. 15, nᵒ 4, p. 680, 2023.

[2] A. G. Adeniyi et J. O. Ighalo, « Biosorption of pollutants by plant leaves: An empirical review », *J. Environ. Chem. Eng.*, vol. 7, nᵒ 3, p. 103100, juin 2019, doi: 10.1016/j.jece.2019.103100.

[3] Md. T.-A. Hassan, M. Hossain, et M. Hossain, « Mechanism of Basic Violet 3 Adsorption on Used Black Tea Leaves from Neutral Solution », oct. 2007.

[4] A. Stavrinou, C. A. Aggelopoulos, et C. D. Tsakiroglou, « Exploring the adsorption mechanisms of cationic and anionic dyes onto agricultural waste peels of banana, cucumber and potato: Adsorption kinetics and equilibrium isotherms as a tool », *J. Environ. Chem. Eng.*, vol. 6, nᵒ 6, p. 6958-6970, déc. 2018, doi: 10.1016/j.jece.2018.10.063.

[5] N. T. Abdel-Ghani, G. A. El-Chaghaby, E.-S. A. Rawash, et E. C. Lima, « Magnetic activated carbon nanocomposite from Nigella sativa L. waste (MNSA) for the removal of Coomassie brilliant blue dye from aqueous solution: Statistical design of experiments for optimization of the adsorption conditions », *J. Adv. Res.*, vol. 17, p. 55-63, mai 2019, doi: 10.1016/j.jare.2018.12.004.

[6] C. Pearce, J. Lloyd, et J. Guthrie, « The removal of colour from textile wastewater using whole bacterial cells: a review », *Dyes Pigments*, vol. 58, nᵒ 3, p. 179-196, 2003.

[7] M. Benjelloun, Y. Miyah, G. Akdemir Evrendilek, F. Zerrouq, et S. Lairini, « Recent Advances in Adsorption Kinetic Models: Their Application to Dye Types », *Arab. J. Chem.*, vol. 14, nᵒ 4, p. 103031, avr. 2021, doi: 10.1016/j.arabjc.2021.103031.

[8] Y. Dai *et al.*, « Utilizations of agricultural waste as adsorbent for the removal of contaminants: A review », *Chemosphere*, vol. 211, p. 235-253, 2018.

[9] S. Yadav, A. Yadav, N. Bagotia, A. K. Sharma, et S. Kumar, « Adsorptive potential of modified plant-based adsorbents for sequestration of dyes and heavy metals from wastewater - A review », *J. Water Process Eng.*, vol. 42, p. 102148, août 2021, doi: 10.1016/j.jwpe.2021.102148.

[10] « Water | Free Full-Text | Review on Methylene Blue: Its Properties, Uses, Toxicity and Photodegradation ». Consulté le: 13 décembre 2023. [En ligne]. Disponible sur: https://www.mdpi.com/2073-4441/14/2/242

[11] N. Bouchelkia *et al.*, « Jujube stones based highly efficient activated carbon for methylene blue adsorption: Kinetics and isotherms modeling, thermodynamics and mechanism study,

optimization via response surface methodology and machine learning approaches », *Process Saf. Environ. Prot.*, vol. 170, p. 513-535, 2023, doi: 10.1016/j.psep.2022.12.028.

[12] L. Yu, D. P. Gamliel, B. Markunas, et J. A. Valla, « A Promising Solution for Food Waste: Preparing Activated Carbons for Phenol Removal from Water Streams », *ACS Omega*, vol. 6, nº 13, p. 8870-8883, avr. 2021, doi: 10.1021/acsomega.0c06029.

[13] L. Liang, S. Zhang, G. A. Goenaga, X. Meng, T. A. Zawodzinski, et A. J. Ragauskas, « Chemically Cross-Linked Cellulose Nanocrystal Aerogels for Effective Removal of Cation Dye », *Front. Chem.*, vol. 8, p. 570, juill. 2020, doi: 10.3389/fchem.2020.00570.

[14] S. Pandey, E. Fosso-Kankeu, et J. Ramontja, « Efficient and rapid adsorption characteristics of templating xanthan gum-graft-poly (aniline) and silica nanocomposite toward removal of toxic methylene blue dyes », présenté à 9th International Conference on Advances in Science, Engineering, Technology and Waste Management (ASETWM-2017), 2017, p. 27-28.

[15] A. H. Jawad, A. Kadhum, et Y. Ngoh, « Applicability of dragon fruit (Hylocereus polyrhizus) peels as low-cost biosorbent for adsorption of methylene blue from aqueous solution: Kinetics, equilibrium and thermodynamics studies », *Desalination Water Treat.*, vol. 109, mai 2018, doi: 10.5004/dwt.2018.21976.

[16] A. Nasar et S. Shakoor, « Utilization of Punica granatum peel as an eco-friendly biosorbent for the removal of methylene blue dye from aqueous solution », *J. Appl. Biotechnol. Bioeng.*, vol. 5, sept. 2018, doi: 10.15406/jabb.2018.05.00145.

[17] K. Madi *et al.*, « Green Fabrication of ZnO Nanoparticles and ZnO/rGO Nanocomposites from Algerian Date Syrup Extract: Synthesis, Characterization, and Augmented Photocatalytic Efficiency in Methylene Blue Degradation », *Catalysts*, vol. 14, nº 1, p. 62, 2024.

[18] A. N. E. H. Sid *et al.*, « Comparative investigation of the effect of eggshellpowder and calcium carbonate as additivesin eco-friendly polymer drilling fluids », *Sustainability*, vol. 15, nº 4, p. 3375, 2023.

[19] M. Smara *et al.*, « Efficiency of Hydrogen Peroxide and Fenton Reagent for Polycyclic Aromatic Hydrocarbon Degradation in Contaminated Soil: Insights from Experimental and Predictive Modeling », *Processes*, vol. 12, nº 3, p. 621, 2024.

[20] M. I. Kanjal *et al.*, « A Study of Treatment of Reactive Red 45 Dye by Advanced Oxidation Processes and Toxicity Evaluation Using Bioassays », *Sustainability*, vol. 15, nº 9, p. 7256, 2023.

[21] S. S. Shah, T. Sharma, B. A. Dar, et R. K. Bamezai, « Adsorptive removal of methyl orange dye from aqueous solution using populous leaves: Insights from kinetics, thermodynamics and computational studies », *Environ. Chem. Ecotoxicol.*, vol. 3, p. 172-181, 2021, doi: 10.1016/j.enceco.2021.05.002.

[22] R. Kumar et M. A. Barakat, « Decolourization of hazardous brilliant green from aqueous solution using binary oxidized cactus fruit peel », *Chem. Eng. J.*, vol. 226, p. 377-383, juin 2013, doi: 10.1016/j.cej.2013.04.063.

[23] N. D. Shooto, C. S. Nkutha, N. R. Guilande, et E. B. Naidoo, « Pristine and modified mucuna beans adsorptive studies of toxic lead ions and methylene blue dye from aqueous solution », *South Afr. J. Chem. Eng.*, vol. 31, p. 33-43, janv. 2020, doi: 10.1016/j.sajce.2019.12.001.

[24] K. K. Wong, C. K. Lee, K. S. Low, et M. J. Haron, « Removal of Cu and Pb by tartaric acid modified rice husk from aqueous solutions », *Chemosphere*, vol. 50, n° 1, p. 23-28, janv. 2003, doi: 10.1016/S0045-6535(02)00598-2.

[25] A. Guediri, A. Bouguettoucha, D. Chebli, N. Chafai, et A. Amrane, « Molecular dynamic simulation and DFT computational studies on the adsorption performances of methylene blue in aqueous solutions by orange peel-modified phosphoric acid », *J. Mol. Struct.*, vol. 1202, p. 127290, 2020.

[26] A. Guediri, A. Bouguettoucha, D. Chebli, et A. Amrane, « The use of encapsulation as a proposed solution to avoid problems encountered with conventional materials in powder form: Application in methylene blue removal from aqueous solutions », *J. Mol. Liq.*, vol. 316, p. 113841, oct. 2020, doi: 10.1016/j.molliq.2020.113841.

[27] T. Yumak, « Surface characteristics and electrochemical properties of activated carbon obtained from different parts of Pinus pinaster », *Colloids Surf. Physicochem. Eng. Asp.*, vol. 625, p. 126982, sept. 2021, doi: 10.1016/j.colsurfa.2021.126982.

[28] H. Ait Ahsaine *et al.*, « Cationic dyes adsorption onto high surface area 'almond shell' activated carbon: Kinetics, equilibrium isotherms and surface statistical modeling », *Mater. Today Chem.*, vol. 8, p. 121-132, juin 2018, doi: 10.1016/j.mtchem.2018.03.004.

[29] C. Djama, D. Chebli, A. Bouguettoucha, I. Doudou, et A. Amrane, « Statistical physics modelling of azo dyes biosorption onto modified powder of Acorus calamus in batch reactor », *Biomass Convers. Biorefinery*, vol. 13, n° 2, p. 1013-1028, janv. 2023, doi: 10.1007/s13399-020-01190-2.
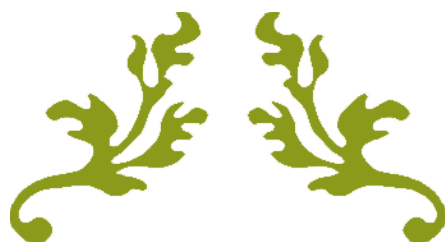
[30] R. Aravindhan, J. R. Rao, et B. U. Nair, « Application of a chemically modified green macro alga as a biosorbent for phenol removal », *J. Environ. Manage.*, vol. 90, nᵒ 5, p. 1877-1883, 2009.

[31] F. Sakr, S. Alahiane, A. Sennaoui, M. Dinne, I. Bakas, et A. Assabbane, « Removal of cationic dye (Methylene Blue) from aqueous solution by adsorption on two type of biomaterial of South Morocco », *Mater. Today Proc.*, vol. 22, p. 93-96, 2020, doi: 10.1016/j.matpr.2019.08.101.

[32] Y. Miyah, A. Lahrichi, et M. Idrissi, « Removal of cationic dye -Methylene bleu- from aqueous solution by adsorption onto corn cob powder calcined », vol. 7, p. 96-104, janv. 2016.

[33] M. Zamouche *et al.*, « Predictive Model Based on K-Nearest Neighbor Coupled with the Gray Wolf Optimizer Algorithm (KNN_GWO) for Estimating the Amount of Phenol Adsorption on Powdered Activated Carbon », *Water*, vol. 15, nᵒ 3, p. 493, 2023.

[34] A. Guediri *et al.*, « The Enhanced Adsorption Capacity of Ziziphus jujuba Stones Modified with Ortho-Phosphoric Acid for Organic Dye Removal: A Gaussian Process Regression Approach », *Water*, vol. 16, nᵒ 9, p. 1208, 2024.

[35] C. Djama *et al.*, « Experimental and Theoretical Study of Methylene Blue Adsorption on a New Raw Material, Cynara scolymus—A Statistical Physics Assessment », *Sustainability*, vol. 15, nᵒ 13, Art. nᵒ 13, janv. 2023, doi: 10.3390/su151310364.

[36] S. Shrestha, « Chemical, Structural and Elemental Characterization of Biosorbents Using FE-SEM, SEM-EDX, XRD/XRPD and ATR-FTIR Techniques », *J. Chem. Eng. Process Technol.*, vol. 7, nᵒ 3, 2016, doi: 10.4172/2157-7048.1000295.

[37] R. Dod, G. Banerjee, et S. Saini, « Adsorption of methylene blue using green pea peels (Pisum sativum): A cost-effective option for dye-based wastewater treatment », *Biotechnol. Bioprocess Eng.*, vol. 17, nᵒ 4, p. 862-874, août 2012, doi: 10.1007/s12257-011-0614-5.

[38] A. Shoaib, Nafisa, G. Riaz, Q. Fatima, U. Fatima, et N. Iqbal, « FOURIER-TRANSFORM INFRARED SPECTROSCOPY IDENTIFIED CHANGES IN THE CELL WALL COMPONENTS ASSOCIATED WITH THE SIMULTANEOUS TRAFFICKING OF WHITE MOLD FUNGUS AND COPPER », *Pak. J. Phytopathol.*, vol. 34, nᵒ 2, Art. nᵒ 2, déc. 2022, doi: 10.33866/phytopathol.034.02.0795.

[39] T. M. Eldeeb *et al.*, « Adsorption of methylene blue (MB) dye on ozone, purified and sonicated sawdust biochars », *Biomass Convers. Biorefinery*, vol. 14, nᵒ 8, p. 9361-9383, avr. 2024, doi: 10.1007/s13399-022-03015-w.

[40] T. A. Khan, R. Rahman, I. Ali, E. A. Khan, et A. A. Mukhlif, « Removal of malachite green from aqueous solution using waste pea shells as low-cost adsorbent – adsorption isotherms and dynamics », *Toxicol. Environ. Chem.*, vol. 96, nᵒ 4, p. 569-578, avr. 2014, doi: 10.1080/02772248.2014.969268.

[41] O. O. Namal et E. Kalipci, « Adsorption kinetics of methylene blue using alkali and microwave-modified apricot stones », *Sep. Sci. Technol.*, vol. 54, nᵒ 11, p. 1722-1738, juill. 2019, doi: 10.1080/01496395.2018.1541469.

[42] C. Djama *et al.*, « Experimental and Theoretical Study of Methylene Blue Adsorption on a New Raw Material, Cynarascolymus - A statistical Physics Assessment », Engineering, preprint, mai 2023. doi: 10.20944/preprints202305.0418.v1.

[43] D. Blau, L. Bach, M. Scott, et S. Rubin, « Clark Moustakas (1923–2012): Scholar, teacher, colleague and friend. », *Humanist. Psychol.*, vol. 41, nᵒ 1, p. 97-99, janv. 2013, doi: 10.1080/08873267.2013.752695.

[44] O. Amrhar, L. El Gana, et M. Mobarak, « Calculation of adsorption isotherms by statistical physics models: a review », *Environ. Chem. Lett.*, vol. 19, nᵒ 6, p. 4519-4547, déc. 2021, doi: 10.1007/s10311-021-01279-8.

[45] M. Ben Yahia, M. Tounsi, F. Aouaini, S. Knani, M. Ben Yahia, et A. Ben Lamine, « A statistical physics study of the interaction of [7]-helicene with alkali cations (K $^+$ and Cs $^+$): new insights on microscopic adsorption behavior », *RSC Adv.*, vol. 7, nᵒ 71, p. 44712-44723, 2017, doi: 10.1039/C7RA08387D.

[46] L. Sellaoui, H. Guedidi, S. Knani, L. Reinert, L. Duclaux, et A. Ben Lamine, « Application of statistical physics formalism to the modeling of adsorption isotherms of ibuprofen on activated carbon », *Fluid Phase Equilibria*, vol. 387, p. 103-110, févr. 2015, doi: 10.1016/j.fluid.2014.12.018.

[47] S. Mahmoudi, Z. Chemat-Djenni, A. Bouguettoucha, A. Guediri, D. Chebli, et A. Gil, « Removal of Pb (II) from aqueous solutions by new layered double hydroxides adsorbent MgCuCaAl-LDH: Free Gibbs energy, entropy and internal energy studies », *Inorg. Chem. Commun.*, vol. 144, p. 109910, oct. 2022, doi: 10.1016/j.inoche.2022.109910.

[48] A. Yazidi, L. Sellaoui, G. L. Dotto, A. Bonilla-Petriciolet, A. C. Fröhlich, et A. B. Lamine, « Monolayer and multilayer adsorption of pharmaceuticals on activated carbon: Application of advanced statistical physics models », *J. Mol. Liq.*, vol. 283, p. 276-286, juin 2019, doi: 10.1016/j.molliq.2019.03.101.

[49] D. Chaker *et al.*, *Experimental and Theoretical Study of Methylene Blue Adsorption on a New Raw Material, Cynarascolymus - A statistical Physics Assessment*. 2023. doi: 10.20944/preprints202305.0418.v1.

[50] L. Sellaoui *et al.*, « Implementation of a multilayer statistical physics model to interpret the adsorption of food dyes on a chitosan film », *J. Environ. Chem. Eng.*, vol. 9, n° 4, p. 105516, août 2021, doi: 10.1016/j.jece.2021.105516.

[51] A. Guediri, A. Bouguettoucha, D. Chebli, N. Chafai, et A. Amrane, « Molecular dynamic simulation and DFT computational studies on the adsorption performances of methylene blue in aqueous solutions by orange peel-modified phosphoric acid », *J. Mol. Struct.*, vol. 1202, p. 127290, févr. 2020, doi: 10.1016/j.molstruc.2019.127290.

[52] A. Geies, G. S. Gomaa, S. M. Ibrahim, A. F. Al-Hossainy, et F. K. Abdelwadoud, « Experimental and simulated TD-DFT study of malachite green dye and tetrahydroquinoxaline hybrid blend: Its application removal from wastewater », *J. Mol. Struct.*, vol. 1291, p. 136050, nov. 2023, doi: 10.1016/j.molstruc.2023.136050.

[53] A. Guediri, A. Bouguettoucha, D. Chebli, N. Chafai, et A. Amrane, « Molecular dynamic simulation and DFT computational studies on the adsorption performances of methylene blue in aqueous solutions by orange peel-modified phosphoric acid », *J. Mol. Struct.*, vol. 1202, p. 127290, févr. 2020, doi: 10.1016/j.molstruc.2019.127290.

[54] N. Somsesta, C. Piyamawadee, V. Sricharoenchaikul, et D. Aht-Ong, « Adsorption isotherms and kinetics for the removal of cationic dye by Cellulose-based adsorbent biocomposite films », *Korean J. Chem. Eng.*, vol. 37, n° 11, p. 1999-2010, nov. 2020, doi: 10.1007/s11814-020-0602-6.

[55] A. A. Babaei, A. Khataee, E. Ahmadpour, M. Sheydaei, B. Kakavandi, et Z. Alaee, « Optimization of cationic dye adsorption on activated spent tea: Equilibrium, kinetics, thermodynamic and artificial neural network modeling », *Korean J. Chem. Eng.*, vol. 33, n° 4, p. 1352-1361, avr. 2016, doi: 10.1007/s11814-014-0334-6.

[56] S. Chen *et al.*, « Study on the adsorption of dyestuffs with different properties by sludge-rice husk biochar: Adsorption capacity, isotherm, kinetic, thermodynamics and mechanism », *J. Mol. Liq.*, vol. 285, p. 62-74, juill. 2019, doi: 10.1016/j.molliq.2019.04.035.

[57] R. K. Ghosh, D. P. Ray, S. Debnath, A. Tewari, et I. Das, « Optimization of process parameters for methylene blue removal by jute stick using response surface methodology », *Environ. Prog. Sustain. Energy*, vol. 38, n° 5, p. 13146, 2019, doi: 10.1002/ep.13146.

[58] M. Danish *et al.*, « Optimization of banana trunk-activated carbon production for methylene blue-contaminated water treatment », *Appl. Water Sci.*, vol. 8, nº 1, p. 9, janv. 2018, doi: 10.1007/s13201-018-0644-7.

[59] K. N. Aboua, Y. A. Yobouet, K. B. Yao, D. L. Goné, et A. Trokourey, « Investigation of dye adsorption onto activated carbon from the shells of Macoré fruit », *J. Environ. Manage.*, vol. 156, p. 10-14, juin 2015, doi: 10.1016/j.jenvman.2015.03.006.

CHAPTER IV

IV.1 Introduction

Water resources encompass roughly 70% of the surface of our planet, which are crucial for the survival of living organisms and play a pivotal role in industrial and agricultural production [1]. However, over the past few decades, water resources have faced significant degradation, particularly due to the growth of the dye industry [2]. The wastewater generated by this industry contains a diverse array of pollutants, including azo dyes, pyridine, benzidine, heavy metal ions, cyanide, aromatic compounds, and landfill leachate, among others[3], [4]. Many of these pollutants, especially the chemical structures of most dyes, are characterized by their stability and complexity, making them challenging to degrade solely through natural environmental purification processes.

Methylene blue (MB), a water-soluble phenothiazine salt a prevalent blue and cationic type of dye, It exhibits a molecular weight of 319.85 g/mol and is characterized by the chemical formula $C_{16}H_{18}N_3Sl$, finds wide applications as a chemical indicator, dye, biological stain, and pharmaceutical agent [5]. However, it has garnered attention in the context of dye pollution due to its notable biotoxicity [6]. Moreover, when MB accumulates at certain concentrations, it can pose health risks to both animals and humans, potentially leading to biological abnormalities and even cancer [7]. Various sewage treatment technologies [8], such as coagulation [9], chemical oxidation [10], [11], [12], adsorption [13], [14], and photodegradation [15], have been developed to address the presence of MB in contaminated water . Among these methods, adsorption technology is a particularly suitable approach due to its versatility, cost-effectiveness, and high removal efficiency [16]. Nevertheless, the efficacy of adsorption is significantly influenced by the physicochemical properties of the adsorbents used, leading to substantial variability in removal efficiency. Therefore, selecting an appropriate adsorption material plays a pivotal role in determining the effectiveness of MB removal from wastewater, emphasizing the pressing need to develop cost-effective and highly efficient adsorbents.

The utilization of waste derived from fruits and vegetables for the development of adsorbent materials presents an opportunity for the efficient utilization of these waste resources [17], [18].

83

Consequently, there has been a focused investigation into the modification of biomass to enhance its adsorption capabilities [19]. Among the various approaches, chemical activation has garnered significant attention due to its capacity for rapid activation, resulting in the attainment of elevated specific surface areas and a profusion of pore structures. Multiple research studies have underscored the effectiveness of alkali molten pyrolysis as a means to increase the surface area of the biosorbent substantially. In this context, potassium hydroxide (KOH) has emerged as a commonly employed activating reagent for chemical activation. Several types of biomass including bamboo waste [20], coconut shell [21], jotaba fruits [22], soybean oil cake [23], and coconut leaves [24], have been discovered in the literature to have a high potential for removing pollutants from aqueous media.

In this study, particular attention was devoted to the preparation, characterization, and modeling of the adsorption behavior exhibited by an adsorbent material derived from fruit and vegetable waste, aiming at the effective removal of methylene blue from aqueous solutions. The process involved the collection, drying, grinding, sieving, washing, and treatment of fruit and vegetable peels with KOH to create the adsorbent material. Surface chemistry and morphological features of the adsorbent material were meticulously examined using FTIR spectroscopy and scanning electron microscopy (SEM), along with the experimental determination of the zero point charge (pHpzc). A series of adsorption experiments were meticulously conducted to scrutinize the kinetics and equilibrium of methylene blue (MB) adsorption onto the adsorbent material across varying temperatures and pH levels. The acquired adsorption data were subjected to rigorous analysis employing both kinetic and isotherm models to effectively simulate the adsorption phenomenon. Furthermore, advanced computational methodologies, including density functional theory (DFT) and molecular dynamics simulations, were employed to delve into the electronic properties and compute a spectrum of reactivity descriptors. This work stands out for

its innovative nature in several respects. Firstly, it pioneers the creative use of fruit and vegetable waste for producing an adsorbent material, thereby paving the way for sustainable valorization of agricultural resources. Secondly, this study adopts an integrated approach, combining thorough characterization of the adsorbent material with advanced experimental techniques and sophisticated computational models to model the adsorption process.

IV.2 Resultats and discussion

IV.2.1 Adsorption characterization

➢ **FT-IR**
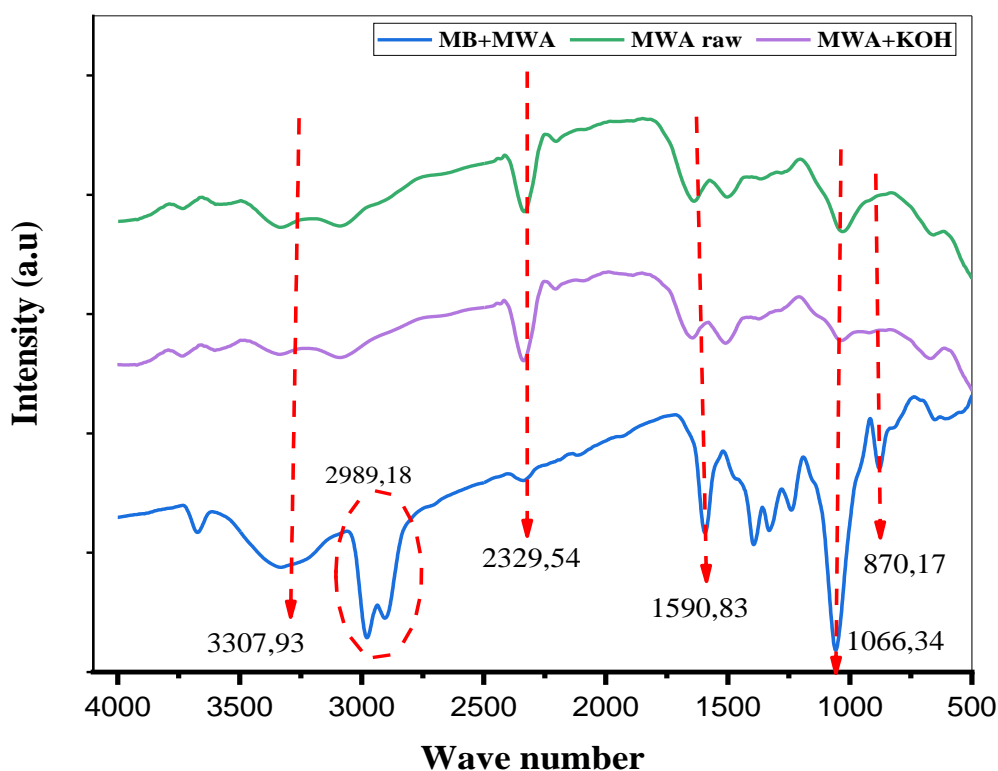
Figure IV. 1: FTIR spectra of MWA before and after MB dye adsorption.

Fig. IV.1 depicts the functional groups observed in the Fourier-Transform Infrared (FTIR) spectra of MWA both before and after MB adsorption. The FTIR peaks corresponding to different functional groups of MB, along with their assignments, are concisely summarized in **Table IV.1**.

Table IV. 1: IR Band Characteristics: Peak Location and Shape of Main Chemical Functional Groups in MWA Biosorbent Analyzed via FTIR [25], [26].

FTIR Wavenumbers (cm−1)	Assignments
3307.93	-OH, Hydroxyl group for alpha-cellulose band Broad
2986.18	symmetrical stretching C-H of -CH_2 band
2329.54	–COO Carbon dioxide band Small
1590.83	C=C side ring stretching
1066.34	C–O–C Ethers Very tiny sharp band
870.17	absorption of C–H in-plane bending vibration

> **SEM**

Fig. IV.2 exhibit scanning electron microscope imagery depicting activated biomass derived from food waste, specifically peels from various fruits and vegetables sourced from a restaurant, through KOH activation. Noteworthy alterations are discernible between the surfaces of the raw materials and the activated counterparts, characterized by the emergence of numerous pores. KOH activation of the mixed waste biomass facilitated the formation of a distinctive porous surface featuring spheroidal attributes. This spherical morphology potentially initiates the formation of spherical carbon, catalyzed by the disruption of bonds within the lignocellulosic biomass structure induced by the alkaline nature of KOH. Consequently, surface irregularities manifest in the form of sporadic cracks and pits.
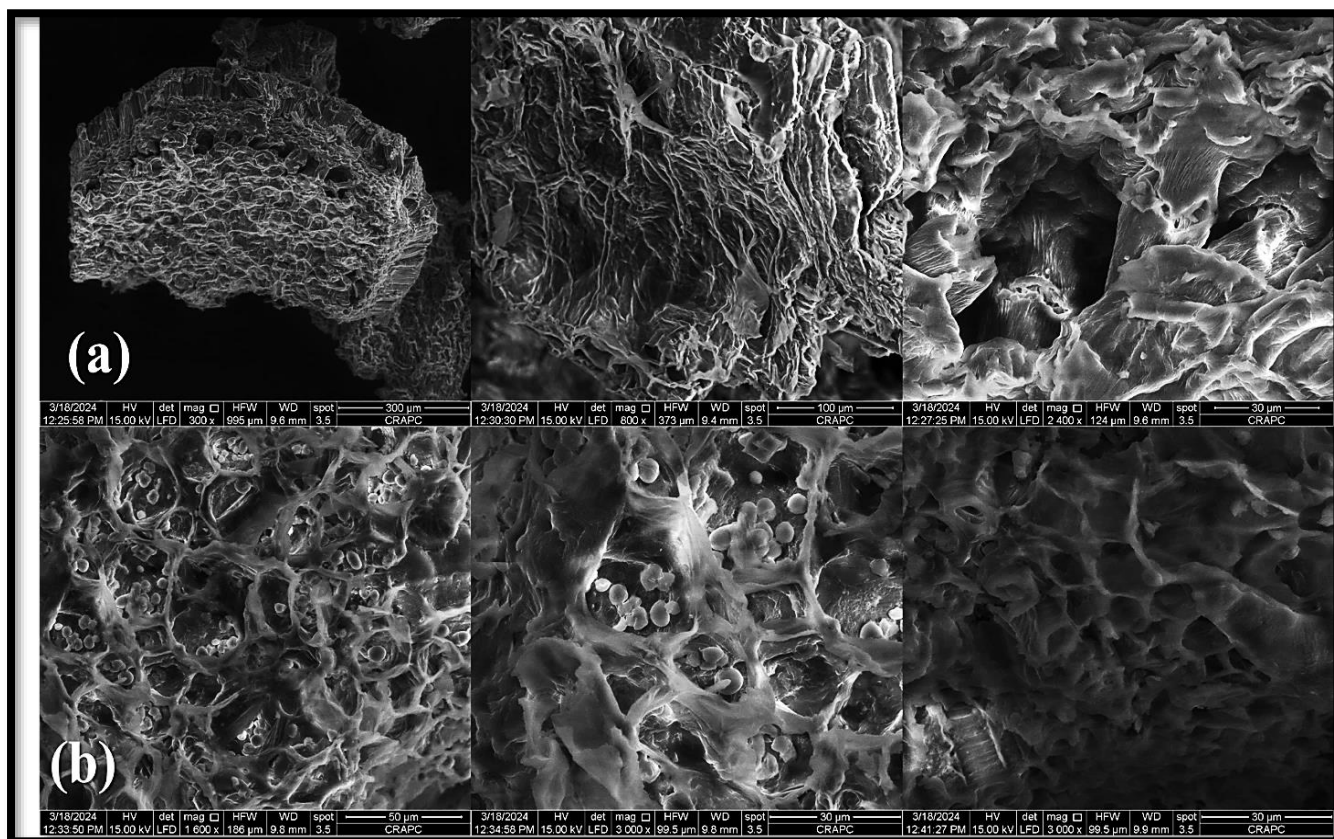
Figure IV. 2: *SEM images of (a) raw material, (b) activated biomass (MWA).*

➢ **The zero-charge point**

The **Fig. IV.3** illustrates the zero charge point value for MWA. The pH$_{PZC}$ for MWA is 6.23, indicating a nearly neutral sample. Following KOH modification, there is an increase in the presence of alkaline functional groups on the biomass surface. Consequently, when the pH is below 6.23, the surface of MWA carries a positive charge, whereas when the pH exceeds 6.23, the surface becomes negatively charged.
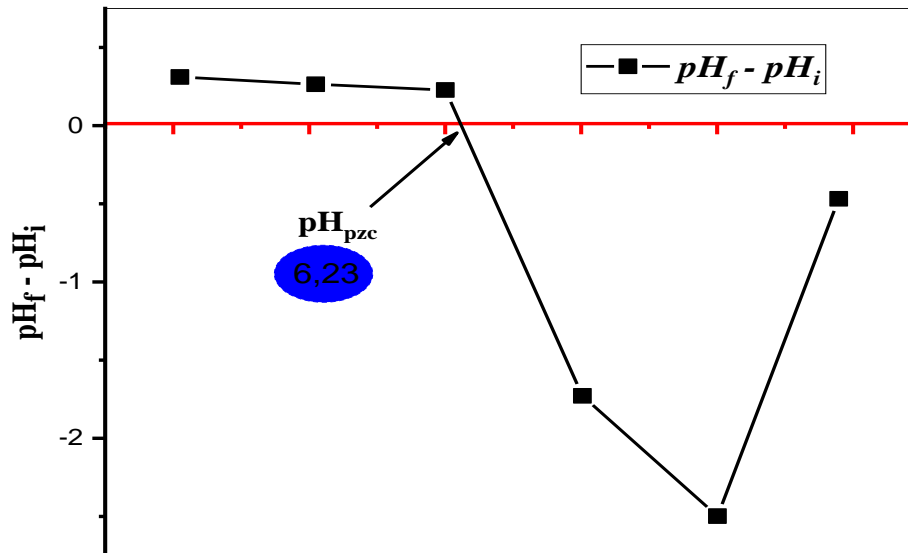
Figure IV. 3: The change of ΔpH about MWA at different pH.

IV.3 Functionality of the MB adsorption method

IV.3.1 Effect of biosorbent dose

The quantity of adsorbent employed plays a critical role in shaping adsorption dynamics, impacting the equilibrium between the adsorbent and the adsorbate in the system. The **Fig. IV.4** illustrates the influence of adsorbent dosage on the removal efficiency and adsorption capacity of MWA in MB adsorption. Notably, the removal efficiency experiences a substantial rise as the adsorbent dose increases from 0.2, 0.4, 1, and 2 g/L, reaching near-complete removal at 2 g/L, this behavior is attributed to the proliferation of active sites. However, the adsorption capacity plateaus beyond a certain threshold, potentially due to a relative decrease in MB molecules per unit of adsorbent. Consequently, an optimal adsorbent dosage of 1 g/L is identified to harness the maximum adsorption capacity, resulting in a removal rate of 95.98%.
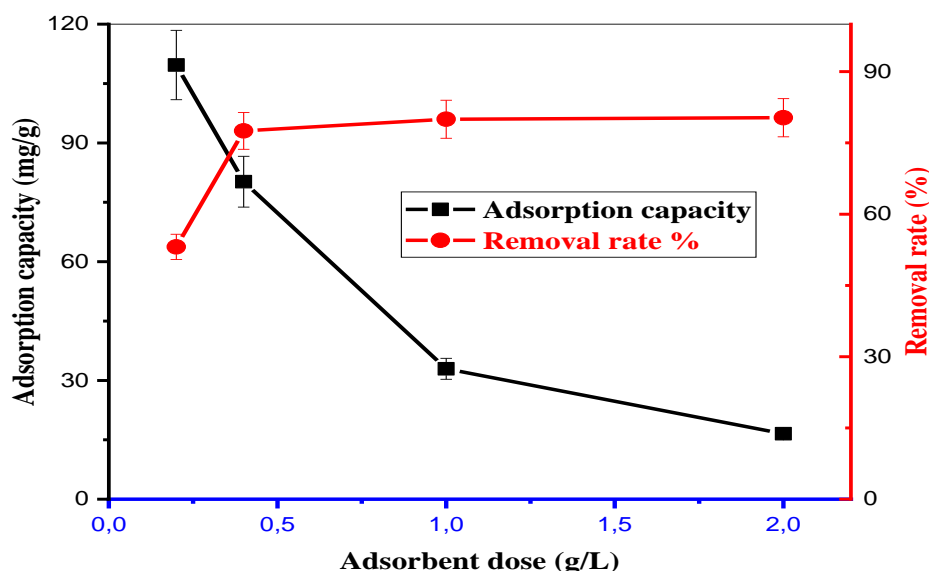
Figure IV. 4: Effect of adsorption dose of MB on MWA.

IV.3.2 Effect of solution pH and ionic strength

A particular salts, such as $NaNO_3$, Na_2SO_4, NaCl, and KCl, can have an impact on the adsorption capacity of biosorbents, Uniform concentrations of the employed agents, specifically 0.1 mol/L for selts, were maintained, while varying concentrations of the dye ranging from 20 to 100 mg/L were employed. Subsequent to the dissolution of salts in 50 ml of the MB dye, 50 mg of MWA adsorbent was introduced at 20°C under ambient pH conditions. The resultant mixtures underwent stirring using a multi-post magnetic stirrer for a duration of 24 hours, followed by centrifugation and subsequent analysis. The effectiveness of elimination of cationic pollutants from aqueous solutions is often significantly reduced when salt is available.

Fig. IV.5a demonstrates the impact of ionic strength on the MWA adsorption of MB. With the ionic strength, there was a pronounced decrease in the adsorbed quantity for material, diminishing from 219.07, 76.34, and 70.26 to 22.11 mg/g (without salts, NaSO4, NaNO3, and KCl). This decline signifies an adverse influence of salts on the adsorption process, likely stemming from the decomposition of inorganic salts into cationic and anionic ions. This process instigates competition between MB molecules and cations (Na+ and K+) for adsorption onto

the adsorbents. The adsorption capacity of a biosorbent for MB is significantly influenced by the pH parameter, affecting surface charges, the ionic state of biomass functional groups, and MB ionization. **Fig. IV.5b** illustrates the exploration of the initial solution pH impact on MB removal rate and adsorption capacity by MWA.

The consequential effect of pH on the biosorbent's MB adsorption performance is evident, characterized by a substantial augmentation in the adsorbed quantity, escalating from 39.56 to 72.71 mg/g within the pH range of 2 to 4. Meanwhile, the quantity of MB adsorbed exhibited relative constancy within the pH range of 4 to 12. Notably, pH 8 was selected as the optimal condition for the entirety of subsequent experiments. The observed variation in MB adsorption performance can be elucidated by the relationship between pH fluctuations and the corresponding modulation of negative charges on the MWA biosorbent surface. This phenomenon is attributed to the pH at the point of zero charge of MWA, which is determined to be 6.23. With an increase in solution pH, there is a concomitant rise in the negative charges present on the MWA surface. Consequently, under alkaline pH conditions, there is an augmented availability of negative charges on the adsorbent surface. This heightened accessibility of negative charges facilitates and enhances the favorability of the adsorption of MB, owing to its cationic nature.
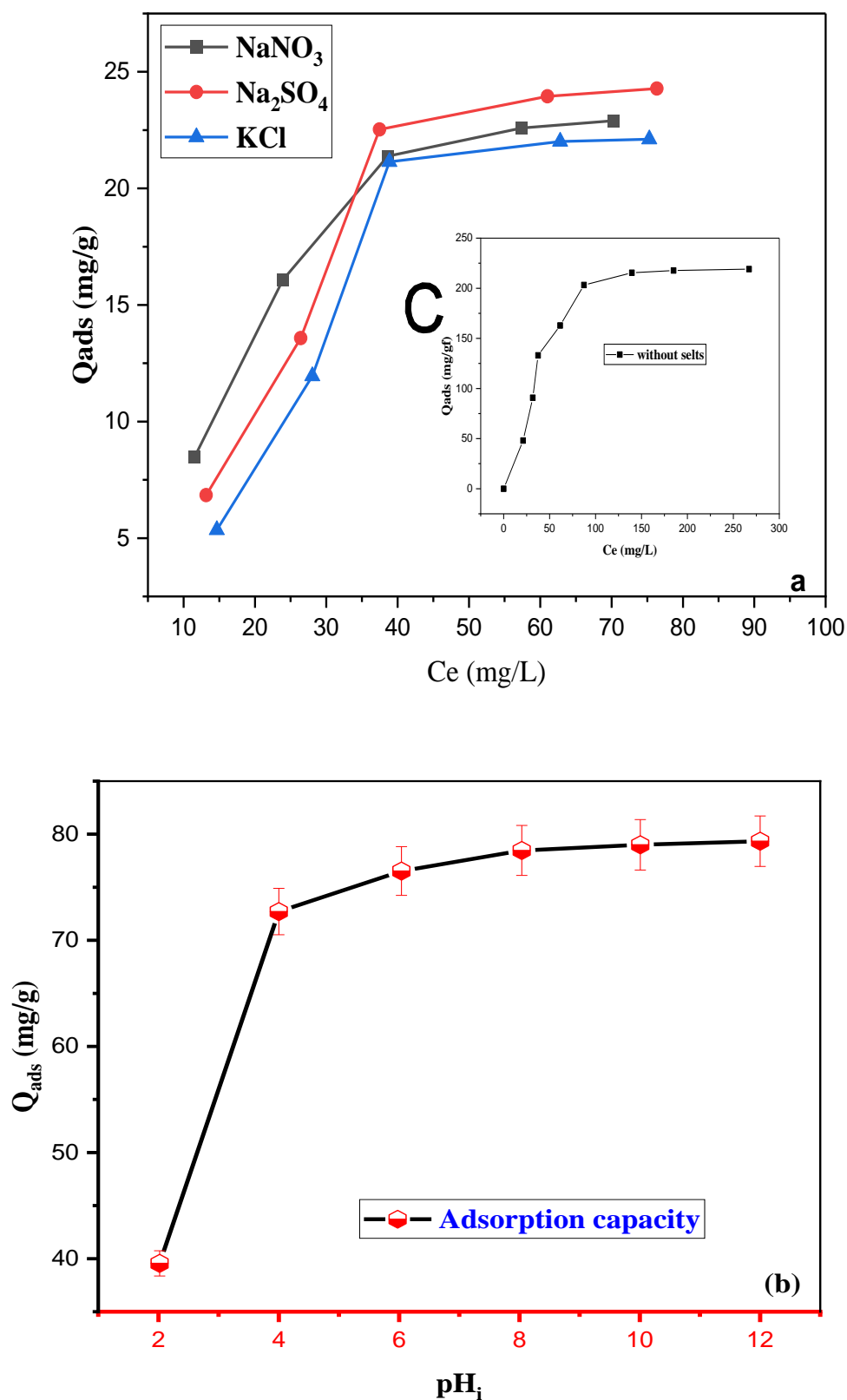
Figure IV. 5: *ionic strength (a), (b) and Effect of solution pH on the amount of MB adsorbed onto MWA.*

IV.4 Kinetics and isotherms of MB adsorption
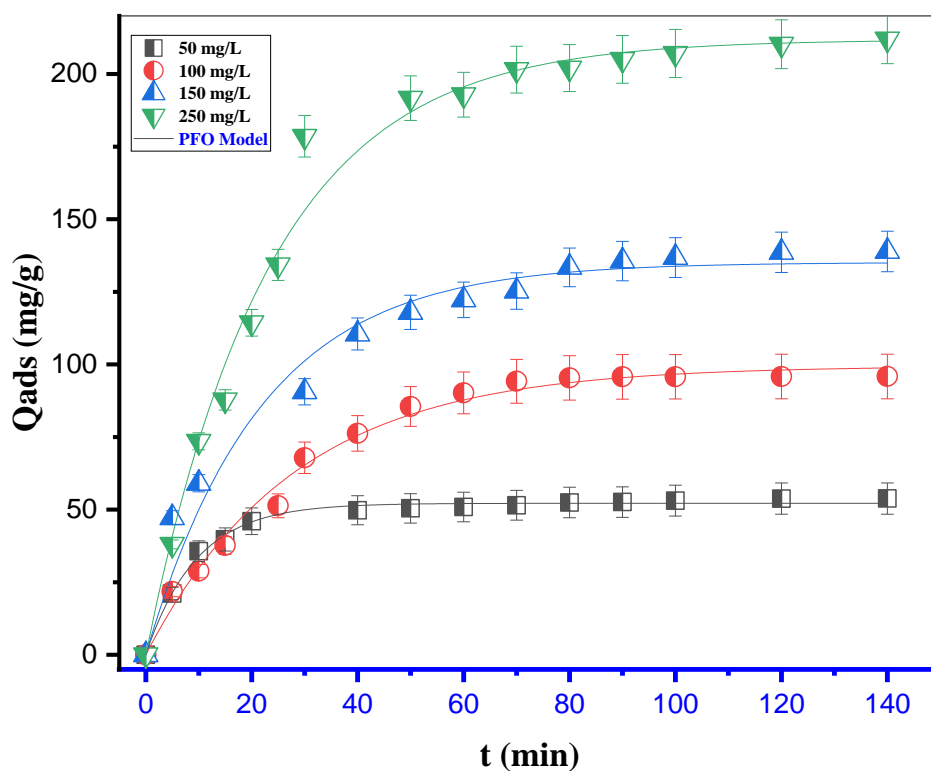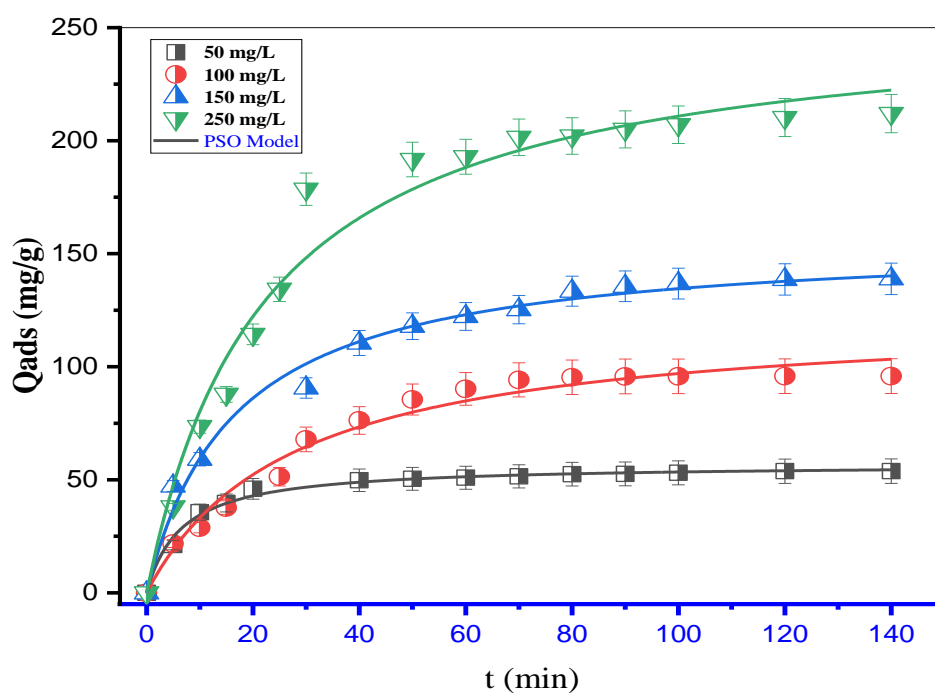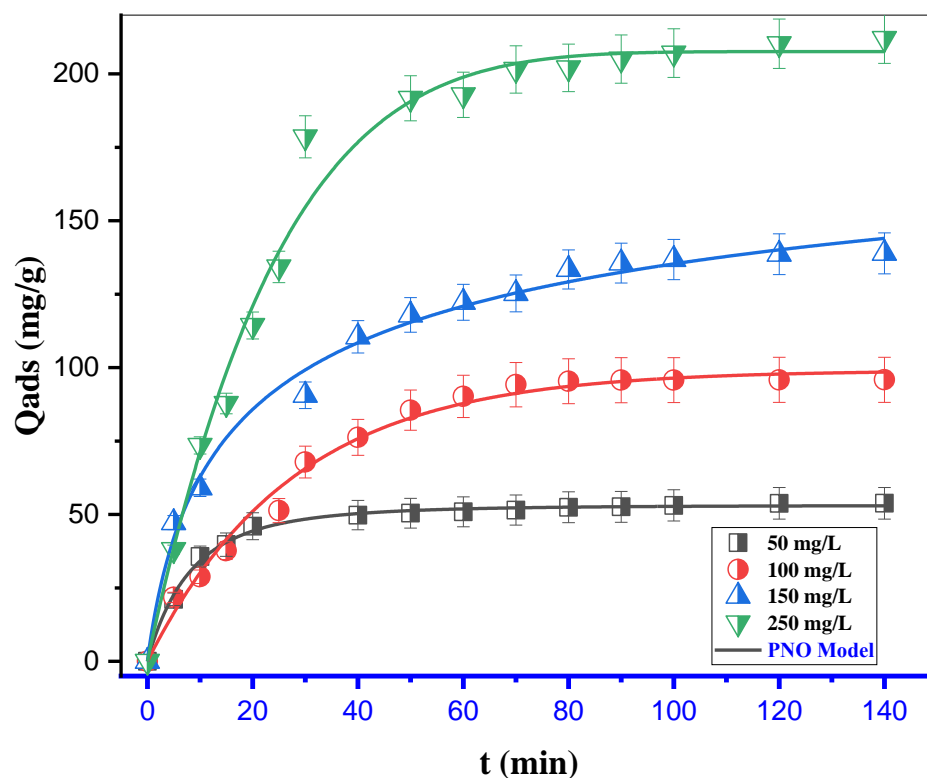
***Figure IV. 6:** kinetics models' adsorption of MB on MWA from aqueous solution at pH 8.*

Adsorption kinetics, which involves the determination of the quantity of adsorbate adhering to the adsorbent at constant concentration over varying time intervals, plays a pivotal role in understanding the dynamic adsorption process. The diverse constants associated with PFO, PSO, and PNO kinetic models have been elucidated in **Table IV.2**. The absorption profiles of different concentrations at distinct time points are depicted in **Fig. IV.6**. Notably, the PSO kinetic model exhibited the highest correlation coefficient, indicating its superior fitting to the empirical data. In accordance with the PSO kinetic model, the adsorption of the adsorbate onto the adsorbent is directly proportional to the available binding sites on the sorbent, affirming a chemisorptive nature of the dye molecule interaction. The data further reveal a substantial adsorption of dye molecules within the initial 40 minutes, with a subsequent diminishing sorption trend as the duration extends. Approximately 90% of the solution was adsorbed within the initial 60 minutes, suggesting an equilibrium time that could be considered for future batch experiments.

Table IV. 2: Parameters fitting nonlinear data of kinetics adsorption.

models	Parameters	50 mg/g	100 mg/g	150mg/g	250mg/g
PFO	Q_e	52.197	99.465	135.147	211.874
	K_1	0.104	0.035	0.046	0.042
	R^2	**0.994**	**0.990**	**0.969**	**0.986**
PSO	Q_e	56.954	123.410	156.594	257.535
	K_2	0.00267	$2.975^E\text{-}4$	$3,900^E\text{-}4$	$1.754^E\text{-}4$
	R^2	**0.991**	**0.978**	**0.988**	**0.974**
PNO	Q_e	53.134	99.085	236.873	207.583
	k_n	0.004	$6.075^E\text{-}7$	4.620	0.0100
	N	1,319	1	4.620	0.823
	R^2	**0.996**	**0.988**	**0.990**	**0.985**

The results of the study were used to characterize Langmuir and Freundlich isotherms illustreted in **(Fig. IV.7 and Table IV.3)**. The elevated correlation coefficients ($R^2 > 0.99$) underscore the superior suitability of the Langmuir model in describing the equilibrium adsorption data for MB on the surface of MWA. This is attributed to a monolayer coverage of MB, indicative of a homogeneously distributed array of active sites on the surface of biosorbent. The maximum adsorption capacity of a monolayer of MB on MWA was determined to be 129.93 mg/g at 10 °C, exhibiting an augmentation to 258.42 mg/g at 40 °C. The Freundlich isotherm reveals a notable affinity for MB adsorption on MWA, as evidenced by values of 1/n within the range of 0 to 1. Conversely, lower R^2 values imply the inadequacy of the model in accommodating experimental data. The application of two conventional models for constructing the dynamics of MB uptake proves insufficient. Consequently, the nuanced and

regulated interaction between MB and MWA necessitates theoretical treatment employing sophisticated models.
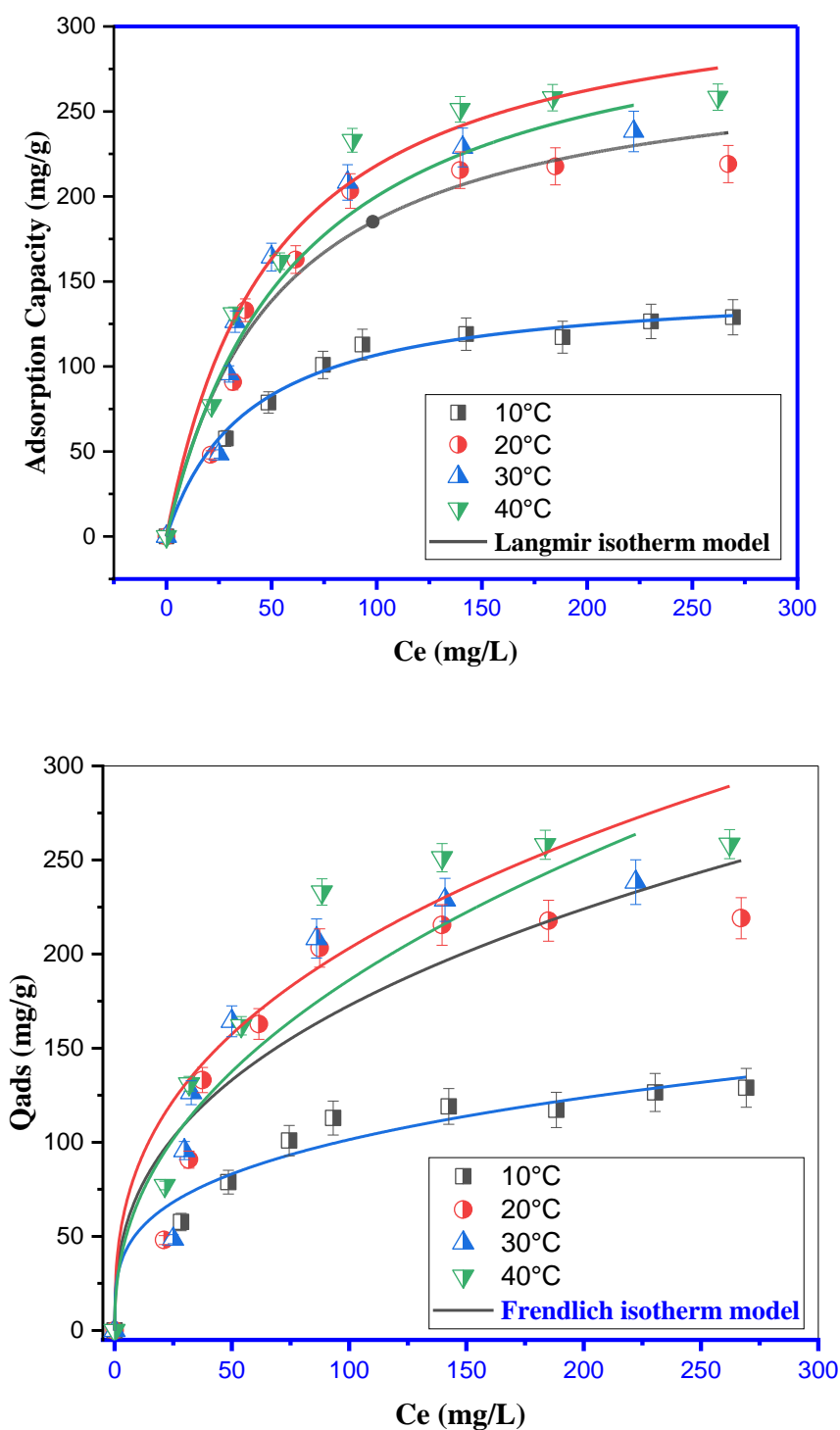
Figure IV. 7: *Isotherms of the adsorption of MB on MWA from aqueous solution at pH 8.*

Table IV. 3: Parameters fitting nonlinear data of isotherms.

Models	Parameters	10 °C	20 °C	30 °C	40°C
Langmuir	Q_m(mg • g^{-1})	129.930	234.259	249.877	258.420
	K_L (L • mg^{-1})	0.025	0.019	0.016	0.019
	R^2	**0.989**	**0.947**	**0.977**	**0.937**
Freundlich	N	3.493	2.662	2.293	2.726
	K_F(mg•g^{-1})(L/mg)$^{1/n}$	27.142	30.623	24.996	37.502
	R^2	**0.962**	**0.883**	**0.889**	**0.932**

Fig. IV.8 elucidated advanced models, denoted as ME$_1$ and ME$_2$, employed for comprehending the adsorption dynamics of MB on the MWA biomass, as evidenced by the correlation coefficients (R^2) provided in **Table IV.4**. Among the sophisticated statistical physics models considered, the most adept in capturing the intricacies of MB adsorption onto the MWA adsorbent was determined to be ME$_2$, specifically characterized as the double-energy single-layer model.
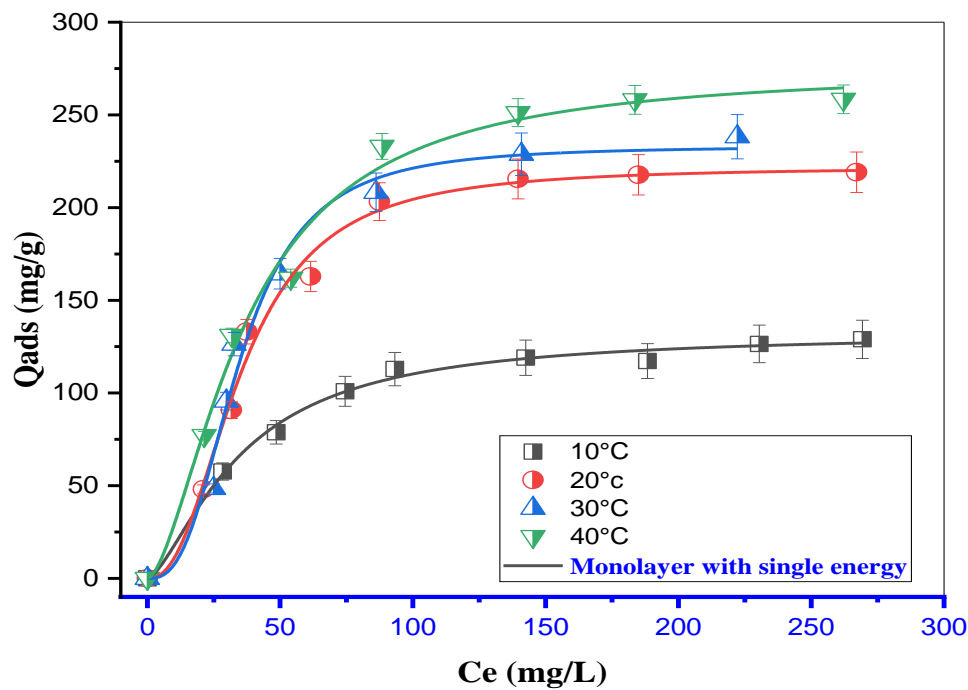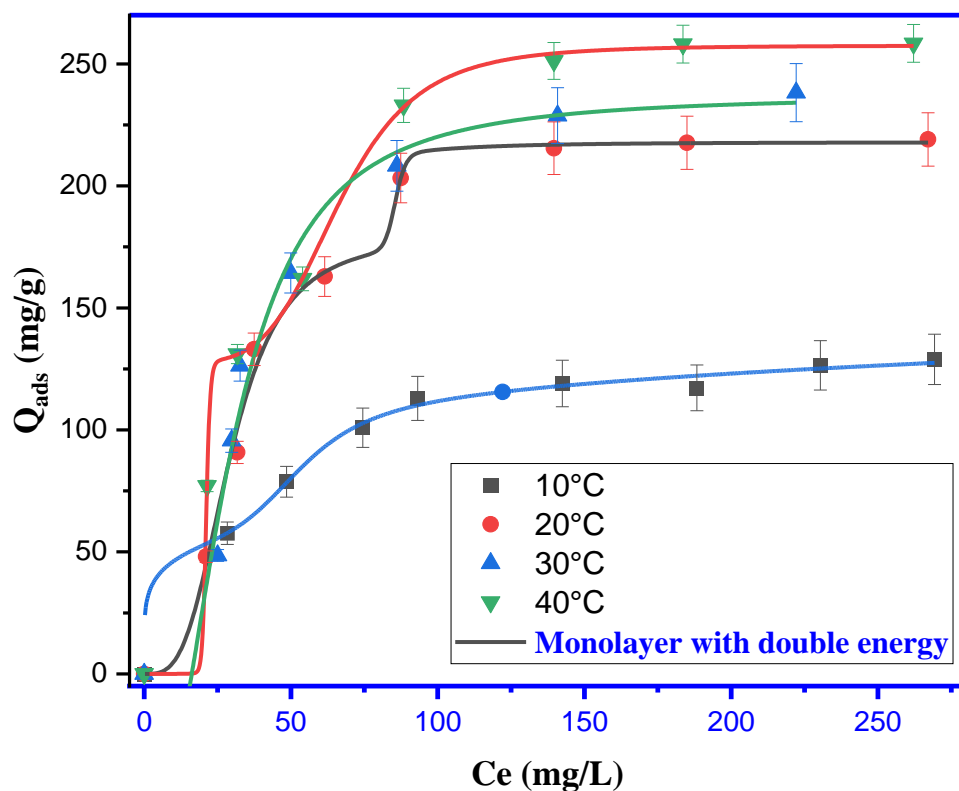
***Figure IV. 8:** The findings were acquired from fitting isotherm data, the adsorption of MB onto MWA adsorbent, were analyzed using ME1 and ME2 models.*

***Table IV. 4:** The determined parameter values for advanced models.*

Models	Parametrs	T = 283 K	T = 293 K	T = 303 K	313 K
ME$_1$	n	1.508	2.363	2.759	1.649
	N$_m$	88.039	93.854	84.474	166.764
	C$_{1/2}$	34.863	35.270	34.671	36.926
	R^2	**0.994**	**0.992**	**0.983**	**0.991**
ME$_2$	n$_1$	4.751	3.315	0.791	32.389
	n$_2$	0.180	48.228	2.262	4.928
	N$_{m1}$	9.262	53.953	82.548	3.937
	N$_{m2}$	76.571	51.953	0.348	168.192
	C$_1$	53.447	29.370	1.192^E-13	21.142
	C$_2$	33.115	85.524	28.643	66.243
	R^2	**0.997**	**0.996**	**0.988**	**0.999**

IV.5 Steric parametrs

Since steric parameters shed light on the specificity of the adsorbed species for the adsorption sites, interpreting them is a crucial first step in comprehending the adsorption equilibrium.

The following provides specifics on "**Parameter n**" is the initial steric parameter. It shows how many species are adsorbed on an adsorption site at equilibrium. This parameter, allows one to infer the possible orientation of molecules or ions on an adsorption site and provides insight into the degree of clustering of those molecules or ions. the main steric properties [27]. The determination of the n parameter gives rise to three distinct scenarios characterizing the adsorption shape and mechanism: For Si where (n > 1), the adsorption of MB transpires in a vertical orientation, facilitated by a multi-interaction process. Conversely, when (n < 1), MB adsorption occurs horizontally through a multi-docking process, wherein multiple MWA functional groups can bind to a single molecule of the studied dye. The condition where (n = 1) signifies the attachment of the adsorbed species to an adsorption site in a non-parallel configuration, indicative of a mono-adsorbate process leading to the formation of a monomer [28], [29].

In **Fig. IV.9**, the values of the n parameter are depicted at temperatures of 283, 293, 303, and 313 K, and the corresponding values are tabulated in **Table IV.5**. Specifically, the n_1 values associated with these temperatures were determined as 4.751, 3.315, 0.791, and 3.389, while the n_2 values were found to be 4.751, 3.315, 8.088, and 32.389 at 283, 293, 303, and 313 K, respectively. The interaction between MB and MWA displayed a vertical (non-parallel) arrangement, indicative of a multimolecular mechanism, as suggested by the n_1 values. Additionally, the second variable n_2 exhibited molecule adopted a vertical setting, reflecting a multimolecular mode.

The number of adsorption sites occupied in a unit mass of adsorbent is defined by the steric parameter known as **the N_m**. Additionally, it shows how many adsorption sites are

accessible for species that are adsorbed at equilibrium. The upward trajectory of this parameter is the inverse of that of parameter n; as n rises, fewer accessible adsorption sites are available, and vice versa [30].

Fig. IV.9 shows how receptor site density (Nm) varies with temperature. As the temperature rose, there was a tendency toward a reduction in the densities of the MWA receptor sites, namely Nm_1 and Nm_2. An augmentation in the quantity of molecules. collected (n_1 and n_2 per site) is connected with this event, suggesting that there is a greater propensity for aggregation when the temperature rises.

As a steric parameter, $\mathbf{Q_{sat}}$ **(the saturation adsorption amount)** is reliant on other steric parameters ($Q_{sat,i}=N_{mi}*n_i$). In line with the most applicable statistical physics model, Q_{sat} can be described in terms of the number of species adsorbed per adsorption site, the density of adsorption sites, and/or the creation of layers [27]. This statistic makes it possible to evaluate how well the adsorbent used in the adsorption process is working [29].

The temperature-dependent fluctuation of the total saturation adsorption amount was illustrated visually in **Fig. IV.9**. A significant sensitivity to temperature changes was seen in the total adsorbed quantity at saturation. In particular, a rise in temperature resulted in a fall in the amount adsorbed, which may be attributed to the exothermic nature of the adsorption process, which is a hallmark of traditional adsorption phenomena.
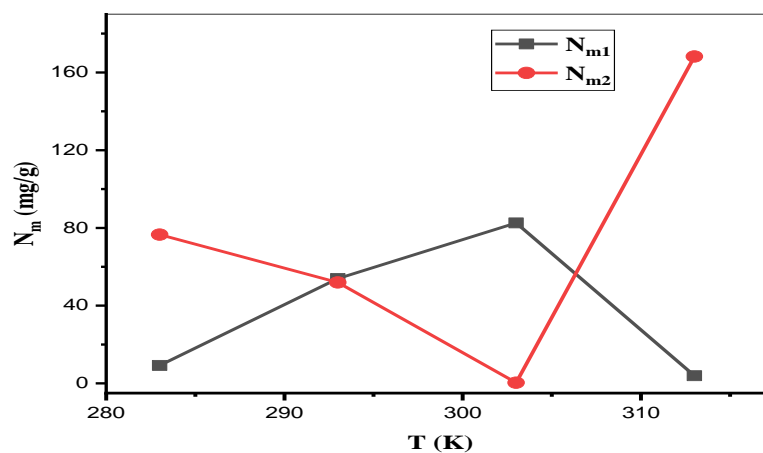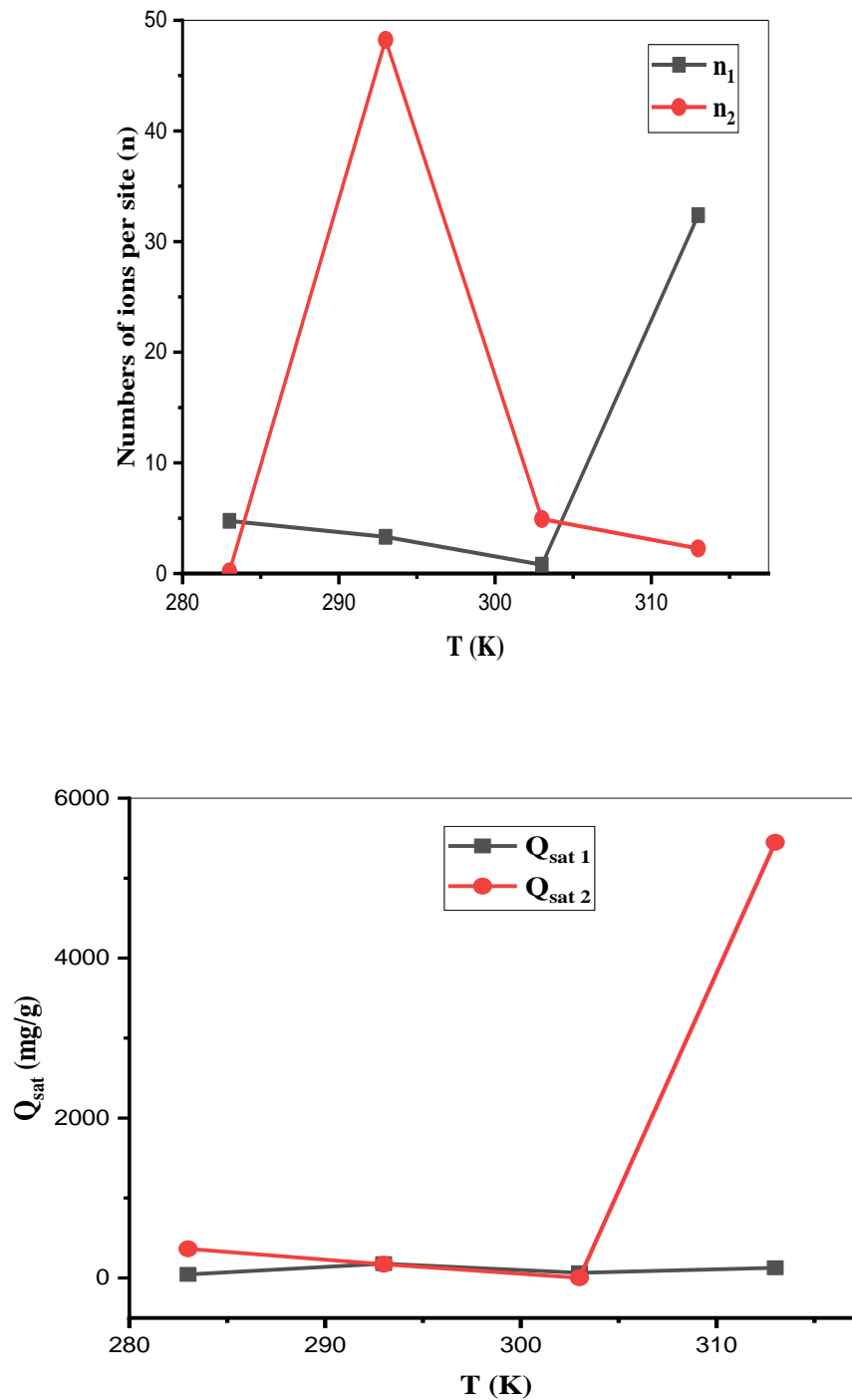
Figure IV. 9: The temperature-dependent changes in Nm, n, and Qsat for MB-MWA adsorption.

IV.6 Thermodynamic study

The use of the complex Double-energy single-layer model (ME_2) allows thermodynamic quantities such as entropy, Gibbs free energy, and internal energy to be calculated.

Table IV. 5: Thermodynamics function according to the ME2 model [31].

Function	Equation	Number	
Entropy	$$\frac{S_a}{K_B} = N_1\left[ln\left(1 + \left(\frac{C_e}{C_1}\right)^{n_1 m}\right) + \frac{n_1 ln\left(\frac{C_1}{C_e}\right)}{1 + \left(\frac{C_1}{C_e}\right)^{n_1 m}}\right]$$ $$+ N_2\left[ln\left(1 + \left(\frac{C_e}{C_2}\right)^{n_2}\right) + \frac{n_2 ln\left(\frac{C_2}{C_e}\right)}{1 + \left(\frac{C_2}{C_e}\right)^{n_2}}\right]$$	**(IV.1)**	S_a: Entropy K_B: Boltzmann constant (J/K). G: Gibbs free enthalpy
Gibbs free enthalpy	$$G = K_B T ln\left(\frac{C_e}{Z_v}\right)\left[\frac{Q_{sat1}}{1 + (\frac{C_1}{C_e})^{n_1 m}} + \frac{Q_{sat2}}{1 + (\frac{C_2}{C_e})^{mn_2}}\right]$$ $$Z_v = \frac{Z_{gtr}}{V} = \left(\frac{2\pi m K_B T}{h^2}\right)^{3/2}$$	**(IV.2)**	Z_v: Translation partition function per unit volume. Z_{gtr}: The translation partition function.
Internal energy	$$E_{int} = K_B T\left[N_{1s}\frac{ln(\frac{C_e}{Z_v}) + n_{1m}ln(\frac{C_1}{C_e})}{1 + (\frac{C_1}{C_e})^{n_1 m}}\right.$$ $$\left. + N_{2s}\frac{ln(\frac{C_e}{Z_v}) + n_2 m ln(\frac{C_2}{C_e})}{1 + (\frac{C_2}{C_e})^{n_2 m}}\right]$$	**(IV.3)**	E_{int}: System internal energy (J/mol) V: Volume(L). h: Planck constant (J/s) m: Adsorbent mass (g)

The evaluation of **internal energy (E_{int})** provides a thorough approach to assessing the various energy contributions within the MB adsorption system [28], [30]. The overarching representation of internal energy is expressed by **Equation (IV.3)**, as outlined in **Table IV.5**. The internal energy values for the investigated adsorption system are graphically depicted in **Fig. IV.10**. Remarkably, all documented internal energy values exhibit negativity, indicating that energy is released at the same time as the Methylene Blue adsorption systems spontaneously form.

The calculation of **Gibbs free enthalpy** involves the application of **Equation (IV.2)**, elucidated in **Table IV.5**, with dependence on the ME_2. Subsequently, the graphical representation of Gibbs free enthalpy is conducted in relation to adsorbate concentrations across various temperatures for the MWA adsorbent, as depicted in **Fig IV.10**. The observation within

Fig. IV.10 emphasizes the negative values of Gibbs free energy, indicative of the spontaneous nature of the adsorption process. Furthermore, a rise in temperature is associated with a concurrent decrease in free enthalpy, suggesting a consequential reduction in the efficacy of the adsorption process [32].

The data presented in **Fig. IV.10**, illustrating **the entropy** variation based on the utilization of the ME_2 model as per **Equation (IV.1)** outlined in **Table IV.5**, reveals two distinct concentration-dependent behaviors. Notably, at lower concentrations ($C_{1/2} > C$), there is a conspicuous increase in entropy, indicative of heightened molecular disorder. This phenomenon suggests that MB molecules undergo random movement across the surfaces of the biosorbent MWA, facilitated by the abundant active sites provided by MWA at low concentrations. This, in turn, enhances the adsorption process. Conversely, at higher concentrations ($C_{1/2} < C$), an opposing trend is observed. The concentration increment results in a reduction of entropy, which can be attributed to a plausible decrease in the number of available receptor sites on MWA for adsorption as the concentration rises. This insight highlights the intricate interplay between concentration levels, molecular dynamics, and the availability of active sites in governing the entropy variations within the Methylene Blue adsorption system [33], [34].
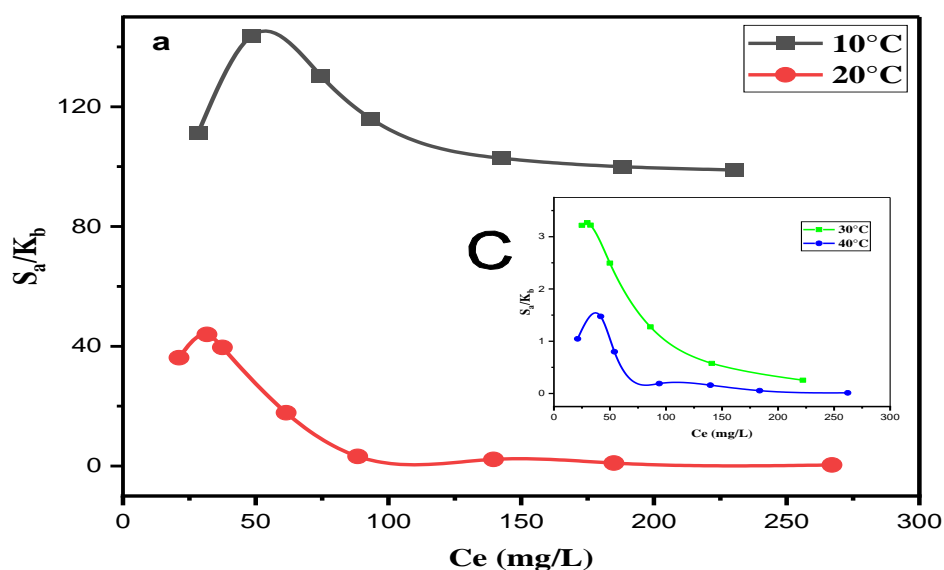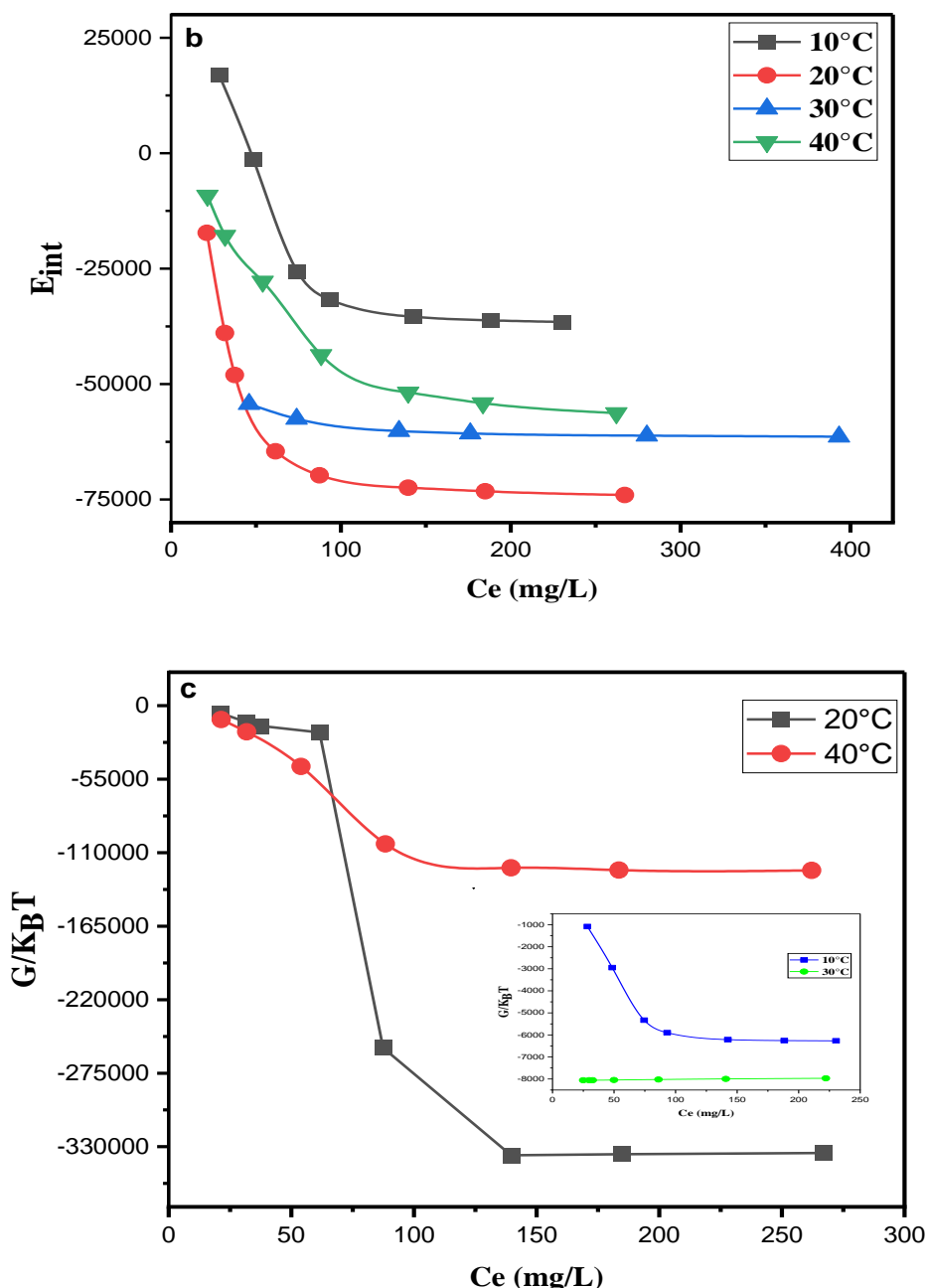
Figure IV. 10: *The progression of entropy (a), internal energy (b), and free enthalpy (c) concerning the absorption of MB by an MWA was investigated as a function of concentration at various temperatures.*

IV.7 Application of Density Functional Theory and Molecular Dynamics Simulations

IV.7.1   Molecular Orbital and Reactivity Measures

In this investigation, the B3LYP method was employed to compute the reactivity indices via Density Functional Theory, aiming to identify the adsorption sites of the MB. **Fig. IV.11** presents the molecular electrostatic potential (MEP), as well as the HOMO and LUMO Orbital, highlighting active regions and discerning reactive sites within the MB. Based on the MEP

Fig.IV.11(d), areas highlighted in red and yellow denote electrophilic regions (electron-donating), while blue regions signify nucleophilic areas. As per the analysis, the HOMO orbitals are concentrated around the amino groups N (38) and carbons C (3), C (2), and C (4) of the MB molecules. Conversely, the LUMO orbitals predominantly localize near the amino groups N (19) and carbons C (11), C (12), and C (13) of the molecule, indicating these specific atoms as primary active sites.

Quantum chemical parameters were utilized to examine the reactivity of molecules. The inclination of molecules to donate electrons is linked with the E_{HOMO}, whereas the propensity of molecules to accept electrons is linked with the E_{LUMO} [35]. The quantum chemical characteristics of MB, as determined by the DFT/B3LYP technique, are shown in **Table IV.6**. Hardness **(η)** provides insight into a molecule's ability to retain electrons within its environment. A lower hardness value suggests that the chemical compound is highly reactive and less stable [36]. Furthermore, a diminished **ΔE_{GAP}** value signifies heightened molecular reactivity, promoting the adsorption of MB onto the cellulose surface, thus indicating a highly stable adsorption process. The lower χ values allowing species to achieve electron equilibrium more readily, thereby enhancing their reactivity [37]. In contrast, global softness **(S)** signifies the general inclination of a molecule to undergo chemical reactions. Meanwhile, electronic chemical potential **(μ)** aids in ascertaining the direction of electron transfer during the condensation of molecules [38].

The electrophilicity index **(ω)** reflects the molecules' capacity to capture electrons, potentially leading to an increased adsorption process as the ω value decreases. A reduced $\omega-$ value signifies an increased propensity for electron donation, whereas a higher $\omega+$ value of a chemical species indicates a superior ability to accept electron density [39].

Table IV. 6: *Quantum Chemical Parameters (eV) of MB Molecules in Aqueous Solution Determination.*

Parameter (ev)	E_{HOMO}	ELU_{MO}	ΔE^{Gap}	μ	η	X	S	ω	ω^+	$\omega-$	ΔN_{max}
Value	-0.13462	-0.00277	0.13185	0.00277	-0.13739	0.13739	7.584376	0.143163	0.009684	0.078379	2.084
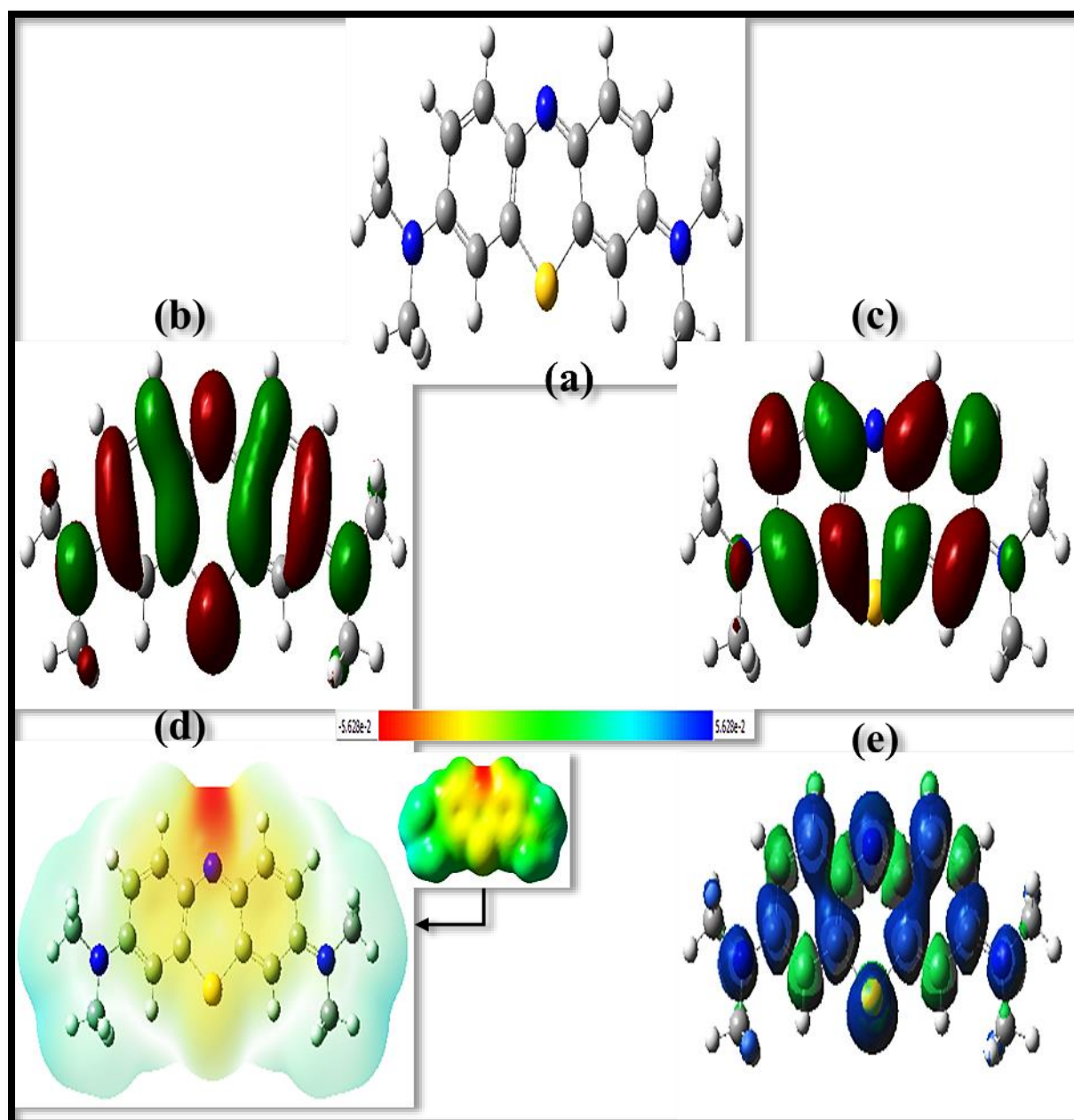
Figure IV. 11: *(a) Enhanced Molecular Architectures, Density Mapping of Frontier Molecular Orbitals (HOMO (b), LUMO (c)), (e) electron density from spin sfc, and (f) Molecular Electrostatic Potential (MEP) Evaluation for MB.*

IV.7.2   Molecular Dynamic Simulation study

MD simulation was utilized to compute adsorption energies governing the interaction between molecules and the graphite (1 0 1) surface. **Table IV.7** presents the calculated descriptors by the adsorption locator, along with the total energy, expressed in kcal/mol, associated with the substrate-adsorbate arrangements. It encompasses the summation of energy contributions from adsorbate components, rigid adsorption energy, and deformation energy. This metric encapsulates the collective influence of both rigid adsorption energy and deformation energy on the adsorbate components. **Table IV.7** also illustrates (dE_{ads}/dN_i), indicating the energies of MB configurations when a single adsorbate component is removed. Negative $E_{adsorption}$ numbers serve as indicators of the adsorption process' exothermic (chemisorption) and spontaneous nature, with a stable and strong surface, is further supported by the rigid adsorption energy values.
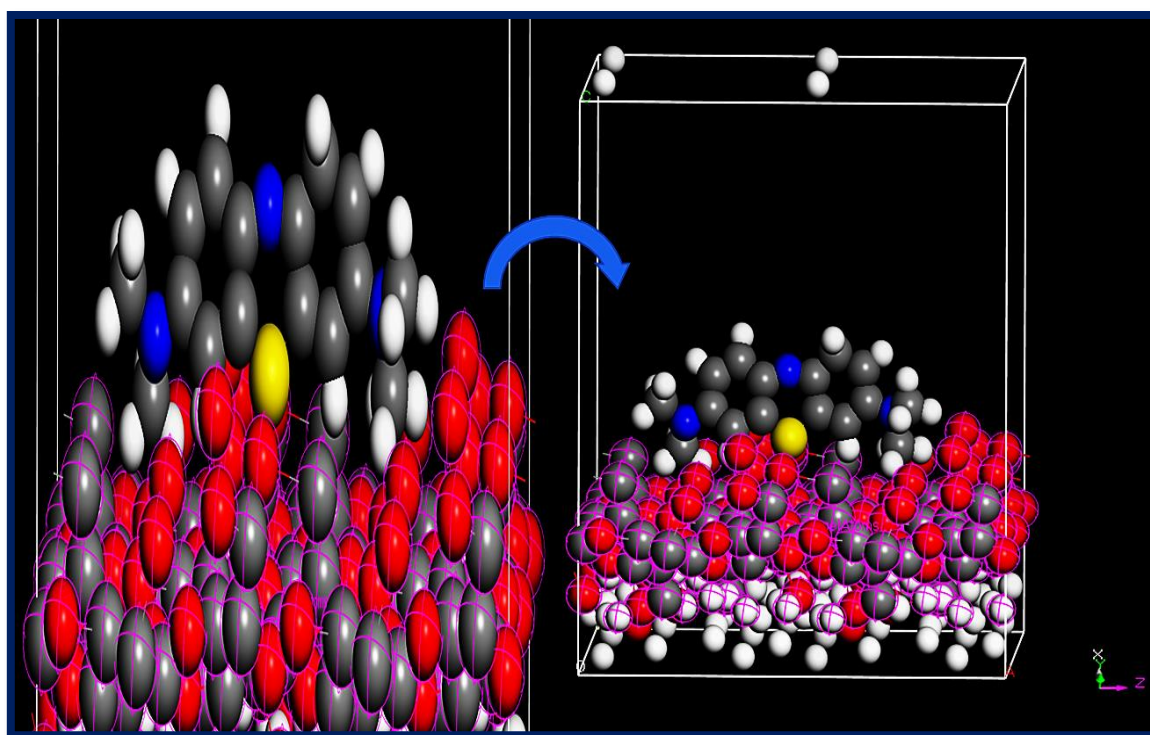
Figure IV. 12: Alternative views of stable adsorption configurations for MB on cellulose (1 0 1) obtained through the. Adsorption Locator module

Table IV. 7: MDS-generated results for the adsorption process of MB onto cellulose.

Adsorption energy, Kcal/mol	Rigid adsorption energy, Kcal/mol	Deformation energy, Kcal/mol	BM: d Fad/dNi	Total energy, Kcal/mol
-16.366	-17.102	0.735	-16.366	-83.757

IV.8   Comparative Analysis of Results with Published Findings

The adsorption capacity, as outlined in **Table IV.11**, discloses a significant maximum adsorbed quantity of 258.48 mg/g concerning the absorption of MB per the MWA adsorbent, as predicted by the Langmuir equilibrium model.

Table IV. 8: *Comparative Evaluation of Adsorption Capacities for MB Dye Across Different Adsorbents.*

Adsorbent	Adsorption capacity	Reference
Pristine wild sugarcane	20.917 mg/g	[40]
Solid waste of lemongrass	122.12 mg/g	[41]
Cassava bagasse	170.13 mg/g	[42]
Cucumis sativus peels	21.45 mg/g	[43]
Fig leaf	41.7 mg/g	[44]
This article	258.48 mg/g	

IV.9   Conclusion

This study has presented a comprehensive exploration aimed at optimizing adsorption efficiency using agricultural waste biomass for the removal of organic pollutants, with a specific focus on the model pollutant Methylene Blue (MB). The activation of biomass derived from food waste, particularly peels sourced from various fruits and vegetables, using KOH has been shown to enhance the adsorption properties through the development of a porous surface morphology. The observed alterations in surface characteristics underscore the efficacy of KOH activation in augmenting the adsorption capacity of the biomass. Characterization of adsorption dynamics revealed the pivotal influence of key parameters such as biosorbent dose and solution

pH. Optimal conditions were identified, demonstrating near-complete MB removal and highlighting the critical role of active sites and surface charge in governing adsorption efficiency. The adsorption capacity plateaued at a biosorbent dose of 1 g/L, achieving a removal rate of 95.98%. Furthermore, molecular dynamics simulations and Density Functional Theory (DFT) computations provided valuable insights into the molecular interactions and reactivity descriptors governing MB adsorption. In summary, this study advances our understanding of adsorption processes utilizing agricultural waste biomass and provides valuable insights and tools for sustainable environmental remediation endeavors. The meticulous optimization of adsorption conditions accurately predicted a maximum MB adsorption capacity, closely aligning with experimental measurements and highlighting the practical applicability of the developed methodologies. The results obtained from each phase of the study were crucial in informing the overall conclusions and implications for future research in this critical field.

Reference chapter IV

[1] H. Hu *et al.*, « NiFe-LDH nanosheet/carbon fiber nanocomposite with enhanced anionic dye adsorption performance », *Applied Surface Science*, vol. 511, p. 145570, mai 2020, doi: 10.1016/j.apsusc.2020.145570.

[2] Md. A. Islam *et al.*, « Removal of dye from polluted water using novel nano manganese oxide-based materials », *Journal of Water Process Engineering*, vol. 32, p. 100911, déc. 2019, doi: 10.1016/j.jwpe.2019.100911.

[3] K. L. Yu *et al.*, « Adsorptive removal of cationic methylene blue and anionic Congo red dyes using wet-torrefied microalgal biochar: Equilibrium, kinetic and mechanism modeling », *Environmental Pollution*, vol. 272, p. 115986, mars 2021, doi: 10.1016/j.envpol.2020.115986.

[4] S.-Y. Li, H.-J. Teng, J.-Z. Guo, Y.-X. Wang, et B. Li, « Enhanced removal of Cr(VI) by nitrogen-doped hydrochar prepared from bamboo and ammonium chloride », *Bioresource Technology*, vol. 342, p. 126028, déc. 2021, doi: 10.1016/j.biortech.2021.126028.

[5] H. Koyuncu et A. R. Kul, « Removal of methylene blue dye from aqueous solution by nonliving lichen (Pseudevernia furfuracea (L.) Zopf.), as a novel biosorbent », *Appl Water Sci*, vol. 10, n° 2, p. 72, févr. 2020, doi: 10.1007/s13201-020-1156-9.

[6] « Water | Free Full-Text | Review on Methylene Blue: Its Properties, Uses, Toxicity and Photodegradation ». Consulté le: 16 janvier 2024. [En ligne]. Disponible sur: https://www.mdpi.com/2073-4441/14/2/242

[7] S. Dardouri et J. Sghaier, « Adsorptive removal of methylene blue from aqueous solution using different agricultural wastes as adsorbents », *Korean J. Chem. Eng.*, vol. 34, n° 4, p. 1037-1043, avr. 2017, doi: 10.1007/s11814-017-0008-2.

[8] S. De Gisi, G. Lofrano, M. Grassi, et M. Notarnicola, « Characteristics and adsorption capacities of low-cost sorbents for wastewater treatment: A review », *Sustainable Materials and Technologies*, vol. 9, p. 10-40, sept. 2016, doi: 10.1016/j.susmat.2016.06.002.

[9] A. N. E. H. Sid *et al.*, « Comparative investigation of the effect of eggshellpowder and calcium carbonate as additivesin eco-friendly polymer drilling fluids », *Sustainability*, vol. 15, n° 4, p. 3375, 2023.

[10] S. Mechati *et al.*, « Modeling and Optimization of Hybrid Fenton and Ultrasound Process for Crystal Violet Degradation Using AI Techniques », *Water*, vol. 15, n° 24, p. 4274, 2023.

[11] M. I. Kanjal *et al.*, « A Study of Treatment of Reactive Red 45 Dye by Advanced Oxidation Processes and Toxicity Evaluation Using Bioassays », *Sustainability*, vol. 15, nᵒ 9, p. 7256, 2023.

[12] M. Kebir *et al.*, « Sunlight Degradation and Mineralization of Food Dye Photoinduced by Homogenous Photo Fenton Fe (III) and Fe (II)/Complex: Surface Response Modeling », 2023.

[13] A. Imessaoudene *et al.*, « Adsorption performance of zeolite for the removal of congo red dye: Factorial design experiments, kinetic, and equilibrium studies », *Separations*, vol. 10, nᵒ 1, p. 57, 2023.

[14] C. Djama *et al.*, « Experimental and Theoretical Study of Methylene Blue Adsorption on a New Raw Material, Cynara scolymus—A Statistical Physics Assessment », *Sustainability*, vol. 15, nᵒ 13, p. 10364, juin 2023, doi: 10.3390/su151310364.

[15] K. Madi *et al.*, « Green Fabrication of ZnO Nanoparticles and ZnO/rGO Nanocomposites from Algerian Date Syrup Extract: Synthesis, Characterization, and Augmented Photocatalytic Efficiency in Methylene Blue Degradation », *Catalysts*, vol. 14, nᵒ 1, p. 62, 2024.

[16] S. A. Mousavi, D. Shahbazi, A. Mahmoudi, P. Mohammadi, et T. Massahi, « Statistical Modeling and Kinetic Studies on the Adsorption of Reactive Red 2 by a Low-Cost Adsorbent: Grape Waste-Based Activated Carbon Using Sulfuric Acid Activator-Assisted Thermal Activation », *Adsorption Science & Technology*, vol. 2021, p. e8404197, nov. 2021, doi: 10.1155/2021/8404197.

[17] « e2-65265.pdf ».

[18] A. I. Osman *et al.*, « Methods to prepare biosorbents and magnetic sorbents for water treatment: a review », *Environ Chem Lett*, vol. 21, nᵒ 4, p. 2337-2398, août 2023, doi: 10.1007/s10311-023-01603-4.

[19] « Removal of methylene blue dye from aqueous solution using immobilized Agrobacterium fabrum biomass along with iron oxide nanoparticles as biosorbent | Environmental Science and Pollution Research ». Consulté le: 17 janvier 2024. [En ligne]. Disponible sur: https://link.springer.com/article/10.1007/s11356-018-2280-z

[20] W. Chen *et al.*, « Insight into KOH activation mechanism during biomass pyrolysis: Chemical reactions between O-containing groups and KOH », *Applied Energy*, vol. 278, p. 115730, nov. 2020, doi: 10.1016/j.apenergy.2020.115730.

[21] W. Tu *et al.*, « A novel activation-hydrochar via hydrothermal carbonization and KOH activation of sewage sludge and coconut shell for biomass wastes: Preparation,

characterization and adsorption properties », *Journal of Colloid and Interface Science*, vol. 593, p. 390-407, juill. 2021, doi: 10.1016/j.jcis.2021.02.133.

[22] L. Spessato *et al.*, « KOH-super activated carbon from biomass waste: Insights into the paracetamol adsorption mechanism and thermal regeneration cycles », *Journal of Hazardous Materials*, vol. 371, p. 499-505, juin 2019, doi: 10.1016/j.jhazmat.2019.02.102.

[23] T. Tay, S. Ucar, et S. Karagöz, « Preparation and characterization of activated carbon from waste biomass », *Journal of Hazardous Materials*, vol. 165, nº 1-3, p. 481-485, juin 2009, doi: 10.1016/j.jhazmat.2008.10.011.

[24] A. H. Jawad et R. Abd Rashid, « KOH-activated carbon developed from biomass waste: adsorption equilibrium, kinetic and thermodynamic studies for Methylene blue uptake », *Desalination and water treatment*, vol. 57, p. 1-11, mars 2016, doi: 10.1080/19443994.2016.1167630.

[25] « Water | Free Full-Text | Review on Methylene Blue: Its Properties, Uses, Toxicity and Photodegradation ». Consulté le: 13 décembre 2023. [En ligne]. Disponible sur: https://www.mdpi.com/2073-4441/14/2/242

[26] R. Md Salim, J. Asik, et M. S. Sarjadi, « Chemical functional groups of extractives, cellulose and lignin extracted from native Leucaena leucocephala bark », *Wood Sci Technol*, vol. 55, nº 2, p. 295-313, mars 2021, doi: 10.1007/s00226-020-01258-2.

[27] C. Djama, D. Chebli, A. Bouguettoucha, I. Doudou, et A. Amrane, « Statistical physics modelling of azo dyes biosorption onto modified powder of Acorus calamus in batch reactor », *Biomass Conv. Bioref.*, vol. 13, nº 2, p. 1013-1028, janv. 2023, doi: 10.1007/s13399-020-01190-2.

[28] A. Yazidi, L. Sellaoui, G. L. Dotto, A. Bonilla-Petriciolet, A. C. Fröhlich, et A. B. Lamine, « Monolayer and multilayer adsorption of pharmaceuticals on activated carbon: Application of advanced statistical physics models », *Journal of Molecular Liquids*, vol. 283, p. 276-286, juin 2019, doi: 10.1016/j.molliq.2019.03.101.

[29] L. Sellaoui *et al.*, « Insights of the adsorption mechanism of methylene blue on brazilian berries seeds: Experiments, phenomenological modelling and DFT calculations », *Chemical Engineering Journal*, vol. 394, p. 125011, août 2020, doi: 10.1016/j.cej.2020.125011.

[30] L. Sellaoui *et al.*, « Implementation of a multilayer statistical physics model to interpret the adsorption of food dyes on a chitosan film », *Journal of Environmental Chemical Engineering*, vol. 9, nº 4, p. 105516, août 2021, doi: 10.1016/j.jece.2021.105516.

[31] L. Sellaoui, H. Guedidi, L. Reinert, S. Knani, L. Duclaux, et A. B. Lamine, « Experimental and theoretical studies of adsorption of ibuprofen on a raw and two chemically modified activated carbons: new physicochemical interpretations », *RSC Advances*.

[32] M. K. Seliem et M. Mobarak, « Cr(VI) uptake by a new adsorbent of CTAB–modified carbonized coal: Experimental and advanced statistical physics studies », *Journal of Molecular Liquids*, vol. 294, p. 111676, nov. 2019, doi: 10.1016/j.molliq.2019.111676.

[33] M. Mobarak *et al.*, « Statistical physics modeling and interpretation of methyl orange adsorption on high–order mesoporous composite of MCM–48 silica with treated rice husk », *Journal of Molecular Liquids*, vol. 285, p. 678-687, juill. 2019, doi: 10.1016/j.molliq.2019.04.116.

[34] L. Sellaoui, H. Guedidi, S. Knani, L. Reinert, L. Duclaux, et A. Ben Lamine, « Application of statistical physics formalism to the modeling of adsorption isotherms of ibuprofen on activated carbon », *Fluid Phase Equilibria*, vol. 387, p. 103-110, févr. 2015, doi: 10.1016/j.fluid.2014.12.018.

[35] K. F. Khaled, « Studies of iron corrosion inhibition using chemical, electrochemical and computer simulation techniques », *Electrochimica Acta*, vol. 55, n° 22, p. 6523-6532, sept. 2010, doi: 10.1016/j.electacta.2010.06.027.

[36] « Anticorrosion Potential of 2-Mesityl-1H-imidazo[4,5-f][1,10]phenanthroline on Mild Steel in Sulfuric Acid Solution: Experimental and Theoretical Study | Industrial & Engineering Chemistry Research ». Consulté le: 29 mars 2024. [En ligne]. Disponible sur: https://pubs.acs.org/doi/abs/10.1021/ie102034c

[37] A. El Asri *et al.*, « Computational and experimental studies of the inhibitory effect of imidazole derivatives for the corrosion of copper in an acid medium », *Journal of Molecular Liquids*, vol. 345, p. 117813, janv. 2022, doi: 10.1016/j.molliq.2021.117813.

[38] J. Attarki *et al.*, « Adsorption mechanism investigation of methylthioninium chloride dye onto some metal phosphates using Monte Carlo dynamic simulations and DFT calculations », *Inorganic Chemistry Communications*, vol. 149, p. 110436, mars 2023, doi: 10.1016/j.inoche.2023.110436.

[39] S.-A. Naicker et M. Moodley, « A computational study of the adsorption of corrosive sulphur on Ag surfaces », *J Mater Sci*, vol. 56, n° 23, p. 13386-13399, août 2021, doi: 10.1007/s10853-021-06120-9.

[40] B. Bharadwaj, S. Dutta, Md. A. Qaiyum, P. P. Samal, B. Dey, et S. Dey, « Pristine wild sugarcane (Saccharum spontaneum) as a biosorbent for removal of methylene blue from wastewater: isotherm, kinetics and regeneration studies », *International Journal of Phytoremediation*, vol. 0, n° 0, p. 1-15, 2023, doi: 10.1080/15226514.2023.2260002.

[41] R. Zein, J. Satrio Purnomo, P. Ramadhani, Safni, M. F. Alif, et C. N. Putri, « Enhancing sorption capacity of methylene blue dye using solid waste of lemongrass biosorbent by modification method », *Arabian Journal of Chemistry*, vol. 16, nᵒ 2, p. 104480, févr. 2023, doi: 10.1016/j.arabjc.2022.104480.

[42] M. Diehl, L. F. O. Silva, C. Schnorr, M. S. Netto, F. S. Bruckmann, et G. L. Dotto, « Cassava bagasse as an alternative biosorbent to uptake methylene blue environmental pollutant from water », *Environ Sci Pollut Res*, vol. 30, nᵒ 18, p. 51920-51931, avr. 2023, doi: 10.1007/s11356-023-26006-4.

[43] S. Shakoor et A. Nasar, « Adsorptive treatment of hazardous methylene blue dye from artificially contaminated water using cucumis sativus peel waste as a low-cost adsorbent », *Groundwater for Sustainable Development*, vol. 5, p. 152-159, sept. 2017, doi: 10.1016/j.gsd.2017.06.005.

[44] S. T. Al-Asadi, F. F. Al-Qaim, H. F. S. Al-Saedi, I. F. Deyab, H. Kamyab, et S. Chelliapan, « Adsorption of methylene blue dye from aqueous solution using low-cost adsorbent: kinetic, isotherm adsorption, and thermodynamic studies », *Environ Monit Assess*, vol. 195, nᵒ 6, p. 676, mai 2023, doi: 10.1007/s10661-023-11334-2.

CHAPTER V

Chapter V: Utilizing Raw Oak Cupule and Response Surface Methodology to Optimize Adsorption Factors for Methylene Blue Elimination

05

V.1 Introduction

In numerous sectors, including cosmetics, pharmaceuticals, and textiles, dyes are extensively utilized. The textile industry, in particular, is known for its significant dye discharge during manufacturing. It is reported that about 20% of the applied dyes end up in the wastewater during the dyeing process, contributing to substantial environmental pollution. The release of dyes into the environment raises significant environmental and health issues due to their intricate chemical structures [1].

Methylene Blue (MB) is widely used across industries, but its improper disposal poses significant environmental and health risks. Studies have shown that MB exhibits teratogenic and embryotoxic effects in both angelfish and rats. Industries like textiles, pharmaceuticals, and cosmetics may release large amounts of MB into the environment [2].

Due to its stable aromatic structure, MB is non-biodegradable and carcinogenic. Exposure to MB is linked to various health issues, including gastrointestinal, respiratory, cardiovascular, neurological, and dermatological complications [3].

Several treatment strategies have been extensively utilized to eliminate dyes from the environment, including biological techniques (involving enzymes and microorganisms), chemical approaches (such as advanced oxidation processes: photocatalysis [4]), and physicochemical methods, with adsorption [5] being the most commonly applied.

Many low-cost sorbents, including industrial waste, natural and/or modified clays, activated carbon, and natural polymers, have been effectively employed in the treatment of contaminated waters to remove different dyes through the sorption process in an aqueous medium.

Chapter V: Utilizing Raw Oak Cupule and Response Surface Methodology to Optimize Adsorption Factors for Methylene Blue Elimination

05

The adsorption process is widely chosen over other dye treatment techniques for wastewater due to its notable benefits, such as its high effectiveness, low cost, straightforward operation, and resilience to the presence of toxic compounds [5], [6].

Nevertheless, because they are all so expensive, a lot of researchers are currently working on creating innovative, low-cost adsorbents that may be used as a substitute for expensive ones to cure polluted waterways. One such example is biomass from agricultural waste [7].

Agricultural waste biomasses, such as garlic peel, orange peel [8], green pea peel [9], rice husk [6], [10], jujube stone [11], and almond shells [12], …eg; Owing to their biomass composition, coupled with their abundance and affordability, these materials have been increasingly utilized in adsorption processes [13].

The present research investigated the potential use of Cellulosic material agricultural waste biomass, such as oak cupules, as adsorbents for the adsorption-based process of treating wastewater.

There is a regional marking on this agricultural product. Furthermore, because of their high consumption, these biomasses made from agricultural waste are widely available. This has led to the massive disposal of waste, which can pose serious issues for the community, particularly when improperly managed or consumed outdoors, which results in additional pollution.

To effectively compare the performance of new adsorbents in dye removal, it is essential to minimize variations in the type of dye being adsorbed. As a result, numerous studies have focused on methylene blue (MB) adsorption using cellulosic materials, given its common use as a standard dye [14].

It is important to note that the success of the adsorption process is influenced by numerous factors. These include the adsorbent's surface area, surface charge, solution isoelectric point, pH, temperature, equilibrium time, and concentration gradient, which acts as the driving force

Chapter V: Utilizing Raw Oak Cupule and Response Surface Methodology to Optimize Adsorption Factors for Methylene Blue Elimination

05

for mass transfer, along with several other parameters that collectively impact the efficiency of adsorption.

This work presents a novel adsorption method by using biomass from agricultural waste as reasonably priced adsorbents to remove dyes. It is notable for incorporating ANOVA modeling to streamline the procedure, providing a viable remedy for environmental issues, and being in line with sustainable development goals. These unique characteristics highlight its potential to drive improvements in wastewater treatment systems and distinguish it from earlier studies. Additionally, it is commonly available for free or at very little cost, making it a cost-effective and easily available adsorbent.

V.2   Materials and Experimental Procedures

V.2.1   Methodological Design

This study utilized the Box-Behnken Design (BBD) within Response Surface Methodology (RSM) to model and analyze the relationship between process factors and the adsorption capacity of the CR in removing MB [15]. Known for its efficiency in optimizing processes by accommodating quadratic responses [16], BBD was employed to examine the effects of key operational parameters pH (A), adsorbent dosage (B), initial concentration of the solution (C), and temperature (D) on the adsorption efficiency. The importance of each factor, along with their interactions and quadratic contributions, was assessed through statistical analysis using Design-Expert Software (version 13.0, Stat-Ease, Minneapolis, USA). Each parameter was tested at three levels (-1, 0, and +1), corresponding to low, medium, and high values, as detailed in **Table V.1**, which summarizes the selected ranges and coded values of these independent variables.

Chapter V: Utilizing Raw Oak Cupule and Response Surface Methodology to Optimize Adsorption Factors for Methylene Blue Elimination

05

Table V. 1: Independent Variables with Corresponding Coded Levels and Actual Value Ranges.

Codes	Factors	Level $_1$(-1)	Level $_2$(0)	Level $_3$(+1)
A	pH	4	7	10
B	Adsorbent dosage(mg)	10	20	30
C	Initial concentration(mg/l)	100	150	200

A series of 29 experiments were conducted to assess the impact of key process variables: pH (ranging from 4 to 10), adsorbent dosage (10 to 30 mg), initial solution concentration (100 to 200 mg/L), and temperature (20 to 40 °C) on the adsorption capacity Q (mg/g) of the CR. A non-linear regression analysis was performed to fit a second-order polynomial (Eq.V.1) to the collected data, facilitating the identification of important model parameters. The quadratic response model, which includes all linear terms, squared terms, and interaction effects, can be formulated as follows [17]:

$$Y = \beta_0 + \sum \beta_i X_j + \sum \beta_{ii} X_i^2 + \sum \beta_i X_i X_j \quad \text{...} \quad (V.1)$$

In this study, Y represents the selected response variable, while β_0 denotes the constant coefficient. The linear coefficients are indicated by β_i, the quadratic coefficients by β_{ii}, and the interaction coefficients by $\beta_{i\text{-}j}$. The variables X_i and X_j correspond to the coded values of the independent factors. The range of these variables was established based on preliminary experimental findings. The absorbance values of Methylene Blue (MB) were measured using a 17000-SHIMADZU Direct Reading Spectrophotometer, calibrated to a maximum wavelength of 663 nm. The adsorption capacity Q (mg/g) of the CR was calculated using **Eq (II.1)**.

Table V.3 presents the experimental matrix for the Box-Behnken Design. To validate the quadratic model, an Analysis of Variance (ANOVA) was performed. The statistical

Chapter V: Utilizing Raw Oak Cupule and Response Surface Methodology to Optimize Adsorption Factors for Methylene Blue Elimination

05

significance and reliability of the model were evaluated using the Fisher value (F-value), the

correlation coefficient (R^2), and the probability value (p-value).

Table V. 2: *Table: Matrix of the 3-Factor Box-Behnken Design (BBD) and Experimental Results for Methylene Blue Adsorption.*

Run	A: pH	B: adsorbent dosage	C: Initial solution concentration	D: T(C)	Q(mg/g)
1	7	20	100	40	50.925
2	7	20	150	30	114.449
3	4	20	150	20	132.09
4	7	30	200	30	126.944
5	7	20	200	20	162.64
6	4	20	200	30	139.659
7	4	20	100	30	89.652
8	4	20	150	40	98.61
9	10	10	150	30	137.906
10	4	30	150	30	92.9133
11	7	30	100	30	64.0067
12	7	30	150	40	85.29
13	7	20	150	30	114.5
14	7	10	150	40	175.17
15	7	20	150	30	114.449
16	10	30	150	30	94.0067
17	7	30	150	20	95.96
18	10	20	150	20	141.99
19	7	20	150	30	114.52
20	7	20	150	30	114.452
21	7	20	200	40	190.755
22	7	10	150	20	174.72
23	10	20	100	30	94.163
24	4	10	150	30	139.36

Chapter V: **Utilizing Raw Oak Cupule and Response Surface Methodology to Optimize Adsorption Factors for Methylene Blue Elimination**

05

25	10	20	150	40	155.76
26	10	20	200	30	174.586
27	7	10	100	30	127.842
28	7	20	100	20	96.17
29	7	10	200	30	194.2

V.3   Results and Discussion

V.3.1   Characterisation

➢   **FTIR**
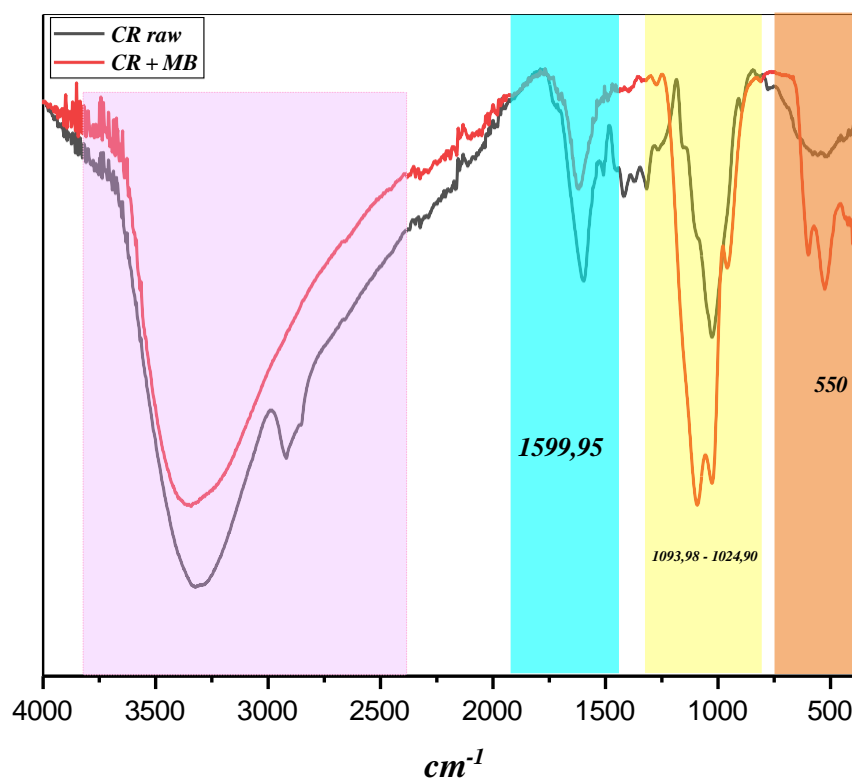
Figure V. 1: *Comparison of FTIR Spectra before and after Methylene Blue Adsorption.*

➢   Bands around 1599.95 cm^{-1} (in blue)

This band is probably associated with the vibrations of groups such as amine groups (-NH2) or C=C in aromatic structures. The increase or shift of this band after MB adsorption (comparing

the before and after spectra) may indicate an interaction between the material and Methylene Blue via chemical bonds or Van der Waals interactions.

➢ The band at 1083.98 - 1024.90 cm^{-1} (yellow)

This region usually corresponds to the stretching vibrations of the C-O bonds.

If this band changes after MB adsorption, it could indicate an interaction with the CR material's oxygen or silicate functional sites.

➢ The band at 550 cm^{-1} (orange)

This low band is often associated with the out-of-plane deformation vibrations of the aromatic groups.

A change in this band may indicate that Methylene Blue is interacting with the metallic or aromatic sites of the CR material.

Broad band between 3000 and 3500 cm^{-1} (in pink)

This region generally corresponds to the stretching vibrations of the hydroxyl groups (-OH).

The differences in this region after MB adsorption suggest possible interactions between Methylene Blue and the hydroxyl groups present in the CR material.

➢ **TGA / DTA**

The **Fig. V.2** shows the TGA and DTA curves of the material analyzed, allowing its thermal decomposition to be observed as a function of temperature. On the TGA curve, a first mass loss is visible between 100°C and 200°C, accompanied by a slight endothermic peak on the DTA curve, corresponding to the evaporation of moisture and some volatile compounds. Then, between 200°C and 700°C, a significant drop in mass is observed on the TGA curve, associated with a marked endothermic peak on the DTA curve, indicating the decomposition of the main

Chapter V: Utilizing Raw Oak Cupule and Response Surface Methodology to Optimize Adsorption Factors for Methylene Blue Elimination

05

organic components such as cellulose and hemicellulose. Above 700°C, the TGA curve stabilizes, indicating the presence of non-decomposable inorganic residues, while the DTA curve remains stable, suggesting no new thermal reactions. This figure shows the thermal degradation stages of a material, typical of a biomass, with a stable final phase due to inorganic residues.
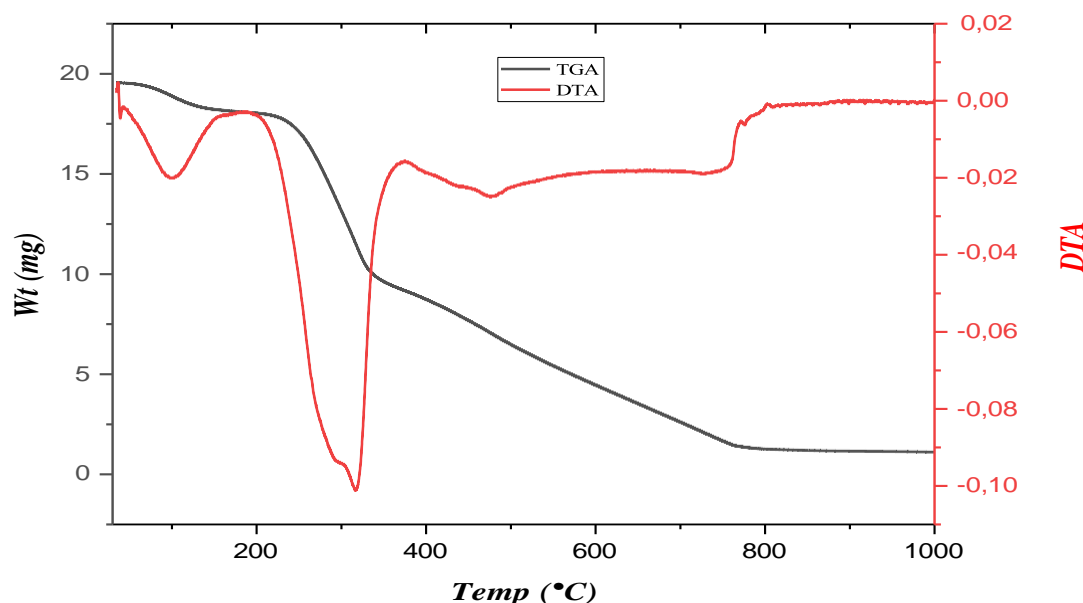
Figure V. 2: the result of thermal decomposition of CR biosorbent.

➢ **Point zero charge**

The zero-point charge denotes the exterior surface charge of the substance. The pH of zero charge (pH$_{pzc}$) is found at the junction of the initial and final pH values. This graph is seen in **Fig V.3**. There was around 7.2 pH (pH$_{pzc}$). This indicates that the surface of the biosorbent is positively charged when the pH is less than 7.2 and charged negatively when the pH is more than 7.2. It is anticipated that a negatively charged surface will encourage adsorption because MB is cationic.

Chapter V: Utilizing Raw Oak Cupule and Response Surface Methodology to Optimize Adsorption Factors for Methylene Blue Elimination

05
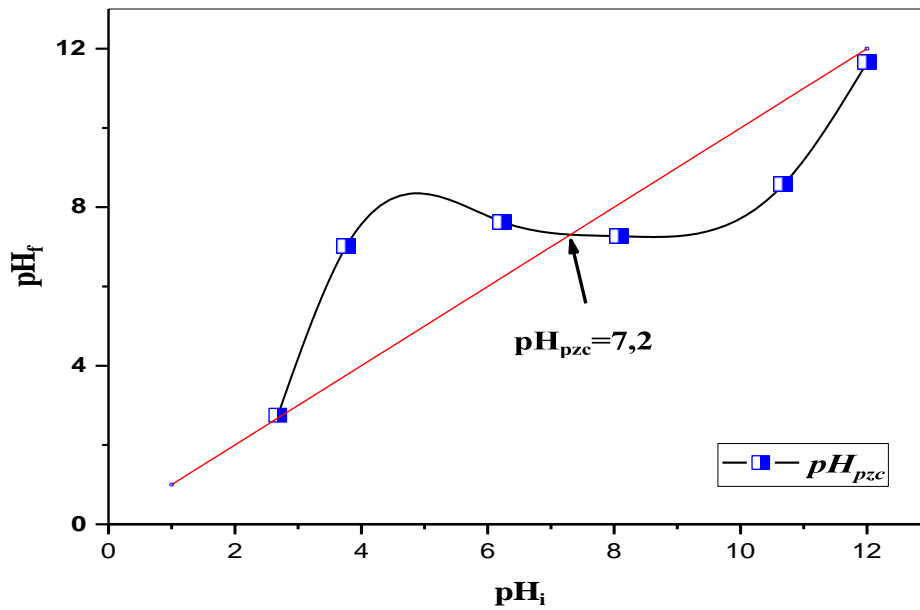
Figure V. 3: *Point zero charges of CR adsorbent.*

V.3.2   Effect of pH :

A constant concentration of MB dye at 100 mg/L and the adsorbent were utilized, with the pH adjusted using 1 M NaOH and 1 M HCl solutions. At low pH, the abundance of H^+ ions creates a repulsive electrostatic environment that inhibits the interaction between Methylene Blue (MB) molecules and the adsorbent's active sites, reducing adsorption efficiency.

Fig. V.4 presented the pH effect for the adsorption capacity, It is noted that the adsorption capacity is increased when the pH is higher than 6, on the other hand when the pH is lower the capacity is small, so from the results, it was evident that the adsorption of methylene blue was the highest in the neutral to page range.

As the pH rises, the concentration of H^+ ions diminish, and the adsorbent surface becomes increasingly negatively charged. This promotes electrostatic attraction between the negatively charged adsorbent and the positively charged MB molecules, enhancing adsorption. At higher ion concentrations, the available adsorption sites on the adsorbent surface become progressively

Chapter V: Utilizing Raw Oak Cupule and Response Surface Methodology to Optimize
Adsorption Factors for Methylene Blue Elimination

05

saturated, limiting further adsorption and causing a reduction in the adsorbent's overall capacity. In contrast, at lower concentrations of MB, the adsorbent has more active sites available, leading to a higher percentage of adsorption. This behavior highlights the importance of pH in optimizing the electrostatic interactions between the adsorbent and MB molecules, particularly when considering the availability of active sites as a function of both pH and dye concentration.
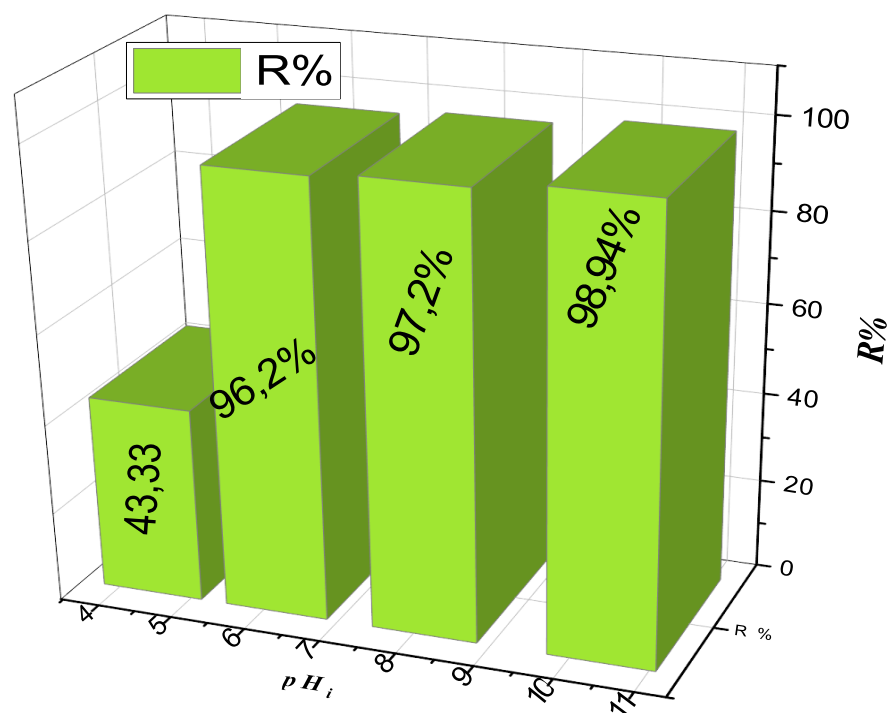
Figure V. 4: *Results of pH effect.*

V.3.3   Effect adsorbent mass

Fig. V.5 highlights the relationship between adsorbent mass and MB adsorption, indicating a reduction in adsorption capacity per unit of adsorbent with increasing mass. Concurrently, there is an observed rise in the adsorption rate, improving overall pollutant removal efficiency.

Chapter V: **Utilizing Raw Oak Cupule and Response Surface Methodology to Optimize Adsorption Factors for Methylene Blue Elimination**

05
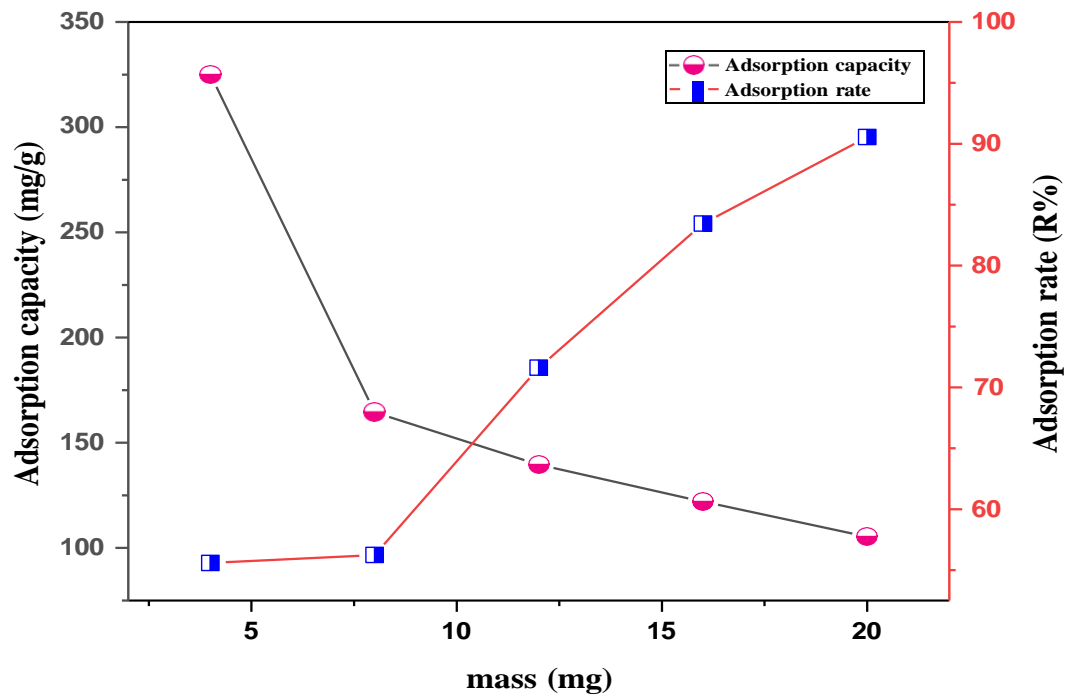
Figure V. 5: Results of biosorbent doge.

This trend may result from the expanded surface area and the increased number of active adsorption sites present on the GP material as its mass grows [18].

V.3.4 Kinetic study

The study of adsorption kinetics is essential for understanding how much adsorbate adheres to the adsorbent over time at a constant concentration. **Table V.3** presents the constants related to the pseudo-first-order (PFO), pseudo-second-order (PSO), and pseudo-nth-order (PNO) kinetic models. Data shown in **Fig. V.6** cover only the first 60 minutes, as adsorption capacity did not exhibit noticeable changes after that time.

Chapter V: Utilizing Raw Oak Cupule and Response Surface Methodology to Optimize Adsorption Factors for Methylene Blue Elimination

05
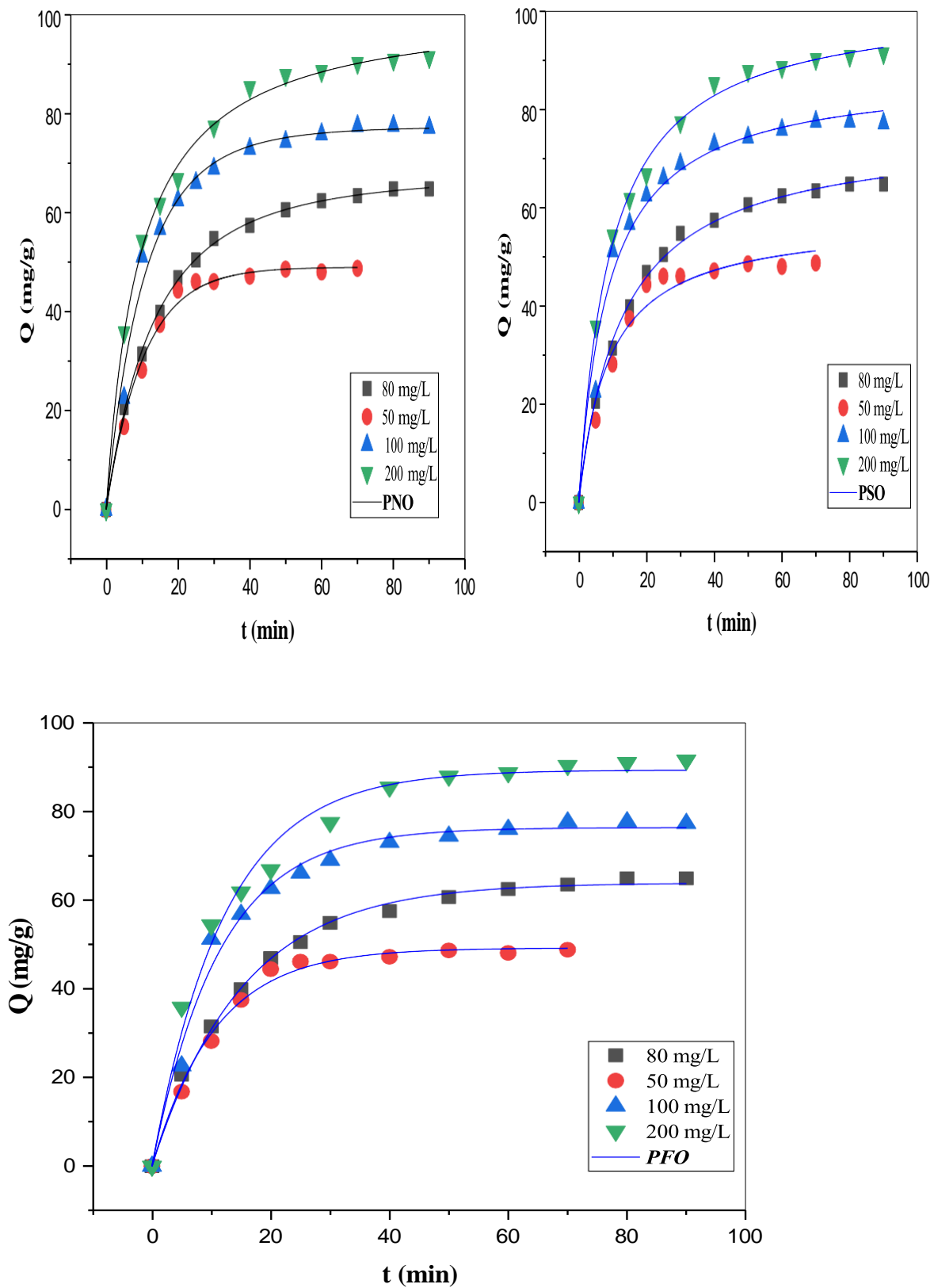
Figure V. 6: *Nonlinear Simulation graphs for Pseudo-First-Order, Pseudo-Second-Order, and Pseudo-nth-Order Kinetic Models.*

Chapter V: Utilizing Raw Oak Cupule and Response Surface Methodology to Optimize Adsorption Factors for Methylene Blue Elimination

05

Table V. 3: Parameter resulting from modeling kinetics of CR on MB.

models	Parameters	50 mg/g	80 mg/g	100mg/g	200mg/g
PFO	Q_e				
	K_1	0.093	0.065	0.088	0.082
	R^2	**0.993**	**0.996**	**0.988**	**0.987**
PSO	Q_e	57.726	75.644	87.538	102.315
	K_2	0.0019	0.001	0.0013	0.001
	R^2	**0.973**	**0.997**	**0.980**	**0.997**
PNO	Q_e	48.994	67.789	77.404	102.1
	k_n	1.112^E-5	0.002	0.0035	3.637^E-4
	N	1	1.407	1.158	1.987
	R^2	**0.999**	**0.991**	**0.997**	**0.996**

The adsorption behavior across various concentrations and time intervals, shown in **Fig. V.6**, indicates that the PSO kinetic model strongly correlated with the experimental results. The initial 40 minutes demonstrated rapid adsorption, followed by a slower rate as time progressed. Nearly 90% of the dye was adsorbed within the first 60 minutes, suggesting this was the equilibrium time for subsequent experiments. The pseudo-nth-order kinetic model provided high correlation coefficients and low average percentage errors, outperforming the PFO and PSO models in describing the experimental data. For dye concentrations of 50, 100, and 200 mg/L, the reaction order (n) was determined to be 1, 1.04, 1.1584, and 1.987, respectively,

Chapter V: Utilizing Raw Oak Cupule and Response Surface Methodology to Optimize Adsorption Factors for Methylene Blue Elimination

05

reflecting the model's ability to capture adsorption kinetics at different concentration levels accurately.

V.3.5   Isotherm study

The results were analyzed to model the adsorption behavior using the Langmuir and Freundlich isotherms, as depicted in **Fig. V.7** and summarized in **Table V.4**. The Langmuir model demonstrated an excellent fit to the experimental data, with correlation coefficients (R^2 > 0.99) indicating its high accuracy in describing the equilibrium adsorption of MB on CR. This outcome suggests the adsorption process involves monolayer coverage, reflecting a uniform distribution of adsorption sites on the biosorbent. The maximum adsorption capacity for MB in a monolayer on CR was found to be 150.29 mg/g at 40 °C, with a further increase to 220.95 mg/g at 20 °C.

Table V. 4: parameter modeling from isotherms study of MB on CR.

Models	Parameters	20 °C	30 °C	40°C
Langmuir	$Q_m(mg \bullet g^{-1})$	229.618	163.118	203.425
	$K_L (L \bullet mg^{-1})$	0.008	0.104	0.008
	R^2	**0.992**	**0.979**	**0.962**
Freundlich	N	4.347	4.734	2.277
	$K_F(mg \bullet g^{-1})(L/mg)^{1/n}$	61.881	50.688	11.552
	R^2	**0.871**	**0.892**	**0.865**

Chapter V: **Utilizing Raw Oak Cupule and Response Surface Methodology to Optimize Adsorption Factors for Methylene Blue Elimination**

05
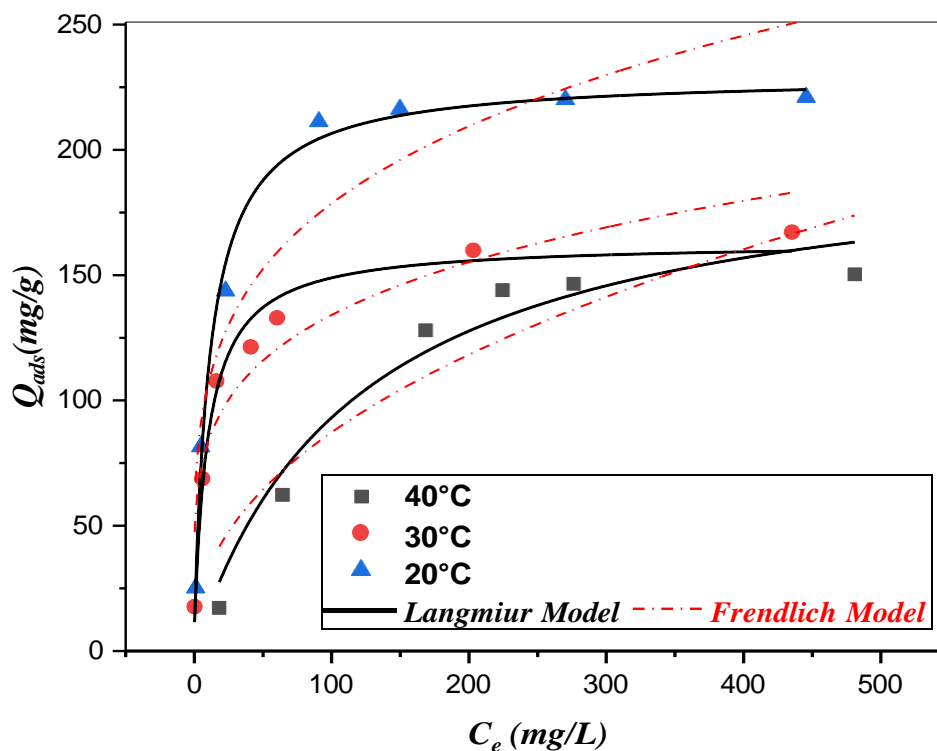
Figure V. 7: Fitting Results of Langmuir and Freundlich Isotherms for Methylene Blue Adsorption onto CR.

The decrease in adsorption efficiency at elevated temperatures is primarily due to desorption, which is facilitated by the strengthening of hydrophobic interactions among MB molecules in the aqueous phase. These interactions reduce the contact between the MB molecules and the adsorbent surface, as higher temperatures promote the detachment of molecules from the surface. This occurs because increased thermal energy enhances the bonding between MB molecules in water, thereby weakening their attraction to the adsorbent surface. The decrease in adsorption efficiency at elevated temperatures is primarily due to desorption, which is facilitated by the strengthening of hydrophobic interactions among MB molecules in the aqueous phase. These interactions reduce the contact between the MB molecules and the adsorbent surface, as higher temperatures promote the detachment of molecules from the surface. This occurs because increased thermal energy enhances the bonding between MB molecules in water, thereby weakening their attraction to the adsorbent surface [9], [19].

Chapter V: **Utilizing Raw Oak Cupule and Response Surface Methodology to Optimize Adsorption Factors for Methylene Blue Elimination**

05

The Freundlich isotherm demonstrates a strong affinity for MB adsorption onto CR, as indicated by 1/n values within the 0 to 1 range. However, the lower R^2 values highlight the model's limitations in accurately representing the experimental data. As such, the use of these traditional models proves inadequate for fully capturing the dynamics of MB uptake. Consequently, the intricate and regulated interactions between MB and MWA necessitate the application of more advanced theoretical models to provide a more precise description.

V.3.6 Advanced isotherms models: Improved Adsorption Models and Data Fitted Procedures in Statistical Physics
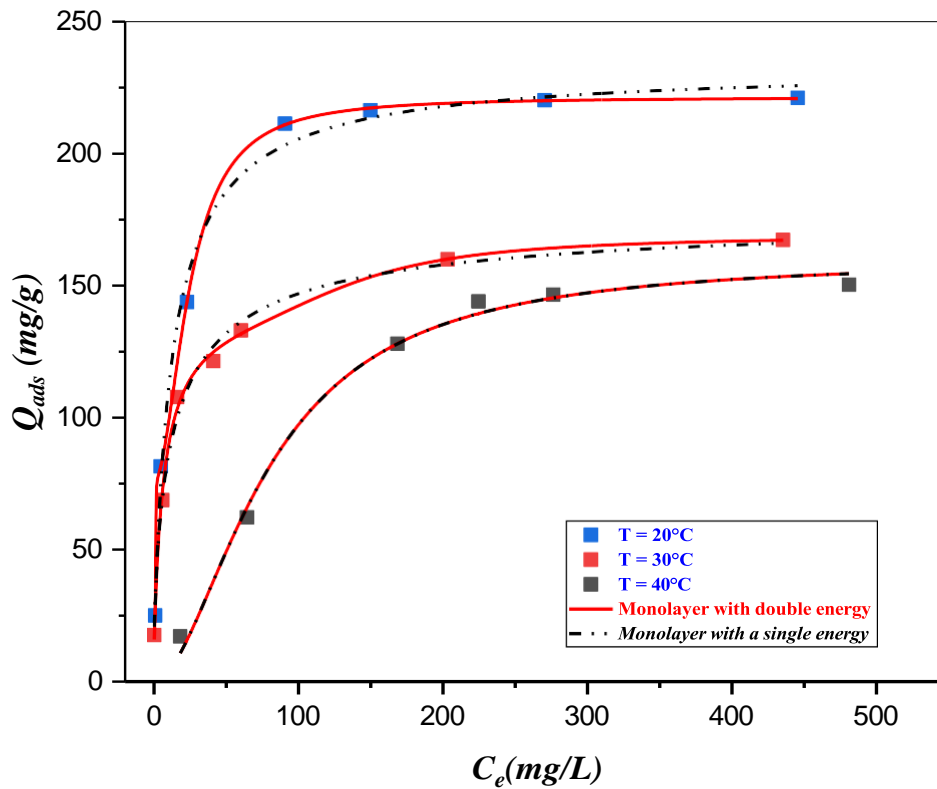
Figure V. 8: Isotherm Fitting Results for Methylene Blue Adsorption onto Cs Using Models ME1 and ME2.

As shown by the correlation coefficients (R^2) in **Table V.5**, **Fig. V.8** explained the sophisticated models, known as ME_1 and ME_2, that were used to understand the adsorption kinetics of MB on the CR bio-mass. It was shown that ME_2, also known as the double-energy

Chapter V: Utilizing Raw Oak Cupule and Response Surface Methodology to Optimize Adsorption Factors for Methylene Blue Elimination

05

single-layer model, was the most effective statistical physics model in describing the complexities of MB adsorption onto the CR bio-adsorbent.

Table V. 5: *The determined parameter values for advanced models.*

	Parametrs	T = 293 K	T = 303 K	313 K
ME$_1$	n	0.933	0.723	1.807
	N$_m$	249.59	246.573	88.715
	C$_{1/2}$	11.739	11.845	78.831
	R^2	**0.993**	**0.992**	**0.993**
ME$_2$	n$_1$	8.353	0.95	0.903
	n$_2$	1.975	3.343	4.928
	N$_{m1}$	8.996	153.311	3.937
	N$_{m2}$	78.904	7.322	88.712
	C$_1$	1.6	6.509	1.135
	C$_2$	24.794	134.314	78.83
	R^2	**0.999**	**0.983**	**0.999**

V.3.7   Steric parameter

Chapter V: Utilizing Raw Oak Cupule and Response Surface Methodology to Optimize Adsorption Factors for Methylene Blue Elimination

05
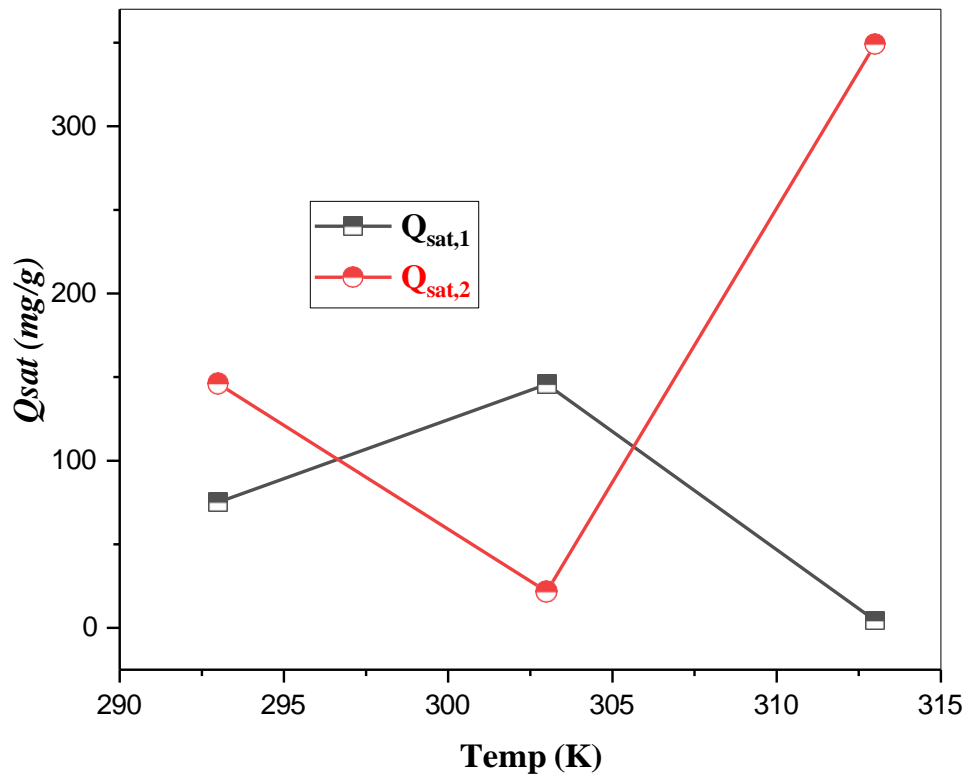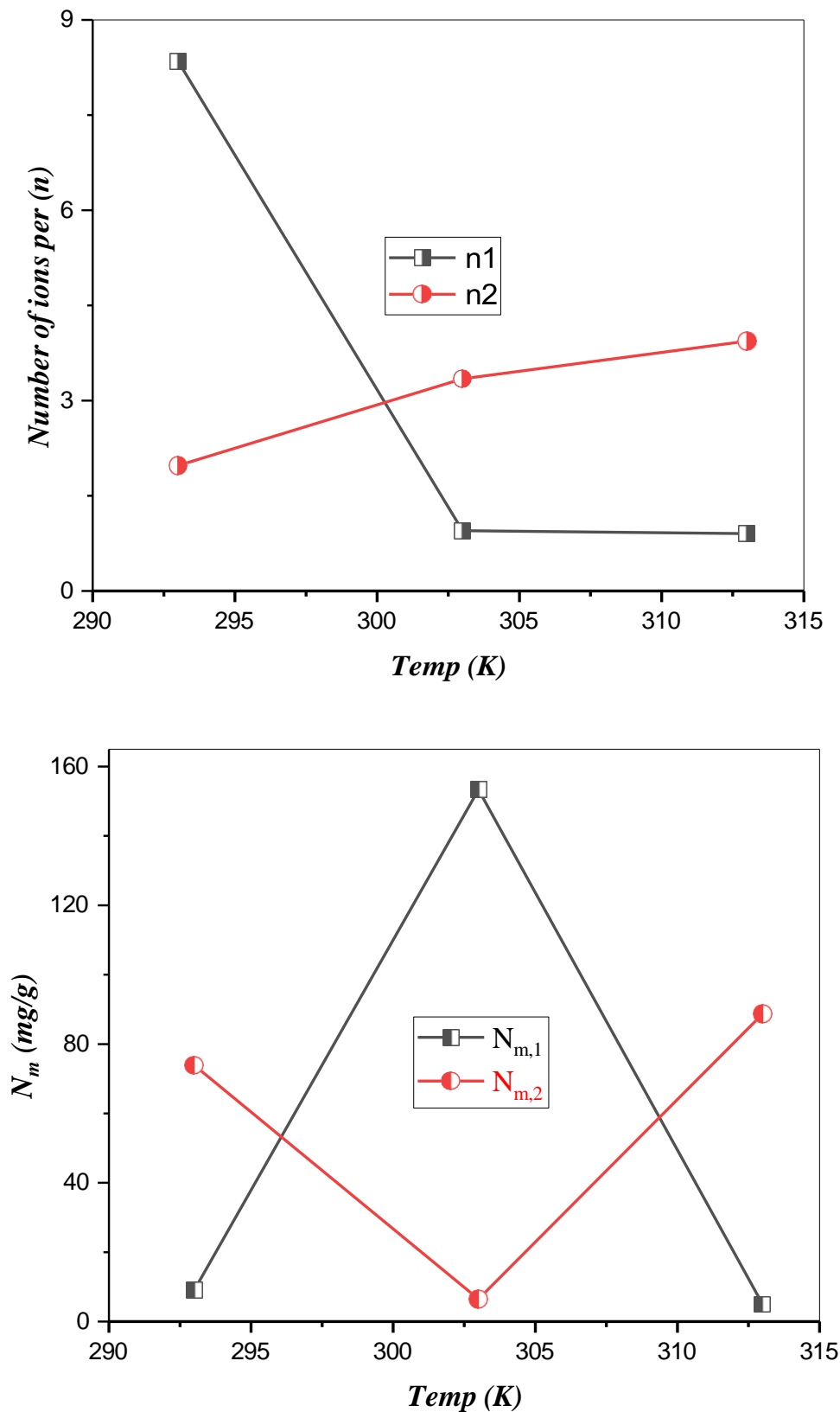
***Figure V. 9:** Temperature-induced variations in Q_{sat}, n, and N_m (mg/g) for MB adsorption into CR.*

Chapter V: Utilizing Raw Oak Cupule and Response Surface Methodology to Optimize Adsorption Factors for Methylene Blue Elimination

05

The steric parameter N_m represents **the number of adsorption sites occupied** per unit of adsorbent and indicates the number of sites accessible to adsorbed species at equilibrium. There is an inverse relationship between Nm and n. As n increases, the number of accessible adsorption sites decreases, whereas a decrease in n leads to an increase in available adsorption sites.

Fig. V.9 illustrates the variation of receptor site density (Nm) as a function of temperature. An increase in temperature is associated with a noticeable decline in the receptor site densities, specifically N_{m1} and N_{m2}, of CR. Concurrently, this reduction is accompanied by an increase in the number of molecules adsorbed per site (n_1 and n_2), indicating an enhanced tendency for molecular aggregation as the temperature rises. This observation suggests that higher temperatures promote greater molecular accumulation at the adsorption sites.

Fig. V.9 illustrates the geometric position (vertical or horizontal) and mechanism (multi–ionic or multimolecular). The parameters n_1 and n_2 correspond to MB molecules adsorbed on the primary and secondary adsorption sites of the CR adsorbent, and their analysis provides insights into the theoretical adsorption mechanism of this water contaminant. These parameters specifically reveal the contribution of both adsorption sites in the removal process. According to the calculated values, the following conclusions were drawn:

n_1 - CR > n_2 - CR à 293 K, n_2 - CR > n_1 - CR à 303 K, et n_2 - CR> n_1 - CR à 323 K.

This pattern shows that both adsorption sites are involved in MB removal but with different degrees of contribution. For instance, at 293 K, the second adsorption site played a dominant role in the removal process, while the first site acted in a secondary capacity (i.e., $n_2 > n_1$). Conversely, at 303 K, the first adsorption site became more active in MB removal than the second. Overall, the two adsorption sites of the CR adsorbent exhibit a strong affinity for MB

Chapter V: Utilizing Raw Oak Cupule and Response Surface Methodology to Optimize Adsorption Factors for Methylene Blue Elimination

05

ions in aqueous solutions. To describe the adsorption behavior of MB on the CR surface, three potential configurations can be considered:

- n_i (i = 1,2) ≤ 0.5: This suggests that the pollutant is adsorbed via at least two sites on the CR surface. In this case, the adsorption process could involve multiple interactions (double, triple interactions, etc.), where the adsorbate is distributed across different surface sites of the adsorbent.

- n_i ≥ 1: Here, a single adsorption site is responsible for pollutant removal. When n_i = 1, the process is likely mono-ionic, while if n_i > 1, it indicates a multi-ionic adsorption process.

- 0.5 < n_i < 1: In this range, the pollutant can be adsorbed through one or two adsorption sites.

Using this model, which assumes that MB can be removed via two active sites, the n_1 values were found to be 8.35, 0.95, and 0.903 at 293, 303, and 313 K, respectively, while n_2 increased from 1.975 to 3.937. The high n_1 values indicate that MB molecules interact with several adsorption sites, suggesting the involvement of multiple adsorption sites. As for the second adsorption site, MB ions also interact with multiple sites at lower temperatures, with n_2 values of 1.975 at 293 K. However, this value rises to 3.937 at 313 K, suggesting that, at higher temperatures, MB ions are mainly adsorbed through a single adsorption site, which depends on the temperature of the aqueous solution.

The saturation adsorption amount Q_{sat} as a steric parameter is influenced by other steric factors and can be expressed as $Q_{sat,i} = N_{m,i} * n_i$, where N_{mi} is the number of species adsorbed per site, and n_i represents the number of available adsorption sites. Based on the most appropriate statistical physics model, Q_{sat} is described in terms of the number of adsorbed molecules per site, the site density, and/or the formation of adsorption layers.

Chapter V: Utilizing Raw Oak Cupule and Response Surface Methodology to Optimize Adsorption Factors for Methylene Blue Elimination

05

Fig. V.9 visually depicts the temperature-dependent variation in the total saturation adsorption amount. The results show a pronounced sensitivity of the total adsorbed quantity to changes in temperature. Specifically, an increase in temperature led to a decrease in the amount of adsorbate at saturation. This trend can be explained by the exothermic nature of the adsorption process, which is characteristic of conventional adsorption behavior.

V.3.8 Thermodynamic study

The complicated Double-energy single-layer model (ME$_2$) is used to compute thermodynamic values such as internal energy, Gibbs free energy, and entropy.

Table V. 6: *Thermodynamics function according to the ME2 model* [20].

Function	Equation		Number	
Gibbs free enthalpy	$$G = K_B T ln\left(\frac{C_e}{Z_v}\right)\left[\frac{Q_{sat1}}{1+\left(\frac{C_1}{C_e}\right)^{n_1 m}}\right.$$ $$\left. + \frac{Q_{sat2}}{1+\left(\frac{C_2}{C_e}\right)^{mn_2}}\right]$$ $$Z_v = \frac{Z_{gtr}}{V} = \left(\frac{2\pi m K_B T}{h^2}\right)^{3/2}$$		**(V.2)**	**K$_B$:** Boltzmann constant (J/K). **G:** Gibbs free enthalpy **Z$_v$:** Translation partition function per unit volume. **Z$_{gtr}$:** The translation partition function.
Internal energy	$$E_{int} = K_B T\left[N_{1s}\frac{ln\left(\frac{C_e}{Z_v}\right)+n_{1m}\,ln\left(\frac{C_1}{C_e}\right)}{1+\left(\frac{C_1}{C_e}\right)^{n_1 m}}\right.$$ $$\left. + N_{2s}\frac{ln\left(\frac{C_e}{Z_v}\right)+n_2\,mln\left(\frac{C_2}{C_e}\right)}{1+\left(\frac{C_2}{C_e}\right)^{n_2 m}}\right]$$		**(V.3)**	**Eint:** System internal energy (J/mol) **V:** Volume(L). **h:** Planck constant (J/s) **m:** Adsorbent mass (g)

Chapter V: Utilizing Raw Oak Cupule and Response Surface Methodology to Optimize Adsorption Factors for Methylene Blue Elimination

05
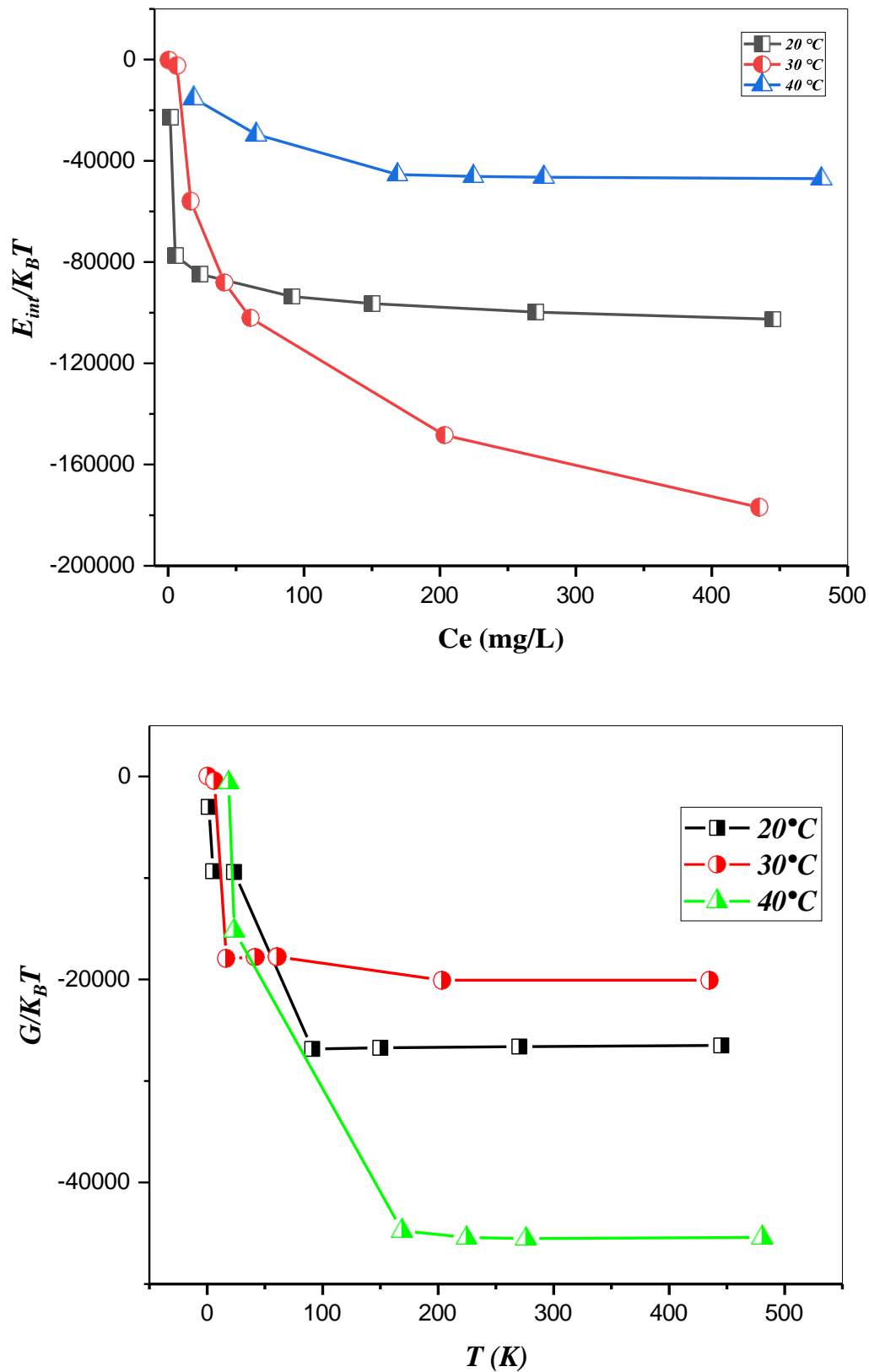
Figure V. 10: *The variation of internal energy (a) and Gibbs free energy (b) during MB*

adsorption onto CR as a function of concentration at different temperatures.

Chapter V: **Utilizing Raw Oak Cupule and Response Surface Methodology to Optimize Adsorption Factors for Methylene Blue Elimination**

05

The assessment of internal energy E_{int} provides a detailed framework for analyzing the various energy components within the MB adsorption system. Equation **(V.3)**, presented in **Table V.6**, describes the general expression for internal energy. The corresponding internal energy values for the studied adsorption system are visually represented in Figure 11. Interestingly, all reported values are negative, signifying that the adsorption process releases energy, thereby confirming the spontaneous formation of the Methylene Blue adsorption system.

In addition, the calculation of Gibbs free energy follows Equation **(V.2)**, also found in Table 6, which is dependent on ME_2. The graph of Gibbs free energy as a function of adsorbate concentration at different temperatures for the CR adsorbent is shown in Figure 11. The data in this figure underscore the negative Gibbs free energy values, reinforcing the spontaneous nature of the adsorption process. Moreover, as the temperature increases, the Gibbs free energy decreases, indicating that the adsorption efficiency diminishes at higher temperatures. This suggests a temperature-dependent weakening in the effectiveness of the adsorption mechanism.

V.3.9 Evaluation of Adsorption Energies

The adsorption energies across different temperatures can be readily estimated by utilizing two half-saturation concentrations (C1 and C2). This can be achieved through the application of the following two equations (Eqs **V.4** et **V.5**), which allow for the straightforward calculation of adsorption energies at various temperatures.

$$\Delta E_1 = R\,T\ln\frac{C_s}{C_1} \dots\dots\dots\dots\dots\dots\dots\dots\dots\dots\dots\dots\dots\dots\dots\dots\dots\dots\dots\dots\dots\dots\dots ..(V.4)$$

$$\Delta E_2 = R\,T\ln\frac{C_s}{C_2} \dots\dots\dots\dots\dots\dots ....(V.5)$$

Here, Cs represents the solubility of the molecules in water, and R = 8.314 J/mol·K is the ideal gas constant.

Chapter V: Utilizing Raw Oak Cupule and Response Surface Methodology to Optimize Adsorption Factors for Methylene Blue Elimination

05
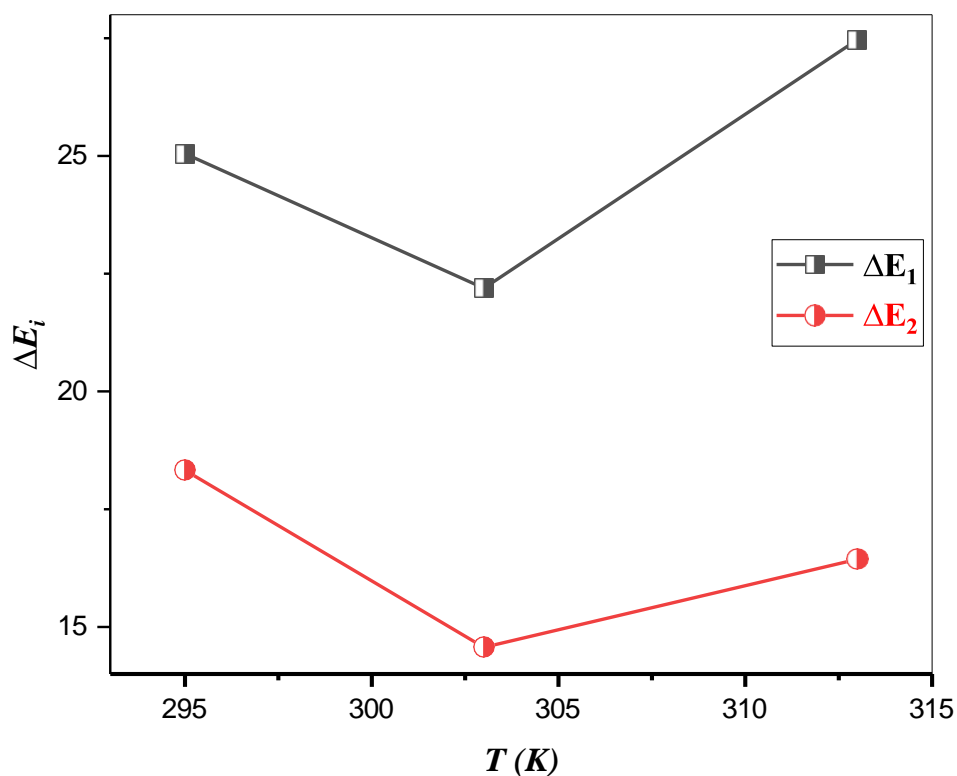
Figure V. 11: *Influence of Temperature on Adsorption Energies.*

Figure 8 illustrates the changes in adsorption energies, which define the interactions between the molecules and the surface of activated carbon (first layer), as well as the interactions between the molecules themselves (second layer), across different temperature conditions for all scenarios tested.

Based on **Fig. V.11**, the adsorption energies for the two layers of MB molecules on the CR surface are less than 40 kJ/mol, indicating that the interactions governing the removal process are primarily physical.

These interactions are likely associated with the formation of electron donor–acceptor complexes. It is also noteworthy that for both systems, E_1 is greater than E_2, which can be explained by the fact that the first adsorption energy reflects the direct interaction between MB molecules and the adsorbent surface.

Chapter V: Utilizing Raw Oak Cupule and Response Surface Methodology to Optimize Adsorption Factors for Methylene Blue Elimination

05

V.3.10 Evaluation of the Box-Behnken Design (BBD) Model

The BBD optimization approach was used to statistically assess the impacts of each process variable separately and in combination on BM removal. These variables were starting solution pH, adsorbent dose, initial solution concentration, and temperature. Analysis of variance (ANOVA) was used to statistically validate the BBD results, and Table 3 provides a summary of the data. With a p-value of smaller than 0.0001, the BBD model's F-value of 31.29 indicates that it is statistically significant for MB adsorption. Additionally, the experimental data and the model's projected values for the MB removal process showed a significant connection [21], as indicated by the corresponding coefficient of estimation (R^2) of 0.91. Additionally, The Adjusted R2 of 0.88 and the Predicted R2 of 0.79 accord rather well [22]. The signal-to-noise ratio is also measured by A_{deq} Precision. More than four is the ideal ratio. An acceptable signal is shown by our percentage of 21.66. The design space may be traversed using this paradigm [23].

It is determined that the BBD model parameters B, C, B_2, and BC are mathematically significant. To get the result of suitable fitness, the remaining BBD model terms with p-values higher than 0.05 were disregarded in a second-order polynomial expression. Therefore, the following **Eq. V.6** mentions the correlation of a second-order polynomial equation comprising the process variables that were evaluated with MB removal:

Q= +120.45+8.84*A-32.51*B+38.84*C-3.92*D+11.81*AD+18.34*CD+9.56*D^2 …. (**V.6**)

In the equation, a positive sign denotes a synergistic interaction between the variables, whereas a negative sign implies an antagonistic or opposing impact. In order to achieve a maximum adsorption capacity of 220.01 mg/g, optimization revealed that the optimal adsorption settings are 10, 10 mg, 200 mg/l, and 40 C of pH, adsorbent dose, starting concentration, and temperature, respectively.

Chapter V: **Utilizing Raw Oak Cupule and Response Surface Methodology to Optimize Adsorption Factors for Methylene Blue Elimination**

05

By comparing the residual distribution and the correlation between the model-predicted and experimental values for MB adsorption, the BBD model was graphically validated. **Fig. V.12(a)** shows the residuals' normal probability curve in the BBD model. A perfect normal distribution and residual independence are shown by the findings, which display a straight-line pattern. The remarkable agreement between the experimental data and the model's predictions is further supported by **Fig. V.12 (b)**, which shows the link between experimental and model-predicted values for MB elimination [24].
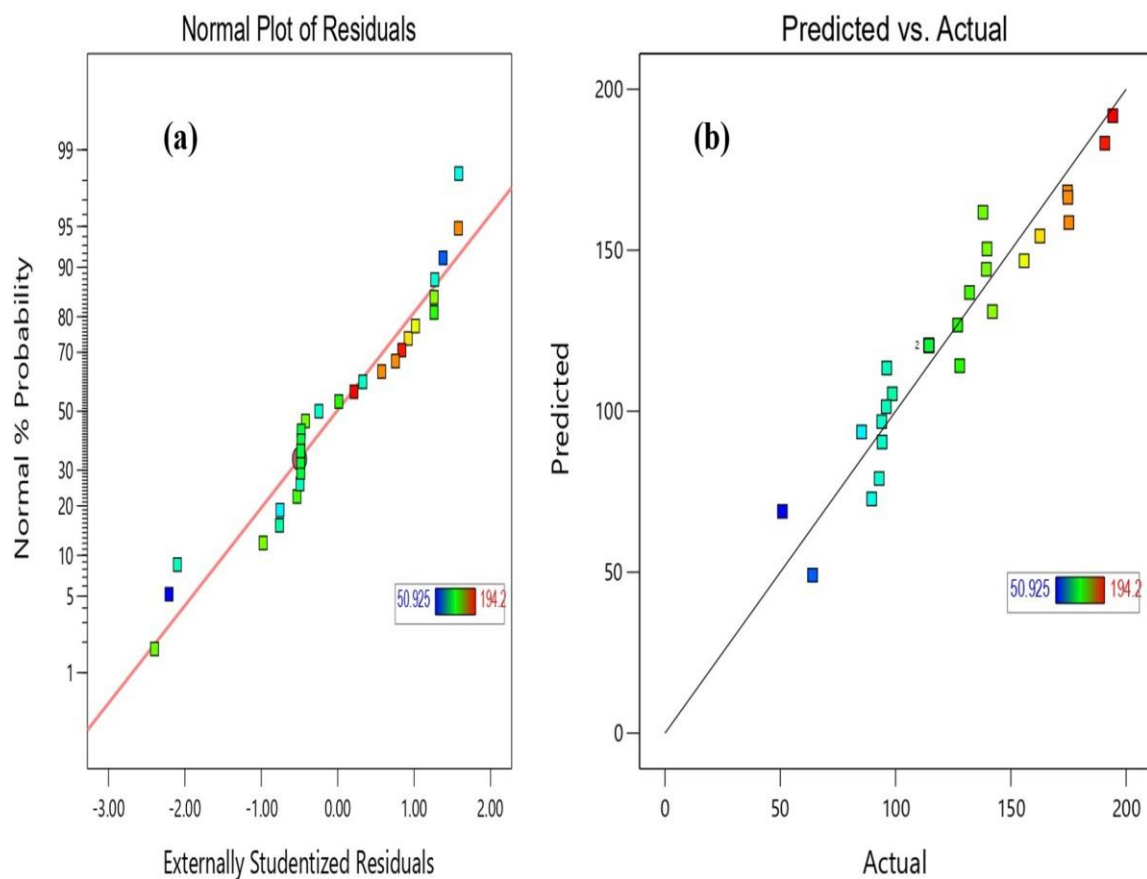
Figure V. 12: *Plots of the residuals for CR adsorption capacity with standard probability (a) and the connection between the real and anticipated values of CR adsorption capacity (b).*

Chapter V: **Utilizing Raw Oak Cupule and Response Surface Methodology to Optimize Adsorption Factors for Methylene Blue Elimination**

05
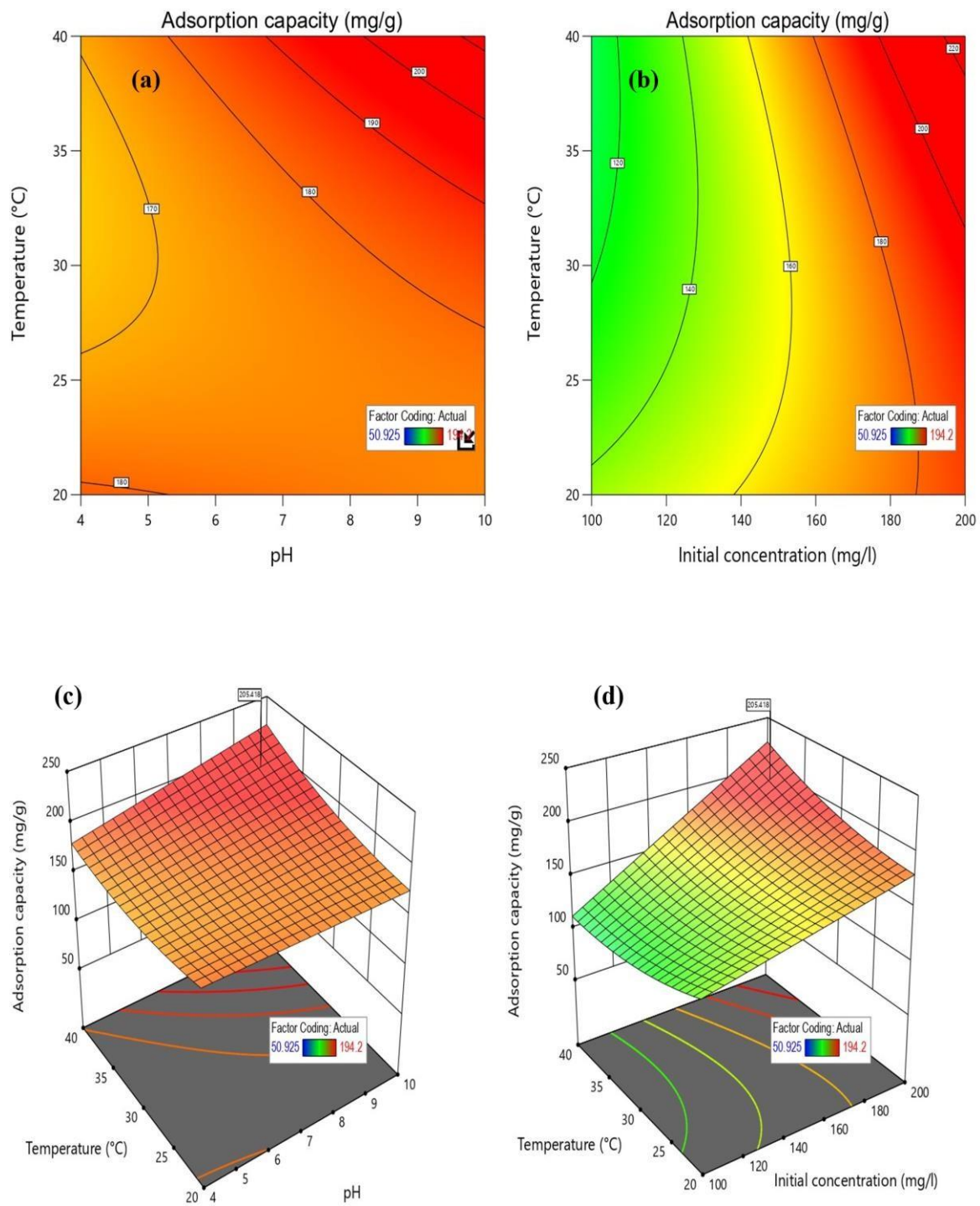
Figure V. 13: *(a) 3D Surface Plot and (b) Contour Plot of Biosorbent Adsorption Capacity*

for MB, Highlighting Interactions between AD (a, d) and DC (b, c).

Chapter V: Utilizing Raw Oak Cupule and Response Surface Methodology to Optimize
Adsorption Factors for Methylene Blue Elimination

05

V.3.11 Interaction Effects on Response Variables and Optimization of Processes

The impacts of two components interacting were examined (**Table V.7**). The P-values for the pH-Temperature (AD) and initial concentration-temperature (CD) interactions were 0.0735 and 0.0081, accordingly, indicating that they were noteworthy.

Table V. 7: ANOVA is used to analyze the adsorption capability of CR.

| Source	Sum of squares	df	Mean square	F-value	P-value	Remarks
Model	34447.81	7	4921.12	31.29	<0.0001	Significant
A-pH	938.58	1	938.58	5.97	0.0235	
B-adsorbent dosage	12680.03	1	12680.03	80.62	<0.0001	
C-Initial concentration	180989.3	1	18098.30	115.06	<0.0001	
D-Temperature	184.55	1	184.55	1.17	0.2910	
AD	558.14	1	558.14	3.55	0.0735	
CD	1345.42	1	1345.42	8.55	0.0081	
D^2	642.79	1	642.79	4.09	0.0562	
Residual	3303.11	21	157.29			

The effects of the remaining interactions, AB, AC, BC, and BD, were found to be negligible.

Fig. V.13 and b show the 3-D surfaces and 2-D contour plots for the AD and CD interactions, respectively. In general, it is discovered that raising the temperature and concentration of the starting solution enhances the ability to add the initial dye concentration, which supplies the required driving force to get around the obstacle to the mass transfer of MB between the aqueous phase and the solid phase, is responsible for the discernible rise in the adsorption capacity. Additionally, the interaction between MB and the biosorbant is improved by the first

Chapter V: Utilizing Raw Oak Cupule and Response Surface Methodology to Optimize
Adsorption Factors for Methylene Blue Elimination

05

dye concentration rise. Consequently, a higher starting MB concentration enhances MB adsorption absorption [25].

The initial solution pH is a critical parameter affecting adsorption capacity Q (mg/g). Analysis at the point of zero charge reveals that adsorption efficiency increases in alkaline conditions. This enhancement is due to the electrostatic attraction between the positively charged dye molecules and the negatively charged surface of the biosorbent in basic media.

V.3.12 Cost estimate

According to this study, agricultural waste materials make a viable adsorbent. CR peel is free and plentiful as garbage. An accurate budget for the necessary materials is included in the Energy and Cost Estimate, which provides a comprehensive prediction of the anticipated production costs. The results are shown in **Table V.8** and provide a meticulous quantification of the energy and costs associated with generating one kilogram of natural green pea peels (CR).

Table V. 8: Cost estimation of CR biosorbent.

unit	Total cost
Cost of cupule collection	0.00 USD
Cost of drying of adsorbent	0.00 USD (dried using the sun)
Milling and sieving	100(1KW/h = 0.035 USD in Algeria)

V.3.13 Comparison of adsorption capacity

In relation to the absorption of MB per the CR adsorbent, the adsorption capability, as shown in **Table V.9**, reveals a noteworthy optimum adsorbed quantity of 220.95 mg/g, as anticipated by the Langmuir equilibrium model.

Chapter V: Utilizing Raw Oak Cupule and Response Surface Methodology to Optimize Adsorption Factors for Methylene Blue Elimination

05

Table V. 9: Comparison of adsorption capacity of MB dye onto CR with an author study.

Material	Dye removal	Adsorption capacity (mg/g)
This study	MB	**220.95**
Green pea peels [9]	MB	207.53
Indian almond [26]	MB	88.6
Wall barley [27]	MB	26.2
Pea haulm [28]	MB	167

V.3.14 Regeneration

The adsorbent material's recycling qualities were crucial in determining how applicable it was.

Fig. V.14 shows the regeneration performance of CR in relation to MB adsorption. It is clear that as the number of usage cycles increased, both the ability for adsorption and desorption efficiency showed a declining trend. CR demonstrated significant adsorption effectiveness for the first six cycles, with removal rates (%) for cycles 1 through 6 of 96.2, 90.01, 80.95, 75.4, 59.1, and 40.75 percent, respectively. However, following six cycles, the adsorbent's removal rate dropped to 33.26 and 10.67%. This downturn is connected to the partial release of MB from the adsorption sites; if MB molecules are not completely released from these sites, they remain on the surface of the biosorbent, reducing its ability to adsorb additional MB molecules and lowering the CR's adsorption capacity. As a result, five cycles were found to be the ideal usage cycle for CR.

Chapter V: Utilizing Raw Oak Cupule and Response Surface Methodology to Optimize Adsorption Factors for Methylene Blue Elimination

05
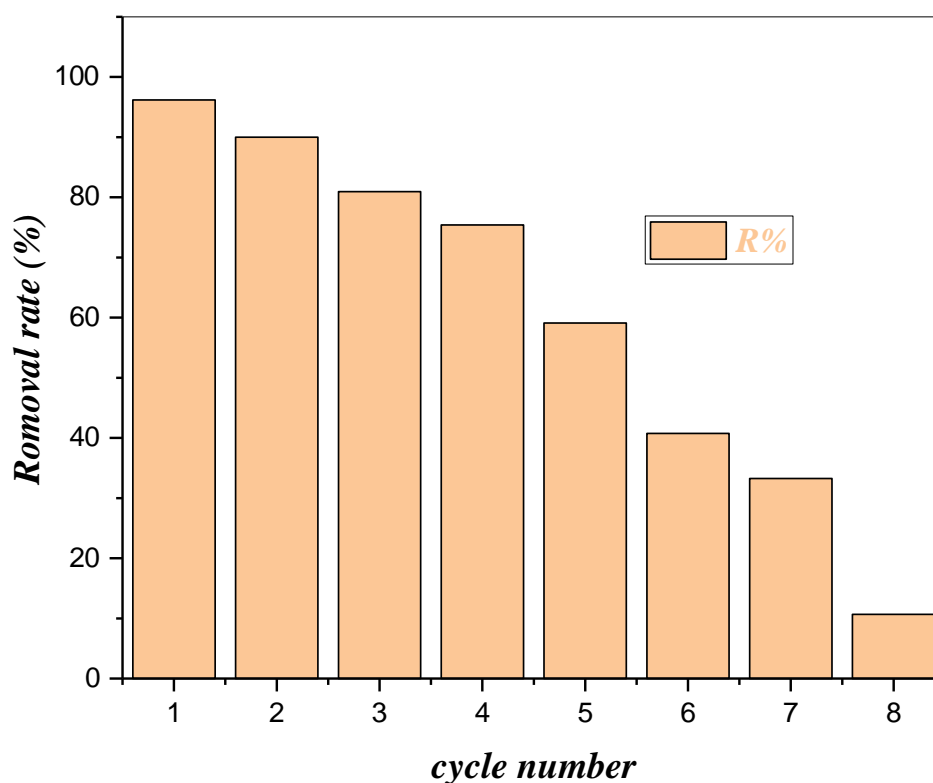
Figure V. 14: Diagram of regeneration cycle Numbers.

V.4. Valorization of Biomass Wastes as Efficient Adsorbents: A Comparative Analysis

The comparative analysis of the adsorption capacities of the three biosorbents reveals valuable insights into their potential for wastewater treatment. Among them, the **Mixed Waste Agriculture (MWA)** adsorbent exhibits the **highest adsorption capacity**, reaching **258.95 mg/g**, positioning it as the most effective material for Methylene Blue removal. This highlights the **importance of utilizing agricultural waste blends**, which combine multiple beneficial properties from various biomass types, thereby enhancing adsorption efficiency. The **oak cupule (CR)** follows with a capacity of **220.95 mg/g**, demonstrating good adsorption potential and emphasizing the **valorization of forestry by-products** that are often underutilized. The **green pea peel (GP)**, with an adsorption capacity of **207.33 mg/g**, while being the least effective among the three, still presents a **novel application of food waste** in pollutant removal. The use of these low-cost, eco-friendly, and abundantly available materials supports **sustainable environmental remediation** and contributes to the **circular economy** by converting waste into valuable adsorbents.

Chapter V: **Utilizing Raw Oak Cupule and Response Surface Methodology to Optimize Adsorption Factors for Methylene Blue Elimination**

05

Table V.10: Comparative Table of Adsorption Capacities

Adsorbent	Adsorption Capacity (mg/g)	Efficiency Ranking	Importance & Novelty
Mixed Waste Agriculture (MWA)	258.95	1st	High efficiency; novel use of mixed biomass; synergy of multiple wastes
Oak Cupule (CR)	220.95	2nd	Effective forestry by-product; underexploited natural material
Green Pea Peel (GP)	207.33	3rd	Promising use of food/agricultural waste; eco-friendly and cheap

Chapter V: Utilizing Raw Oak Cupule and Response Surface Methodology to Optimize Adsorption Factors for Methylene Blue Elimination

05

Reference chapter V

[1] E.-K. Guechi et O. Hamdaoui, « Sorption of malachite green from aqueous solution by potato peel: kinetics and equilibrium modeling using non-linear analysis method », *Arab. J. Chem.*, vol. 9, p. S416-S424, 2016.

[2] Z. H. Mussa, L. R. Al-Ameer, F. F. Al-Qaim, I. F. Deyab, H. Kamyab, et S. Chelliapan, « A comprehensive review on adsorption of methylene blue dye using leaf waste as a bio-sorbent: isotherm adsorption, kinetics, and thermodynamics studies », *Environ. Monit. Assess.*, vol. 195, nº 8, p. 940, août 2023, doi: 10.1007/s10661-023-11432-1.

[3] R. Al-Tohamy *et al.*, « A critical review on the treatment of dye-containing wastewater: Ecotoxicological and health concerns of textile dyes and possible remediation approaches for environmental safety », *Ecotoxicol. Environ. Saf.*, vol. 231, p. 113160, févr. 2022, doi: 10.1016/j.ecoenv.2021.113160.

[4] K. Madi *et al.*, « Green Fabrication of ZnO Nanoparticles and ZnO/rGO Nanocomposites from Algerian Date Syrup Extract: Synthesis, Characterization, and Augmented Photocatalytic Efficiency in Methylene Blue Degradation », *Catalysts*, vol. 14, nº 1, p. 62, 2024.

[5] M. C. Holliday, D. R. Parsons, et S. H. Zein, « Agricultural Pea Waste as a Low-Cost Pollutant Biosorbent for Methylene Blue Removal: Adsorption Kinetics, Isotherm And Thermodynamic Studies », *Biomass Convers. Biorefinery*, mai 2022, doi: 10.1007/s13399-022-02865-8.

[6] K. Philippou, C. Evangelou, I. Ioannidis, et I. Pashalidis, « Pine needle–derived biochar adsorbents for removal of Sm (III) and competitive toxic metals from model aqueous matrices. », *Sustain. Chem. Environ.*, vol. 4, p. 100053, 2023.

[7] M. Rafatullah, O. Sulaiman, R. Hashim, et A. Ahmad, « Adsorption of methylene blue on low-cost adsorbents: a review », *J. Hazard. Mater.*, vol. 177, nº 1-3, p. 70-80, 2010.

[8] A. Guediri, A. Bouguettoucha, D. Chebli, N. Chafai, et A. Amrane, « Molecular dynamic simulation and DFT computational studies on the adsorption performances of methylene blue in aqueous solutions by orange peel-modified phosphoric acid », *J. Mol. Struct.*, vol. 1202, p. 127290, févr. 2020, doi: 10.1016/j.molstruc.2019.127290.

[9] O. R. Benkouachi *et al.*, « Advanced green peel utilization for efficient methylene blue removal: Integrated analysis and predictive modeling », *J. Mol. Liq.*, p. 125951, 2024.

[10] O. Abdelwahab, A. E. Nemr, A. E. Sikaily, et A. Khaled, « USE OF RICE HUSK FOR ADSORPTION OF DIRECT DYES FROM AQUEOUS SOLUTION: A CASE STUDY OF DIRECT F. SCARLET ».

[11] A. Guediri *et al.*, « The Enhanced Adsorption Capacity of Ziziphus jujuba Stones Modified with Ortho-Phosphoric Acid for Organic Dye Removal: A Gaussian Process Regression Approach », *Water*, vol. 16, nº 9, Art. nº 9, janv. 2024, doi: 10.3390/w16091208.

[12] H. Boulika, M. El Hajam, M. Hajji Nabih, N. Idrissi Kandri, et A. Zerouale, « Activated carbon from almond shells using an eco-compatible method: screening, optimization, characterization, and adsorption performance testing », *RSC Adv.*, vol. 12, nº 53, p. 34393-34403, 2022, doi: 10.1039/D2RA06220H.

[13] V. K. Gupta, « Application of low-cost adsorbents for dye removal–a review », *J. Environ. Manage.*, vol. 90, nº 8, p. 2313-2342, 2009.

[14] F. Fadzail, M. Hasan, Z. Mokhtar, et N. Ibrahim, « Removal of naproxen using low-cost Dillenia Indica peels as an activated carbon », *Mater. Today Proc.*, vol. 57, p. 1108-1115, 2022.

[15] A. S. Abdulhameed *et al.*, « Statistical modeling and mechanistic pathway for methylene blue dye removal by high surface area and mesoporous grass-based activated carbon using

Chapter V: Utilizing Raw Oak Cupule and Response Surface Methodology to Optimize Adsorption Factors for Methylene Blue Elimination

05

K2CO3activator », *J. Environ. Chem. Eng.*, vol. 9, nᵒ 4, p. 105530, 2021, doi: 10.1016/j.jece.2021.105530.

[16] F. B. Shahri et A. Niazi, « Synthesis of modified maghemite nanoparticles and its application for removal of acridine Orange from aqueous solutions by using box-Behnken design », *J. Magn. Magn. Mater.*, 2015, doi: 10.1016/j.jmmm.2015.08.054.

[17] A. K. T. Mohammad, A. S. Abdulhameed, et A. H. Jawad, « Box-Behnken design to optimize the synthesis of new crosslinked chitosan-glyoxal/TiO2 nanocomposite: Methyl orange adsorption and mechanism studies », *Int. J. Biol. Macromol.*, vol. 129, p. 98-109, 2019, doi: 10.1016/j.ijbiomac.2019.02.025.

[18] C. Djama *et al.*, « Experimental and Theoretical Study of Methylene Blue Adsorption on a New Raw Material, Cynarascolymus - A statistical Physics Assessment », Engineering, preprint, mai 2023. doi: 10.20944/preprints202305.0418.v1.

[19] O. R. Benkouachi *et al.*, « Innovative Valorization of Agricultural Waste for Enhanced Adsorption Efficiency of Organic Pollutants: Leveraging Density Functional Theory, Molecular Dynamics Simulations, and Advanced Artificial Intelligence Techniques (Ann_Fdb-Lfd, Svm_Fdb-Lfd, Gpr_Fdb-Lfd, and Knn_Fdb-Lfd) », *Mol. Dyn. Simul. Adv. Artif. Intell. Tech. AnnFdb-Lfd SvmFdb-Lfd GprFdb-Lfd KnnFdb-Lfd*, Consulté le: 15 octobre 2024. [En ligne]. Disponible sur: https://papers.ssrn.com/sol3/papers.cfm?abstract_id=4869666

[20] L. Sellaoui, H. Guedidi, L. Reinert, S. Knani, L. Duclaux, et A. B. Lamine, « Experimental and theoretical studies of adsorption of ibuprofen on a raw and two chemically modified activated carbons: new physicochemical interpretations », *RSC Adv.*.

[21] S. S. Moghaddam, M. R. A. Moghaddam, et M. Arami, « Response surface optimization of acid red 119 dye from simulated wastewater using Al based waterworks sludge and polyaluminium chloride as coagulant », *J. Environ. Manage.*, vol. 92, nᵒ 4, p. 1284-1291, 2011, doi: 10.1016/j.jenvman.2010.12.015.

[22] S. Karimifard et M. R. Alavi Moghaddam, « Application of response surface methodology in physicochemical removal of dyes from wastewater: A critical review », *Sci. Total Environ.*, vol. 640-641, p. 772-797, 2018, doi: 10.1016/j.scitotenv.2018.05.355.

[23] S. Soleimani, A. Heydari, M. Fattahi, et A. Motamedisade, « Calcium alginate hydrogels reinforced with cellulose nanocrystals for methylene blue adsorption: Synthesis, characterization, and modelling », *Ind. Crops Prod.*, vol. 192, nᵒ March 2022, p. 115999, 2023, doi: 10.1016/j.indcrop.2022.115999.

[24] A. S. Abdulhameed *et al.*, « Statistical modeling and mechanistic pathway for methylene blue dye removal by high surface area and mesoporous grass-based activated carbon using K2CO3activator », *J. Environ. Chem. Eng.*, vol. 9, nᵒ 4, p. 105530, 2021, doi: 10.1016/j.jece.2021.105530.

[25] R. Subramaniam et S. Kumar Ponnusamy, « Novel adsorbent from agricultural waste (cashew NUT shell) for methylene blue dye removal: Optimization by response surface methodology », *Water Resour. Ind.*, vol. 11, p. 64-70, 2015, doi: 10.1016/j.wri.2015.07.002.

[26] L. Hevira, J. O. Ighalo, H. Aziz, et R. Zein, « Terminalia catappa shell as low-cost biosorbent for the removal of methylene blue from aqueous solutions », *J. Ind. Eng. Chem.*, vol. 97, p. 188-199, 2021.

[27] S. M. Al-Mahmoud, « Kinetic and Thermodynamic Studies for the Efficient Removal of Methylene Blue Using Hordeum Murinum as a New Biosorbent », *Egypt. J. Chem.*, vol. 63, nᵒ 9, p. 3381-3390, 2020.

[28] M. C. Holliday, D. R. Parsons, et S. H. Zein, « Agricultural Pea Waste as a Low-Cost Pollutant Biosorbent for Methylene Blue Removal: Adsorption Kinetics, Isotherm And

Chapter V: **Utilizing Raw Oak Cupule and Response Surface Methodology to Optimize Adsorption Factors for Methylene Blue Elimination**

05

Thermodynamic Studies », *Biomass Convers. Biorefinery*, vol. 14, nº 5, p. 6671-6685, mars 2024, doi: 10.1007/s13399-022-02865-8.
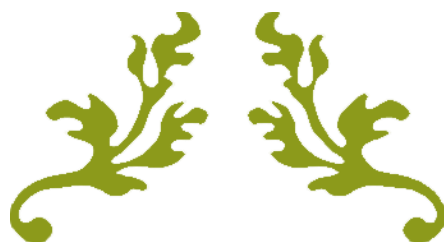
GENERAL CONCLUSION

General conclusion and prospects

Water use is high in the economic world. Their cargoes of organic materials and colors, which are very poisonous and hardly biodegradable, create major disruptions to the aquatic ecosystem once they are released.

The main objective of this work was to develop new materials using simple and inexpensive methods and show how the materials may be used to decontaminate wastewater effluents that include dyes, namely methylene blue. To assess this potential, a variety of experiments were carried out, including kinetics, equilibrium investigations, parameter impacts, and material characterization. To eliminate cationic dyes from wastewater, three main materials have been created and put to use as adsorbents. In particular, GP raw, MWA, and CR raw.

In order to properly position the topic of this thesis, the first chapter will be devoted to a bibliographical investigation. This section will first provide general information on the numerous kinds of dyes, how they are categorized based on various characteristics, and the dangers of using them. After that, research on various water discoloration methods will be discussed, with a focus on the adsorption approach. In addition, comparative tables of various powder precursors utilized in literature and their adsorption effectiveness with several contaminants will be provided, along with information on the various sources of inexpensive adsorbents (natural, industrial, and agricultural leftovers). Numerous factors, such as adsorbent mass, starting dye concentration, duration interaction, pH, temperature, and particle size, things will be studied and noted since they can all affect the adsorption capacity, are included in this chapter.

The next section will provide a detailed description of the characterisation methods used in this thesis as well as the steps involved in preparing the adsorbent materials. This chapter will also include all of the procedures for carrying out the adsorption tests with different parameters. Molecular dynamics simulations (MDS) and density functional theory (DFT), two quantum chemical computations utilized in this work, will also be explained. At the end of this chapter, there will also be a thorough discussion of statistical physical modeling based on the grand canonical ensemble.

Chapter Three provides an extensive examination of the adsorption of Methylene Blue (MB) onto Green Peel (GP) material. The effectiveness of GP as an adsorbent is established through Fourier-transform infrared spectroscopy (FT-IR) analysis. The study systematically

explores the effects of various parameters, including adsorbent mass, pH level, initial MB concentration, and temperature, on the removal efficiency of MB. To analyze the adsorption isotherm data, three models are employed: the single-energy monolayer model (M1), the double-energy monolayer model (M2), and the multilayer model (M3). Among these, the double-energy monolayer model (M2) is identified as the most appropriate representation of the data. The investigation utilizes advanced methodologies, such as statistical physics modeling, steric parameter analysis, thermodynamic evaluations, Density Functional Theory (DFT), regeneration characteristics, Molecular Dynamics Simulation (MDS). Under optimal conditions—specifically, a contact time of 30 minutes, an adsorbent mass of 0.6 g, an initial MB concentration of 400 mg/L, a pH of 6.6, and a temperature of 10°C—the experimental results indicate an MB adsorption capacity of 207.90 mg/g, underscoring the significant potential of GP for MB removal applications.

In Chapter Four, the importance of using agricultural waste to enhance the adsorption of organic pollutants for sustainable environmental remediation is highlighted. This section emphasizes the process of deriving activated biomass from food waste, specifically focusing on the peels of various fruits and vegetables, which are activated using KOH. The maximum monolayer adsorption capacity of Methylene Blue (MB) on the modified waste adsorbent (MWA) was found to be 129.93 mg/g at 10 °C, which increased to 258.42 mg/g at 40 °C. The adsorption capacity stabilized at a biosorbent dose of 1 g/L, resulting in a removal efficiency of 95.98%. Among the advanced statistical physics models analyzed, the ME2 model, defined as the double-energy single-layer model, was identified as the most effective in representing the complexities of MB adsorption onto the MWA adsorbent. This methodology provides essential insights and practical strategies for improving adsorption processes utilizing agricultural waste, thereby supporting sustainable environmental remediation efforts. Notably, the predicted MB uptake of 258.3967 mg/g aligns closely with the experimental measurement of 258.4206 mg/g.

The CR adsorbent from the oak cupule, local residual, is used in the fifth chapter that follows. A homogeneous distribution of adsorption sites on the biosorbent is reflected in the monolayer coverage that occurs throughout the adsorption process. The maximum adsorption capacity for Methylene Blue (MB) on CR was observed to be 150.29 mg/g at 40 °C, which increased to 220.95 mg/g at 20 °C. Furthermore, the adsorption energies for two layers of MB molecules on the CR surface were found to be less than 40 kJ/mol, implying that the interactions responsible for the removal process are mainly physical rather than chemical.

Prospective Applications for Future Development

To advance this study, several enhancements are proposed:

- Innovating encapsulation techniques for powdered adsorbents to improve ease of use and facilitate regeneration, thereby enhancing operational efficiency.

- Conducting in-depth analyses on the transformation and fate of contaminants following adsorption and regeneration phases, ensuring sustained effectiveness and environmental safety.

- Developing and implementing more efficient, rapid production methods for adsorbents to enable scalable deployment and meet larger demand.

Abstract

This thesis investigates the development of novel materials specifically designed for water purification via adsorption. The adsorption capability of three newly prepared adsorbents—green pea peels, mixed food waste, and oak cupule—was evaluated. The mixed food waste was chemically treated with KOH, whereas green pea peels and oak bowl were used in their natural powdered forms. Comprehensive characterization of these materials was conducted through various techniques, including XRD, FTIR, TGA, and SEM analyses. In a batch system, these adsorbents were applied to remove methylene blue (MB) dye, examining factors such as adsorption kinetics, equilibrium behavior, and the effects of pH, contact time, initial concentration, ionic strength, and temperature. High adsorption capacities were achieved, underscoring the effectiveness of the materials. Additionally, advanced methodologies, such as experimental design, were employed to optimize the adsorption process.

Keywords: Adsorption, Green pea peels, Mixed food waste, Oak cupule, Methylene blue.

Resumé

Cette thèse étudie le développement de nouveaux matériaux spécifiquement conçus pour la purification de l'eau par adsorption. La capacité d'adsorption de trois adsorbants nouvellement préparés — les pelures de pois verts, les déchets alimentaires mixtes et la cupule en chêne — a été évaluée. Les déchets alimentaires mélangés ont été traités chimiquement avec du KOH, tandis que les pelures de pois verts et le bol de chêne étaient utilisés sous leur forme naturelle en poudre. La caractérisation complète de ces matériaux a été effectuée au moyen de diverses techniques, y compris des analyses DRX, FTIR, TGA et MEB. Dans un système discontinu, ces adsorbants ont été appliqués pour éliminer le colorant bleu de méthylène (MB), en examinant des facteurs tels que la cinétique d'adsorption, le comportement à l'équilibre et les effets du pH, du temps de contact, de la concentration initiale, de la force ionique et de la température. Des capacités d'adsorption élevées ont été atteintes, ce qui souligne l'efficacité des matériaux. De plus, des méthodologies avancées, telles que la conception expérimentale, ont été utilisées pour optimiser le processus d'adsorption.

Mots-clés : Adsorption, Pelures de pois verts, Déchets alimentaires mixtes, Cupule de chêne, Bleu de méthylène.

ملخص

تدرس هذه الأطروحة تطوير مواد جديدة مصممة خصيصًا لتنقية المياه عن طريق الامتزاز. تم تقييم قدرة الامتزاز لثلاثة امتزازات معدة حديثًا ـ قشور البازلاء الخضراء ومخلفات الطعام المختلطة وكوب البلوط. تمت معالجة نفايات الطعام المختلطة كيميائيًا باستخدام KOH، بينما تم استخدام قشور البازلاء الخضراء ووعاء البلوط في شكل مسحوق طبيعي. وقد أجري التوصيف الكامل لهذه المواد باستخدام تقنيات مختلفة، بما في ذلك تحليلات XRD و FTIR و TGA و SEM. في نظام الدفعات، تم تطبيق هذه الامتزازات لإزالة صبغة الميثيلين الأزرق (MB) من خلال فحص عوامل مثل حركية الامتزاز وسلوك التوازن وتأثيرات الأس الهيدروجيني ووقت التلامس والتركيز الأولي وقوة الأيونات ودرجة الحرارة. وتحققت قدرات امتزازية عالية، مما يؤكد فعالية المواد. بالإضافة إلى ذلك، تم استخدام منهجيات متقدمة مثل التصميم التجريبي لتحسين عملية الامتزاز.

الكلمات الرئيسية: الامتزاز، قشور البازلاء الخضراء، نفايات الطعام المختلطة، كوب البلوط، ميثيلين الأزرق.